AD-A136 984 THE EFFECT OF MASS AND STIFFNESS CHANGES ON THE DAMPING 1/2
FACTOR IN A LARGE..(U) AIR FORCE INST OF TECH
WRIGHT-PATTERSON AFB OH SCHOOL OF ENGI.. D E OLSEN
UNCLASSIFIED DEC 83 AFIT/GSO/AA/83D-2 F/G 22/2 NL

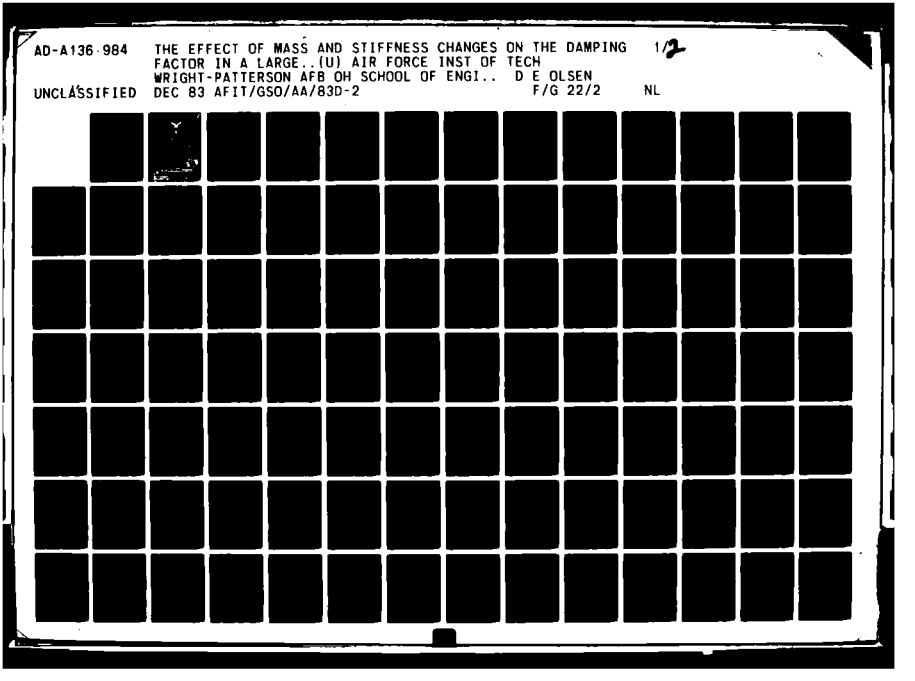

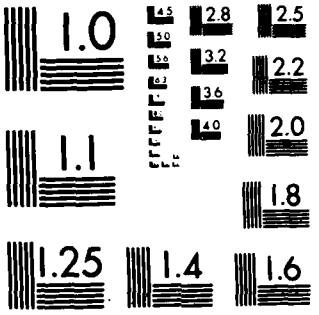

THE EFFECT OF MASS AND STIFFNESS CHANGES ON THE DAMPING FACTOR IN A LARGE SPACE STRUCTURE AS REPRESENTED BY THE CSDL 2 MODEL

THESIS

David E. Olsen
Captain USAF

AFIT/GSO/AA/83D-2

DEPARTMENT OF THE AIR FORCE
AIR UNIVERSITY
AIR FORCE INSTITUTE OF TECHNOLOGY
Wright-Patterson Air Force Base, Ohio

AFIT/GSO/AA/83D-2

THE EFFECT OF MASS AND STIFFNESS CHANGES ON THE DAMPING FACTOR IN A LARGE SPACE STRUCTURE AS REPRESENTED BY THE CSDL 2 MODEL

THESIS

David E. Olsen
Captain USAF

AFIT/GSO/AA/83D-2

Approved for Public Release, Distribution Unlimited

AFIT/GSO/AA/83D-2

THE EFFECT OF MASS AND STIFFNESS CHANGES ON THE DAMPING FACTOR IN A LARGE SPACE STRUCTURE AS REPRESENTED BY THE CSDL 2 MODEL

THESIS

Presented to the Faculty of the School of Engineering
of the Air Force Institute of Technology
Air University
In Partial Fulfillment of the
Requirements for the Degree of
Master of Science in Space Operations

David E. Olsen, B.S.
Captain USAF

December, 1983

Table of Contents

Acknowledgements

The assistance provided by my thesis committe, Major Martin M. Wallace and Dr. Edward J. Dunne, Jr., was instrumental in the development of this research. Their willingness to advise and instruct me during all phases of this thesis is gratefully acknowledged. Additionally, I would like to thank the Design and Analysis Methods Group of the Air Force Flight Dynamics Laboratory, especially Vicky Tischler, for their help in debugging computer programs and in the analysis of the results. Finally, I wish to thank my wife Shelley for her support and understanding during the course of this thesis and our entire AFIT tour.

David E. Olsen

List of Figures

List of Tables

List of Symbols

Symbol	Meaning
B	Actuator system matrix
C	Sensor system matrix
D	n x m matrix of actuator coefficients
E	n x m symmetric damping matrix
I	Identity matrix
K	n x m symmetric stiffness matrix
M	n x m symmetric mass matrix
η	Modal coordinate system
ω	Modal frequency
ω_n	Natural frequency
ω_d	Damped frequency
ϕ	Modal matrix of eigenvectors
q	Generalized coordinate system
σ	Decay
u	Inputs (disturbances)
ζ	Damping factor

Abstract

This investigation was undertaken to determine the sensitivity of the damping factor in a large space structure (LSS) to small changes in nonstructural mass and structural element stiffness. Revision 3 of the ACOSS 2 model, developed by the Charles Stark Drapes Laboratory, Inc. (CSDL), was used as the model of the LSS. Various combinations of the mirror masses in this large space telescope were varie by up to 10%, selected structural elements were stiffened by increasing their cross-sectional areas by 10 and 50%, and, finally, two structural elements in the middle of the telescope were stiffened to represent the addition of a lumped mass located away from the control system sensors and actuators. A control system of 21 collocated sensors and actuators, positioned at the top and bottom of the telescope, was used in this analysis.

The analysis was accomplished using NASTRAN for the finite element analysis, and, after selecting certain vibration modes for further study, the complex conjugate pairs used to determine the damping factors were calculated. This last step was accomplished through spillover reduction and reduction of the closed loop matrix to a lower triangular form. This procedure was repeated for each of the 46 perturbations applied to the model in this research.

The results indicate that the damping factors for the CSDL model are quite sensitive to small perturbations and that it is very difficult to predict the effect that a perturbation to the model will have on the damping factors. If the vibrations in an LSS are to be altered by changing mass or stiffness, a thorough analysis is required to ensure that increasing the damping for one mode does not result in an undesirable change in the damping for another mode.

THE EFFECT OF MASS AND STIFFNESS CHANGES ON THE DAMPING FACTOR IN A LARGE SPACE STRUCTURE AS REPRESENTED BY THE CSDL 2 MODEL

I. Introduction

Background

> "Deployment of large space structures for communications, space defense, power generation, manufacturing, and research has become a major objective of space planners for the mid-1980's and beyond. These systems typically combine large size with extremely rigorous pointing and surface figure performance requirements." (Ref 1:1-1)

In addition to these performance requirements, the mass of a large space structure (LSS) must be kept as small as possible to minimize launch costs and the structure must be designed to be easily assembled once delivered to the proper orbit. These constraints generally "result in highly flexible spacecraft which exhibit poor dimensional precision. Our current ability to conceptualize space systems, to select structural materials, and to build mechanisms for on-orbit construction and deployment has now far outstripped our demonstrated ability to control the resulting structure." (Ref 1:1-1)

In order to study the structural characteristics of an LSS, the Charles Stark Draper Laboratory, Inc. (CSDL) of

Cambridge, MA developed a model representative of an above described structure. This model, known as CSDL 2, is depicted in Figure 1. It is a large space telescope measuring 28 meters tall and 20 meters wide. The beam/truss structure is made of epoxy-graphite tubes varying in diameter from 20 to 40 cm. Including the mirrors, solar panels, and equipment package, the telescope weighs about 9300 kg. Three desired features were incorporated in the design of this model: 1) a structural design based on reasonable sizes and weights, 2) a simple, unclassified optical system with associated performance measures and weights, and 3) a set of disturbances typical of equipment vibration and attitude control. (Ref 2:1) This model is being analyzed in the Active Control of Space Structures (ACOSS) program, sponsored by the Defense Advanced Research Projects Agency (DARPA), to determine the adequacy of various active structural control methods under development. Another effort, the Vibration Control of Space Structures (VCOSS) program, "is intended to study the application of ACOSS technology to an actual spacecraft design", to include specifying the actual control hardware to be used and assessing the controllability of the structure using this hardware. The minimum mass VCOSS model is based on the ACOSS model but has been modified to "reduce the structural mass to the minimum required to maintain structural stability. This system will

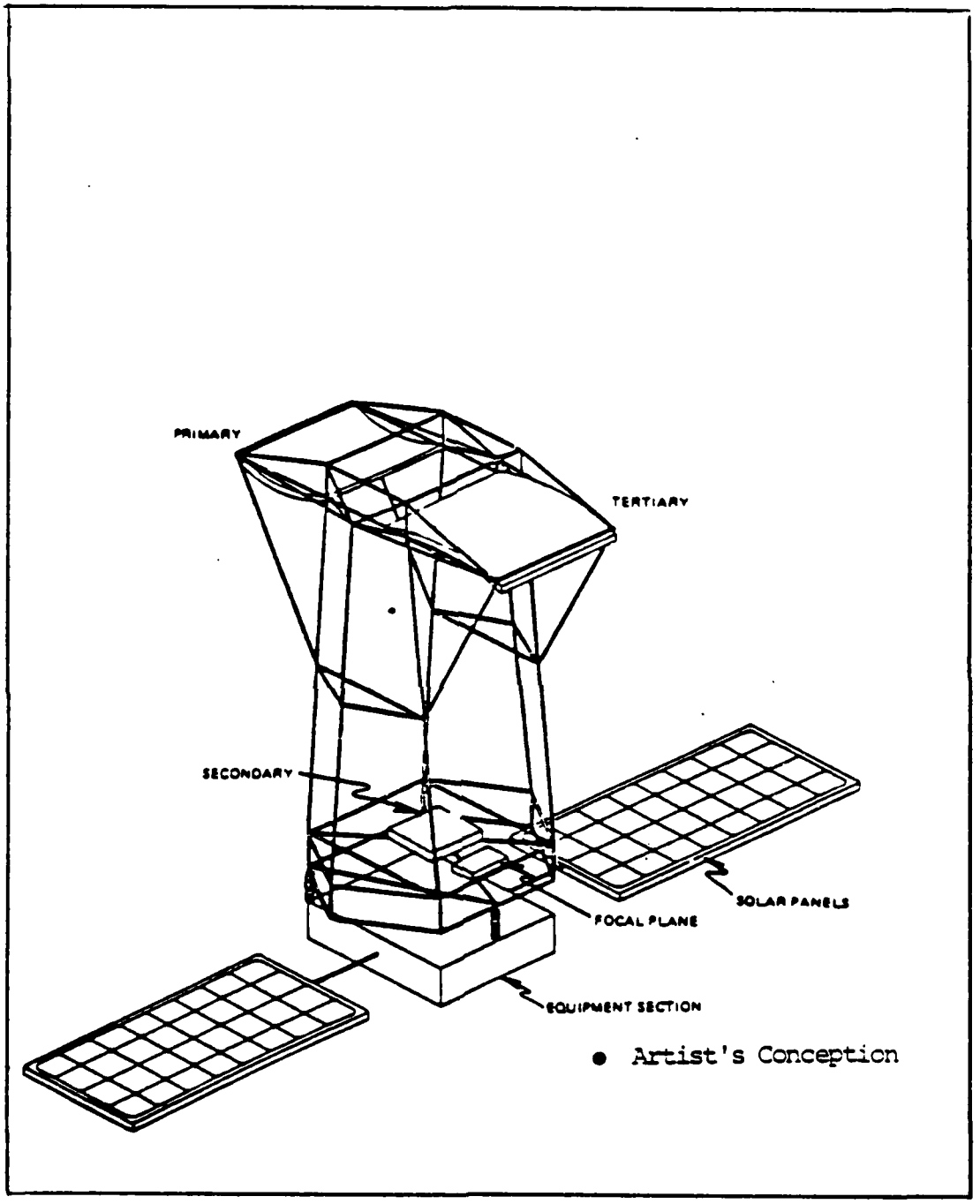

Figure 1. CSDL 2 Conceptual Model

rely entirely on the control system for vibration supression to meet the performance requirements." (Ref 3:1) If hardware requirements are to be specified, the system model must accurately represent the vibrational properties of the actual structure. In this reduced mass structure, the interactions between the mirrors and flexible support structure and between the equipment section and optical support truss are the most important properties. Thus, the modeling of these areas was given particular attention in the VCOSS program, resulting in revision three of the CSDL 2 model. This is the model that is analyzed in this thesis. The wall thickness of the tubes in revision three varies from .03 to .067 cm, the radius ranges from 3.6 to 8.1 cm, and the total weight is down to 8963 kg. This model is thoroughly discussed in reference 3.

The ACOSS FIVE research study has indicated that control system performance associated with detailed structural models "can be extremely sensitive to changes in the structural model" and these sensitivities may result from the "detailed way a portion or all of the structure is built." (Ref 1:4-1).

These research programs use the NASTRAN finite element structural analysis computer program developed by NASA and released to the public in 1969. The NASTRAN program requires, as part of its input data, stiffness and inertia properties for each structural element. Non-structural

masses, such as the mirrors on the CSDL 2 model, are handled as point masses, that is, their mass is assumed to be concentrated at specific points on the structure. These mass distributions are also inputs to the NASTRAN program. NASTRAN can provide, among other things, data on the natural vibration frequency and mode shape associated with each structural element. (Ref 4:316) The natural frequency is the frequency at which the structure will vibrate if there are no external forces being applied to it. The shape that each structural element assumes when it is vibrating is the mode shape of the element. (Ref 5:100) Each structural element will have specific natural frequencies and mode shapes associated with it.

Control system design starts with the finite element structural model, which yields natural frequencies and mode shapes. The control system engineer then selects appropriate actuators, which produce forces or torques, and sensors, used to measure the amount and/or rate of displacement. The next step in the control design process, the determination of where to locate the sensors and actuators, was addressed by the ACOSS FIVE report. (Ref 1:4-15) The desired result of control design is a control system of sensors and actuators that is able to effectively negate an induced vibration without exciting a vibration in the rest of the structure. The set of natural frequencies and

mode shapes associated with a structure (hereafter called the ϕ matrix) can be analyzed in conjunction with the desired location and orientation of the sensors and actuators (called the D matrix) to determine the effectiveness of the control system. The product of the transpose of the ϕ matrix and the D matrix gives the B matrix, whose rows physically correspond to the amplitude of each mode at the various actuator locations. If the sensors and actuators are collocated, then the C matrix, whose columns physically correspond to the amplitude of each mode at the various sensor locations, is the transpose of the B matrix. (Ref 6:2) The B and C matrices can be analyzed to determine the damping factor of the structure, which represents a measure of the total amount of damping (both active and passive) present in the system. (Ref 7:62) There will be a certain amount of damping in the structure that comes from its resistance to bending and twisting. The control system is designed to increase the damping factor and hence cause the magnitude of the vibration to decrease faster than it would in the absence of any active control.

The development of the initial CSDL 2 model was completed by the Draper Laboratory in May of 1980. The product of this effort, the space telescope model, is an example of a typical large space structure that can be used to develop and evaluate control systems for 1) positioning the struc-

ture, and 2) controlling structural vibrations caused by thrustors (actuators) and onboard equipment. As discussed in section five of the ACOSS Model 2 research report (Ref 2), two sets of parameter variations on the CSDL 2 model were input to the NASTRAN program to "assess the sensitivity of the control system to changes in the natural frequencies and mode shapes." (Ref 2:45) The selection of these variations in stiffness and mass distribution represent "two point designs from an infinite number of possible variations" and "In order to fully evaluate the stability limits of a particular control system design, it may be necessary to evaluate several perturbed models." (Ref 2:45)

Objectives of the Research

The objective of this research is to expand the vibrational analysis of a typical LSS, represented by the CSDL 2 model, with respect to variations in beam stiffness and non-structural mass. This research will determine: 1) the effect that these variations have on the controllability of the structure by looking at the change in the damping factor for selected modes of vibration, 2) the particular structural elements or non-structural masses that, when varied slightly, have a significant effect on the magnitude of the damping factor, and 3) the feasibility of adding non-structural mass or stiffening structural elements to increase the controllability of an existing LSS. This

information can be used by structural design engineers to specify allowable manufacturing tolerances for certain structural elements of an LSS and by control engineers to develop or improve control systems capable of handling the wide range of vibrations in an LSS.

Methodology Overview

The analysis of the effect of small variations in stiffness and mass is accomplished using five computer programs. Selected perturbations are applied to the CSDL 2 model and then NASTRAN is run to determine the first 30 frequencies and mode shapes. Program FORMAT reformats the NASTRAN output for input to program SELECT. SELECT picks off the particular modes to be analyzed (12 modes in this research) and formats the data for input to ZETA. In program ZETA, the B and C matrices are calculated from the ϕ matrix and the D matrix, and the output is formatted for input to DOFB34. DOFB34 (Direct Output Feedback 34), through spillover reduction, reduces the closed loop equation matrix to a lower triangular form and produces, among other things, two eigenvector pairs per mode. (Ref 8:49) These pairs are used to calculate the damping factor for the mode; the damping factor is then used as the performance index to determine if the structure is becoming more or less stable as a result of variations in stiffness and mass.

A detailed discussion on the use of these programs is

provided in Appendix B. The equations used in ZETA and the calculating of the damping factor are discussed in Chapter 3. DOFB34 is developed and analyzed in Reference 8 and will not be extensively discussed in this report.

II. The CSDL 2 Model

Basic Model

The CSDL 2 Model (Figure 1) represents a three-mirror, wide-angle optical space telescope. The two major components of this structure are the optical support structure and the equipment section, connected to each other by springs at three points to allow either active or passive vibration isolation. The optical support structure, consisting of the upper mirror support truss, the lower mirror support truss, and the metering truss, contains the four optical surfaces. The upper mirror support truss contains the primary and tertiary mirrors; the secondary mirror and the focal plane are contained in the lower mirror support truss. The metering truss maintains mirror separation and is the key section when examining the focus of the telescope. The equipment section is modeled as a central rigid body with two flexible solar panels cantilevered from it, and is assumed to contain all of the guidance, navigation, control, and power systems required for the operating of the telescope. The full structure is approximately 28 meters high and weighs 8963 kg in the VCOSS strength-controlled design that is analyzed in this research.

The finite element model of the structure (Figure 2) contains 59 node points, 51 of which represent nodes where

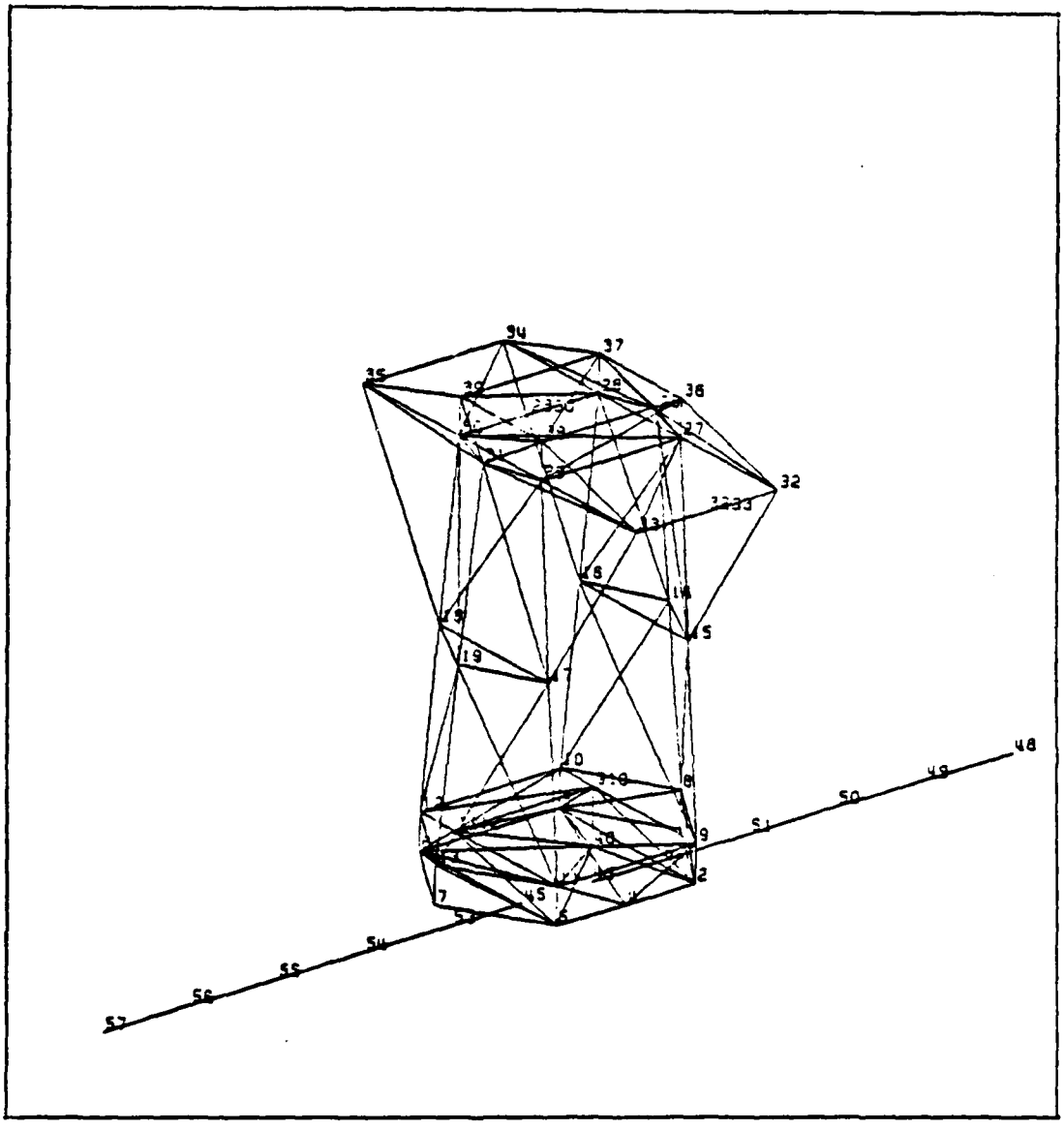

Figure 2. CSDL 2 Finite Element Model

structural elements connect. The other 8 nodes were added to more accurately model the mirrors and equipment section (Ref 3). The coordinates of each node are contained in the NASTRAN input deck (Appendix A) under the title of GRID points. The location of the node points is shown in Figure 2.

There are 137 structural elements in the CSDL 2 model made of epoxy-graphite tubes varying from 3.6 to 8.1 cm in radius. The CBAR entries in the NASTRAN input deck list the node points connected by each structural element. The optical support structure is designed to act as a truss, but it is assumed that all joints allow for a full moment connection. Thus, both bending and axial stiffness are included for all elements. (Ref 2:2) The mass of each structural element is lumped at its node points and is computed by NASTRAN using the cross-sectional area and length of each member and a material density of 1720 kg/m^3. For this VCOSS model, the minimum allowable wall thickness for the epoxy-graphite tubes is .03 cm, and the ratio of radius to thickness (r/t) was defined to be a maximum of 120. The length to radius ratio (l/r) is defined to be a maximum of 400. The natural frequency of each member "was constrained to be greater than 10 hz to prevent significant interaction between systems vibrations and local vibrations." (Ref 3:17) Thus, the radius of each tube is the maximum

value of the three radius values determined by the above criteria. (Ref 9) That is, the radius r is the maximum of:

1) $r = r/t\ (tmin) = 120\ (.0003m) = .036$ meters (1)

2) $r = \frac{1}{400} = (.0025)1$ meters (2)

3) $r = 1.1104 \times 10^{-5}\ \omega 1^2$ meters (3)

where $\omega = 2\pi(10$ hz) radians/second and 1.1104E-05 represents the interaction between the local buckling load, 1/r, Youngs modulus E, area, and a constant, K, that accounts for the end conditions. Additionally, r is rounded to the nearest .0002 m.

The cross-sectional area and moments of inertia for each of the structural elements are listed in the NASTRAN data deck under the title PBAR. In developing this model, the following equations were used by the Draper Laboratory to determine the values for the cross-sectional area A, the moment of inertia I, and the polar moment of inertia J (Ref 9):

$$A = 2\pi rt = \frac{2\pi r^2}{r/t} = \frac{2\pi r^2}{120} = \frac{\pi r^2}{60} \quad (4)$$

$$I_{xx} = I_{yy} = \frac{\pi r^4}{r/t} = \frac{\pi r^4}{120} \quad (5)$$

$$J = \frac{2\pi r^4}{r/t} = \frac{\pi r^4}{60} = 2I \quad (6)$$

The non-structural masses (mirrors, equipment package,

and solar panels) are lumped at 23 node points; these masses and their locations are listed as the CONM2 entries in the NASTRAN input deck.

The eigenvalues and natural frequencies from the 30 mode eigenvalue analysis performed by NASTRAN are listed in Table I. From these 30 modes, the 12 modes marked with an asterisk were selected for further study. These 12 modes were selected because they are the most observable/controllable or have the largest input to the line of sight error. (Ref 1:4-25) The B matrix for these 12 modes is listed in Appendix H. Since the sensors and actuators are collocated, the C matrix is the transpose of the B matrix.

For this research, the control system consists of 21 collocated sensors and actuators located at nodes 9, 10, 11, and 12 on the lower mirror support truss and nodes 27-30 and 32-35 on the upper mirror support truss. This control system was suggested by CSDL in Reference 10. A listing of the node point and orientation associated with each sensor/actuator pair is listed in Appendix G. Figure 3 shows the orientation and location of these pairs on the CSDL 2 model. This control set will be used throughout this research.

Perturbations to the Model

Perturbations to the CSDL 2 model are used to determine the sensitivity of the control system to variations in frequency and mode shape. These perturbations will also aid in the analysis of the effects of system modeling

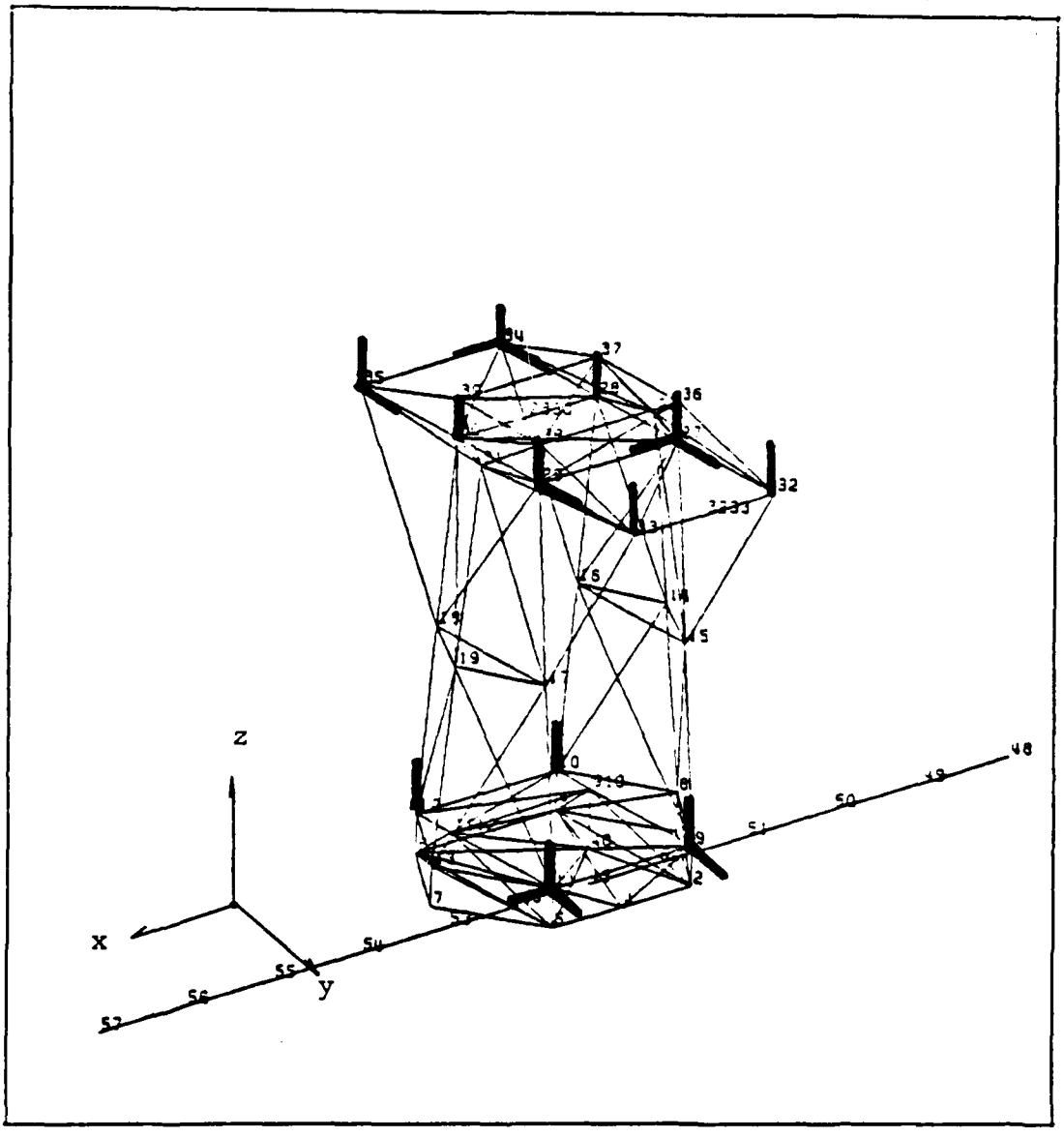

Figure 3. Location and Orientation of the Control System

TABLE I

Eigenvalues and Frequencies for the First 30 Modes

Mode Number	Eigenvalue $(rad/sec)^2$	Frequency (hz)
1	0.0	0.0
2	0.0	0.0
3	0.0	0.0
4*	0.0	0.0
5*	0.0	0.0
6*	0.0	0.0
7*	.51276	.114
8	.85351	.147
9	.88129	.150
10	1.2120	.175
11	8.1889	.455
12*	12.2635	.557
13*	14.0320	.596
14	14.9206	.615
15	15.9854	.636
16	16.2533	.642
17*	26.2311	.815
18	26.2978	.816
19	26.7716	.823
20	33.0992	.916
21*	37.3009	.972
22*	53.0072	1.159
23	94.9786	1.551
24*	124.1206	1.773
25	199.8559	2.250
26	200.5970	2.254
27	465.4279	3.434
28*	470.5175	3.452
29*	627.4820	3.987
30	648.1487	4.052

and manufacturing deviations on the control of the structure. There are an infinite number of possible variations to the CSDL 2 model; this research concentrated on mass changes in the three mirrors and stiffness changes for selected structural elements in the optical support truss. The perturbations were decided upon using a combination of engineering insight and intuition.

The mass perturbations were accomplished by adding or subtracting mass to various combinations of the three mirrors. Because the VCOSS version of the CSDL 2 model was designed "to meet the minimum requirements for local stability and frequency" and the structural elements were sized "to prevent buckling or excessive dynamic interaction" (Ref 3:17), the mass changes were limited to 10 percent or less of the mirror mass. This limitation reduces the impact of increased or decreased mirror mass on a model designed for specific mirror masses. Larger mass changes would result in larger variations of frequency and mode shape, however, the changed model would no longer be representative of a real-world system and a major constraint of the VCOSS program (realistic design) would not be satisfied.

The combinations of mass changes made to the model are listed in Table II. 1, 5, and 10 percent changes were applied to all three mirrors, the secondary and tertiary mir-

TABLE II

Mirror Mass Perturbations to the CSDL 2 Model

Description of Perturbations	Mirror Mass (kg)		
	Primary	Secondary	Tertiary
+1% to all +5% mirrors +10%	1010 1050 1100	808 840 880	1212 1260 1320
-1% -5% -10%	990 950 900	792 760 720	1188 1140 1080
+1% to secondary +5% and tertiary +10% mirrors	1000	808 840 880	1212 1260 1320
-1% -5% -10%		792 760 720	1188 1140 1080
+1% to secondary +5% mirror only +10%	1000	808 840 880	1200
-1% -5% -10%		792 760 720	
+1% to tertiary +5% mirror only +10%	1000	800	1212 1260 1320
-1% -5% -10%			1188 1140 1080

rors, then the secondary and tertiary mirrors by themselves. These percentage changes were added to and subtracted from the original masses. The primary mirror mass was not changed independently of changes to the secondary and tertiary mirror masses because the CSDL 2 model is relatively symmetric and it was felt that the results of changing the mass of only the tertiary mirror would be similar to the results of changing the mass of only the primary mirror. (Both mirrors are in the upper mirror support truss.) A similar assumption was made with regards to changing the masses of only the primary and secondary mirrors.

Stiffness changes to structural elements in the CSDL 2 model are accomplished by changing the cross-sectional area and moments of inertia of the epoxy-graphite tubes. A percentage change is made to the cross-sectional area and then the radius of the tube is determined. The moments of inertia are then calculated using the new radius. Throughout this set of perturbations, r/t is maintained at 120. Because this model already uses the minimum acceptable wall thicknesses, the percentage changes are only added to the values used in the VCOSS model (i.e., the bars are stiffened). For example, one of the perturbations increased the area of CBARs 99-102 by 10 percent. The new area for these CBARs is (1.1) (0.470559E-03) = 0.517615E-03. Using equation (4), $A = \pi r^2/60$ or $r = (60A/\pi)^{\frac{1}{2}} = 0.0994$ meters. Using equations (5) and

(6), I = 0.255572E-05 and J = 0.511144E-05.

A list of the values input to NASTRAN and the CBARs they represent is contained in Table III. The particular elements were selected because they are elements that directly pass the energy of the vibrating mirrors to the rest of the optical support structure. Figures 4 through 12 show the position of the stiffened elements in the structure.

CBARs 44 and 45 (Figure 13) were stiffened to the point of making them solid to simulate an added mass in the middle of the optical support structure. As originally designed, the cross-sectional area of these bars is 0.104152E-03 m^2, r is 0.0446 m, and their length (from their node point coordinates) is 8 meters. The material density for all of the structural elements in the model is 1720 kg/m^3, making the mass of these bars 1.433 kg. This mass was increased by 5, 25, and 50 kg by keeping r constant and increasing the wall thickness t. Finally, the 2 CBARs were made solid, resulting in a mass of 85.988 kg per bar. Table IV lists the NASTRAN input data for these stiffness/mass changes. The values for the 25 kg increase, for example, were derived as follows:

$$\text{mass} = (\text{area})(\text{length})(\text{density})$$

$$\text{Area } A = \frac{\text{mass}}{\text{length} \times \text{density}} = \frac{1.433 + 25}{8(1720)} = .001912 \text{ m}^2$$

$$A = 2\pi rt$$

TABLE III

Stiffness Perturbations to the CSDL 2 Model

Perturbations Set Number	% Increase in A	Old A	New A	New $I_{xx}=I_{yy}$	New J
1	10	.470559E-03	.517615E-03	.255572E-05	.511144E-05
	50	"	.705838E-03	.475573E-05	.951507E-05
2	10	"	.517615E-03	.255572E-05	.511144E-05
		.259503E-03	.285453E-03	.778109E-06	.155622E-05
	50	.470559E-03	.705838E-03	.475573E-05	.951507E-05
		.259503E-03	.389255E-03	.144690E-05	.289381E-05
3	10	.566323E-03	.622955E-03	.370582E-05	.741165E-05
	50	"	.849485E-03	.689101E-05	.137820E-04
4	10	"	.622955E-03	.370582E-05	.741165E-05
	50	"	.849485E-03	.689101E-05	.137820E-04
5	10	.716806E-04	.788487E-04	.593691E-07	.118738E-06
	50	"	.107521E-03	.110397E-06	.220794E-06
6	10	"	.788487E-04	.593691E-07	.118738E-06
	50	"	.107521E-03	.110397E-06	.220794E-06
7	10	.259503E-03	.285453E-03	.778109E-06	.155622E-05
	50	"	.389255E-03	.144690E-05	.289381E-05
8	10	"	.285453E-03	.778109E-06	.155622E-05
	50	"	.389255E-03	.144690E-05	.289381E-05
9 (88&96)	10	.325124E-03	.357636E-03	.122139E-05	.244278E-05
(90&94)		.566323E-03	.622955E-03	.370582E-05	.741146E-05
(92&98)		.348640E-03	.383504E-03	.140447E-05	.280893E-05
(88&96)	50	.325124E-03	.487686E-03	.227118E-05	.454236E-05
(90&94)		.566323E-03	.849485E-03	.689101E-05	.137820E-04
(92&98)		.348640E-03	.522960E-03	.261161E-05	.522322E-04

Set 1: Percent changes in Area added to CBARs 99-102
2: 99-102 & 87-97 (odd)
3: 90 and 94
4: 90
5: 123-126
6: 123-124
7: 76,78,80,81,83,85
8: 76,78,80,81,83,85 & 87-97 (odd)
9: 88-98 (even)

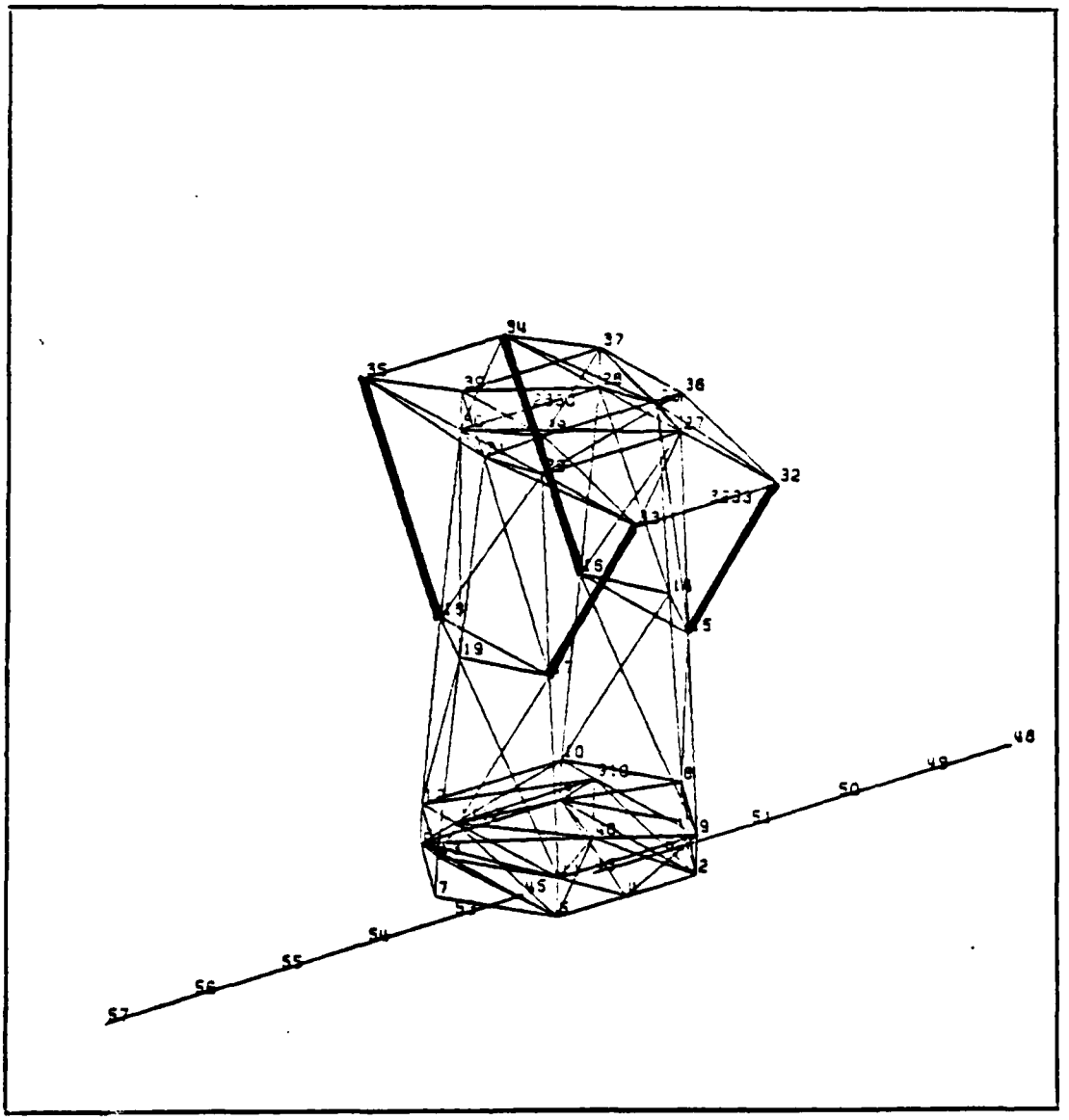

Figure 4. Perturbation Set 1

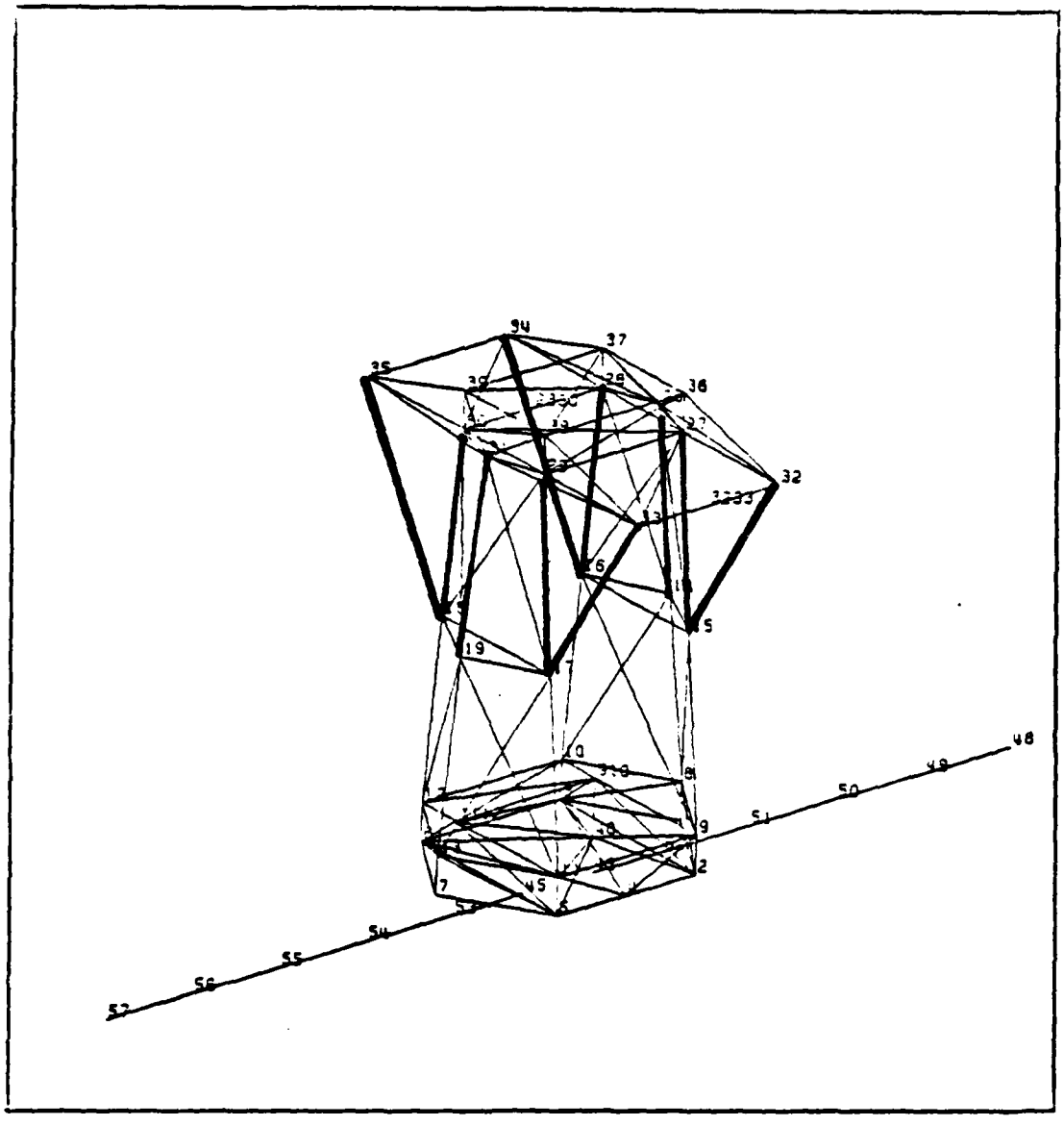

Figure 5. Perturbation Set 2

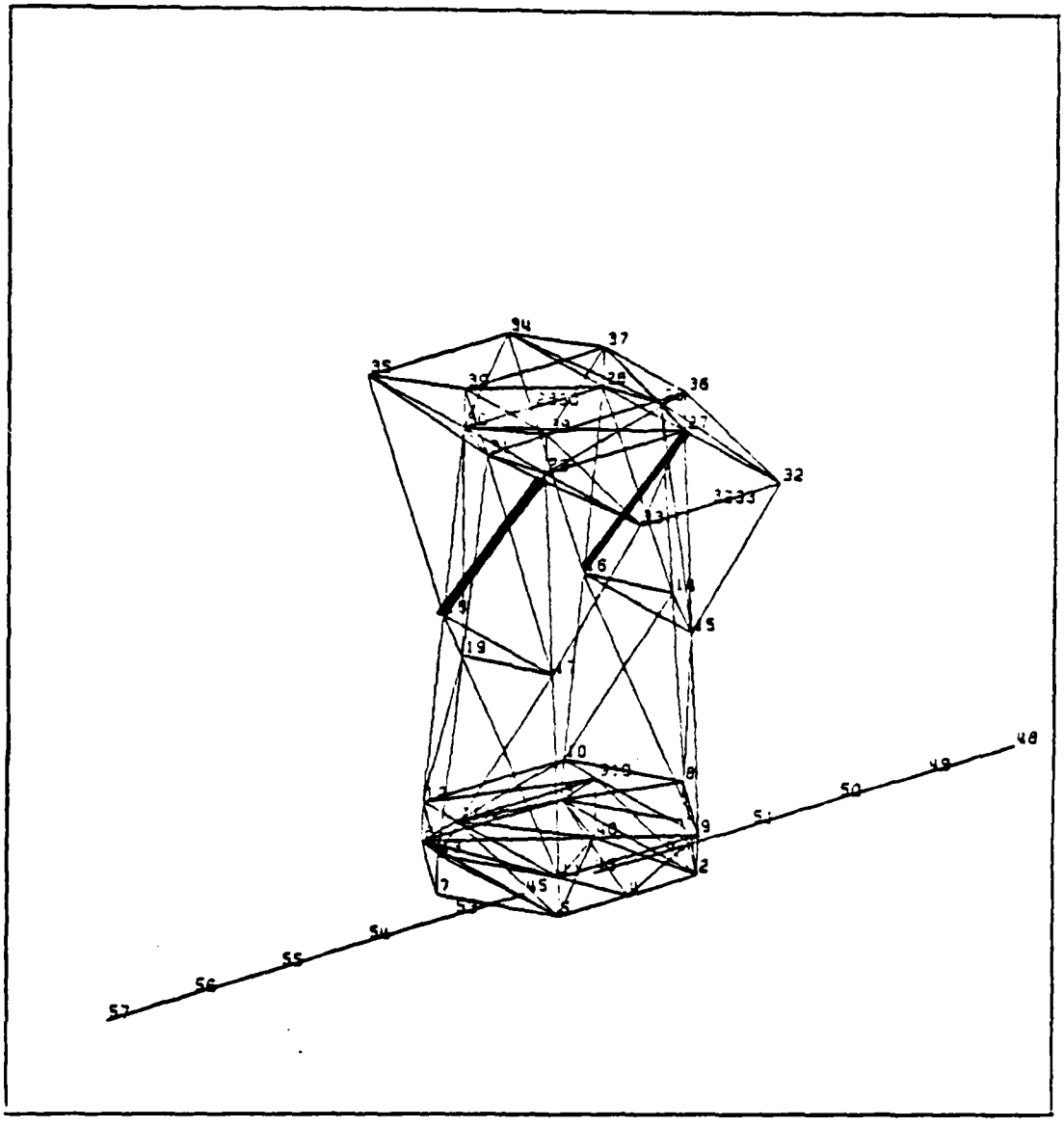

Figure 6. Perturbation Set 3

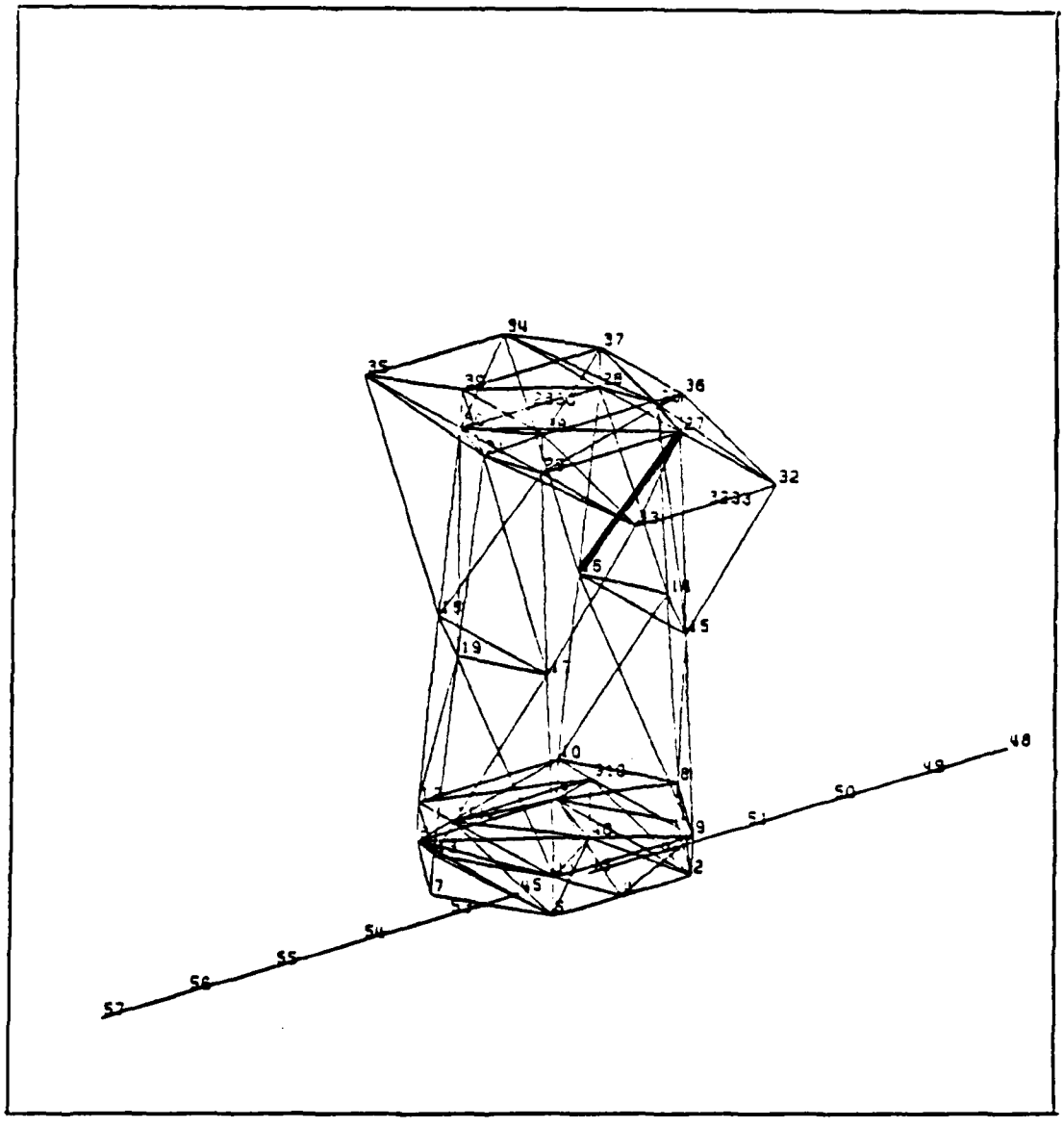

Figure 7. Perturbation Set 4

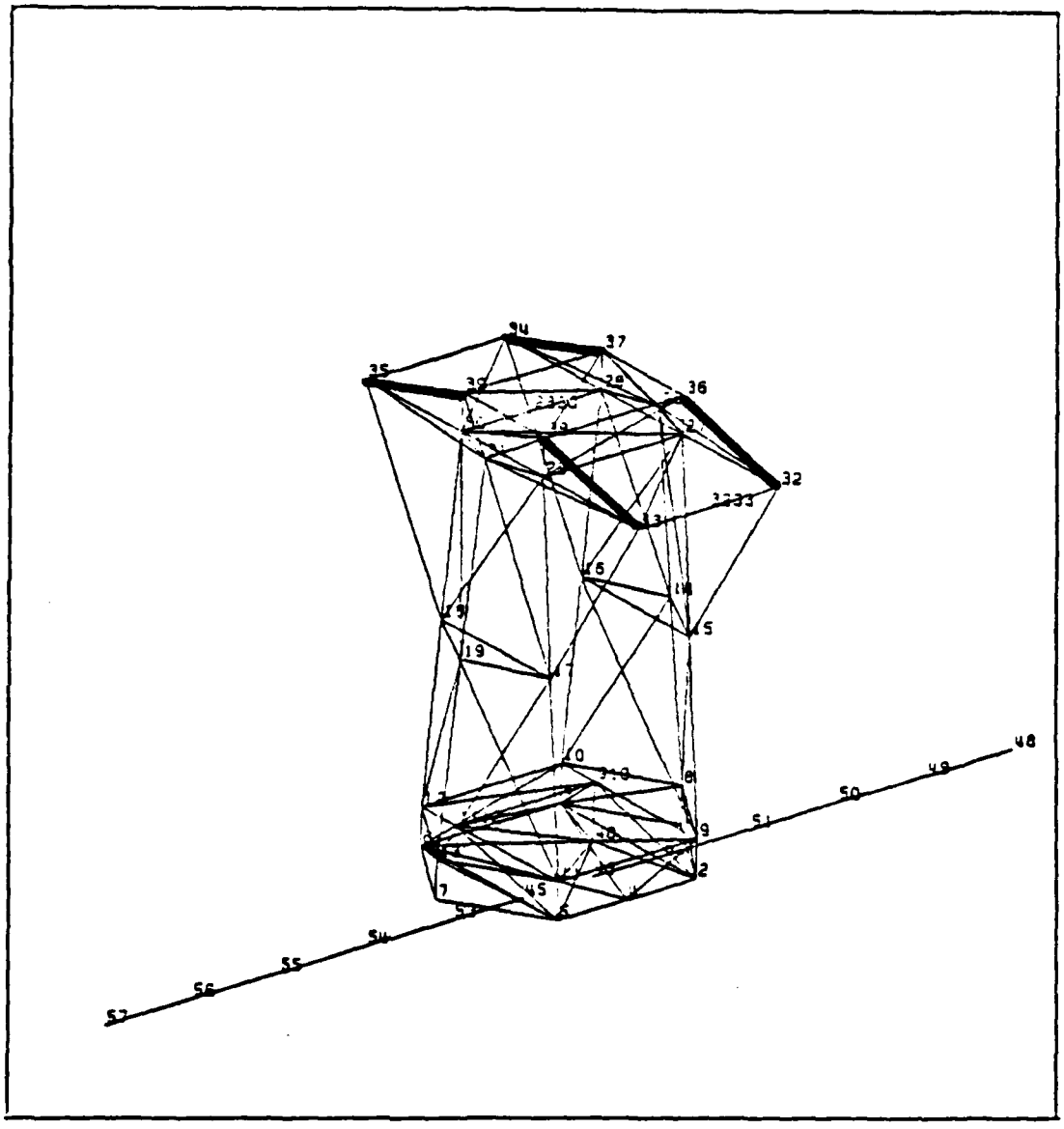

Figure 8. Perturbation Set 5

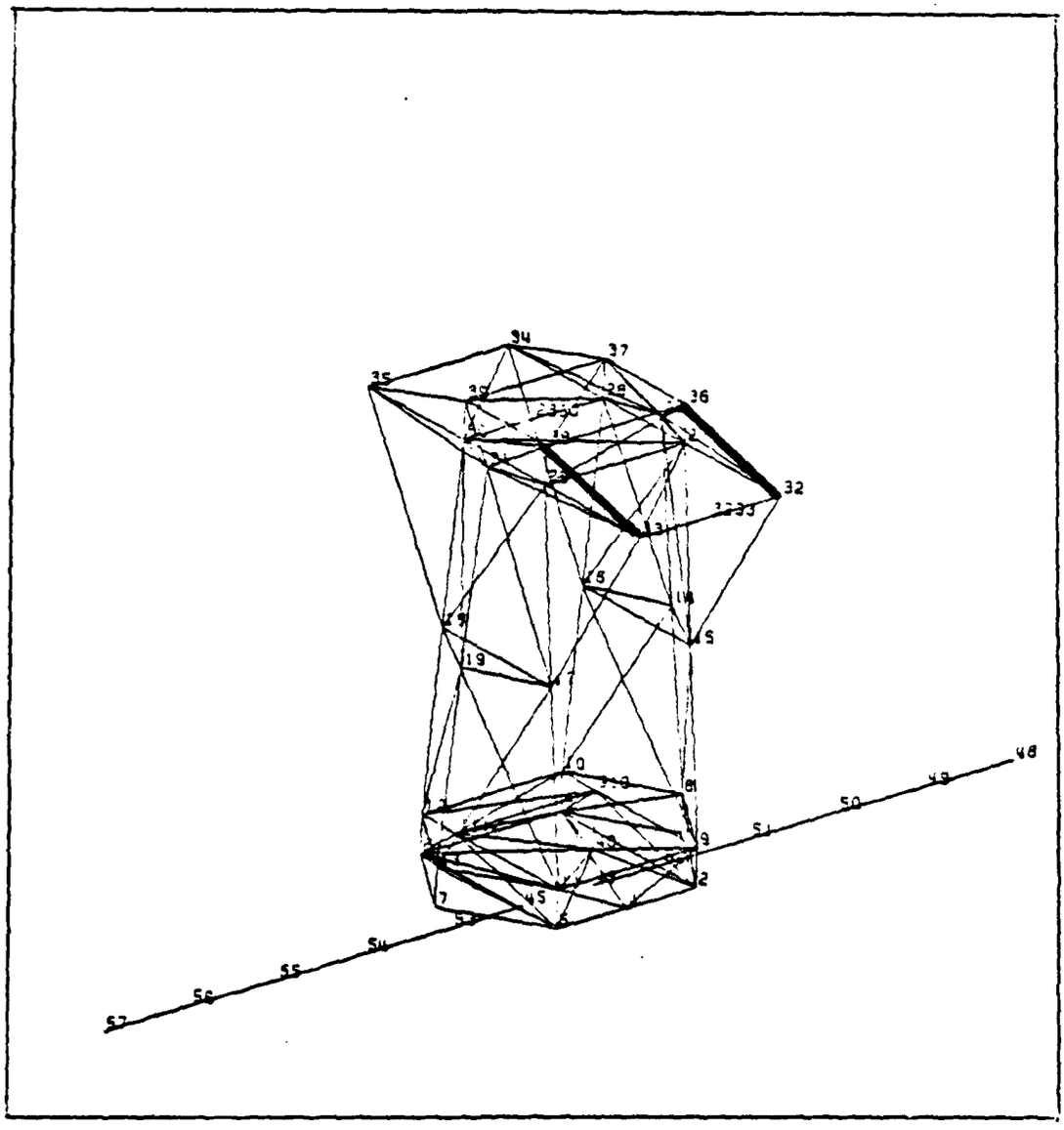

Figure 9. Perturbation Set 6

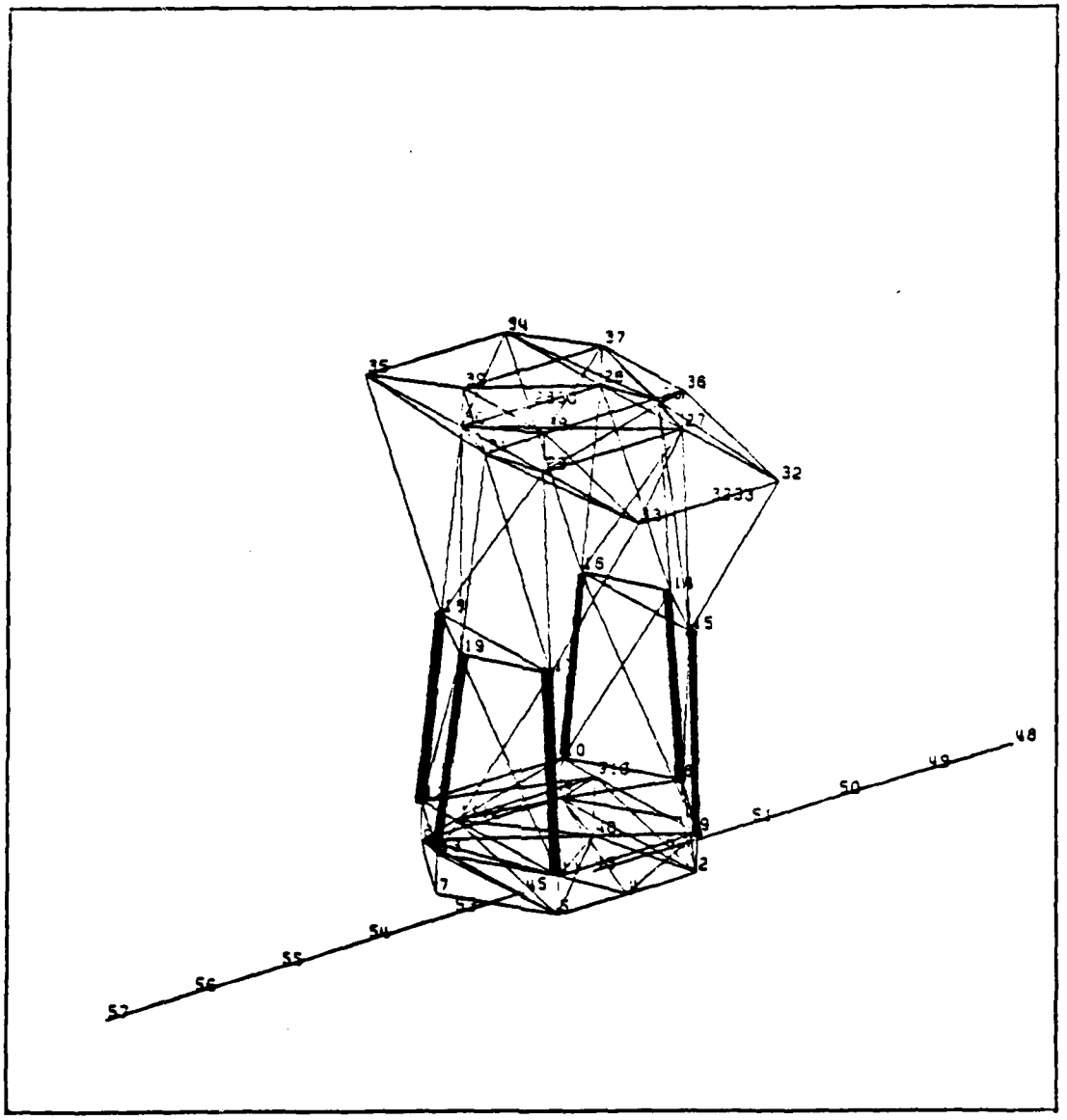

Figure 10. Perturbation Set 7

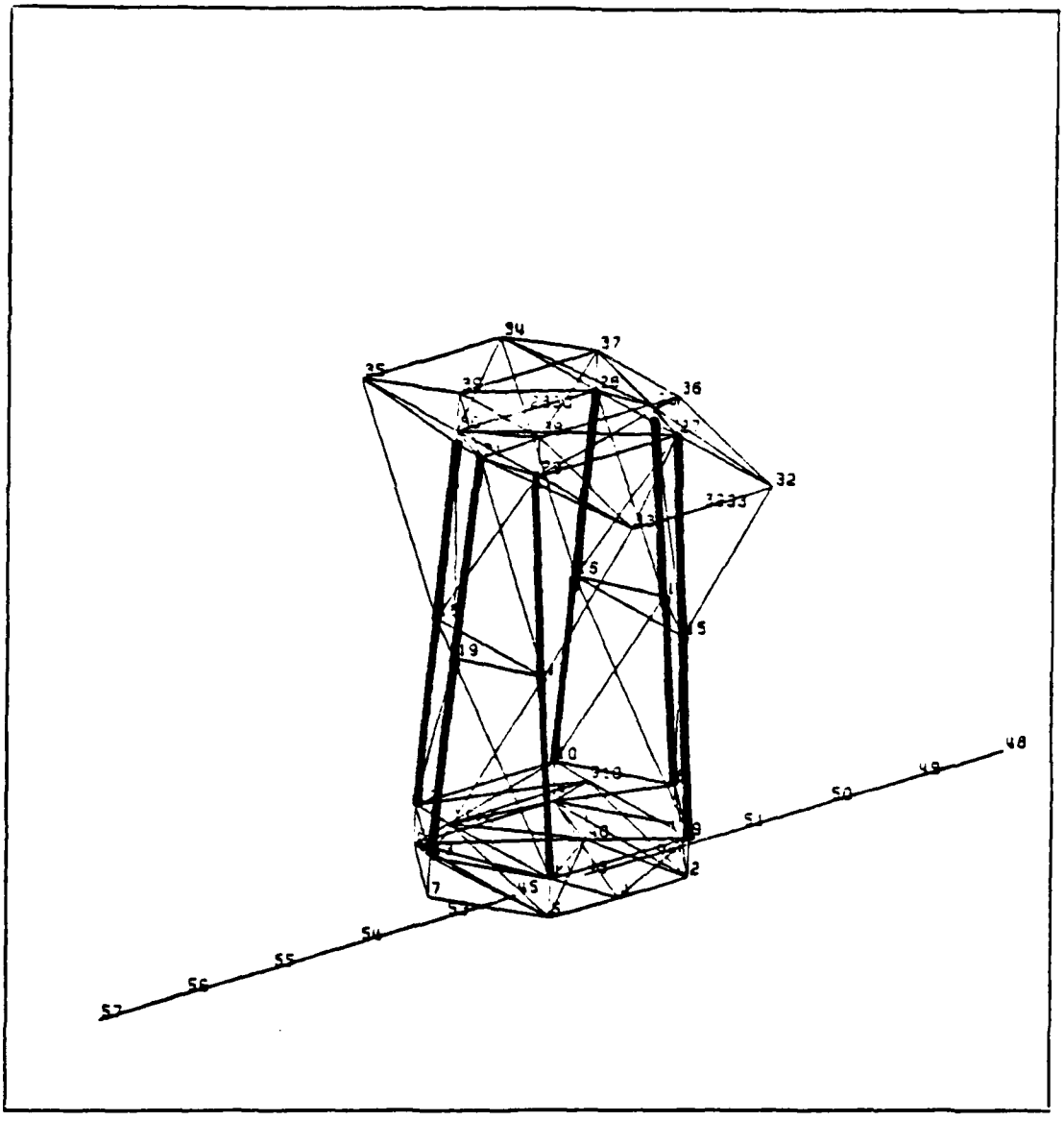

Figure 11. Perturbation Set 8

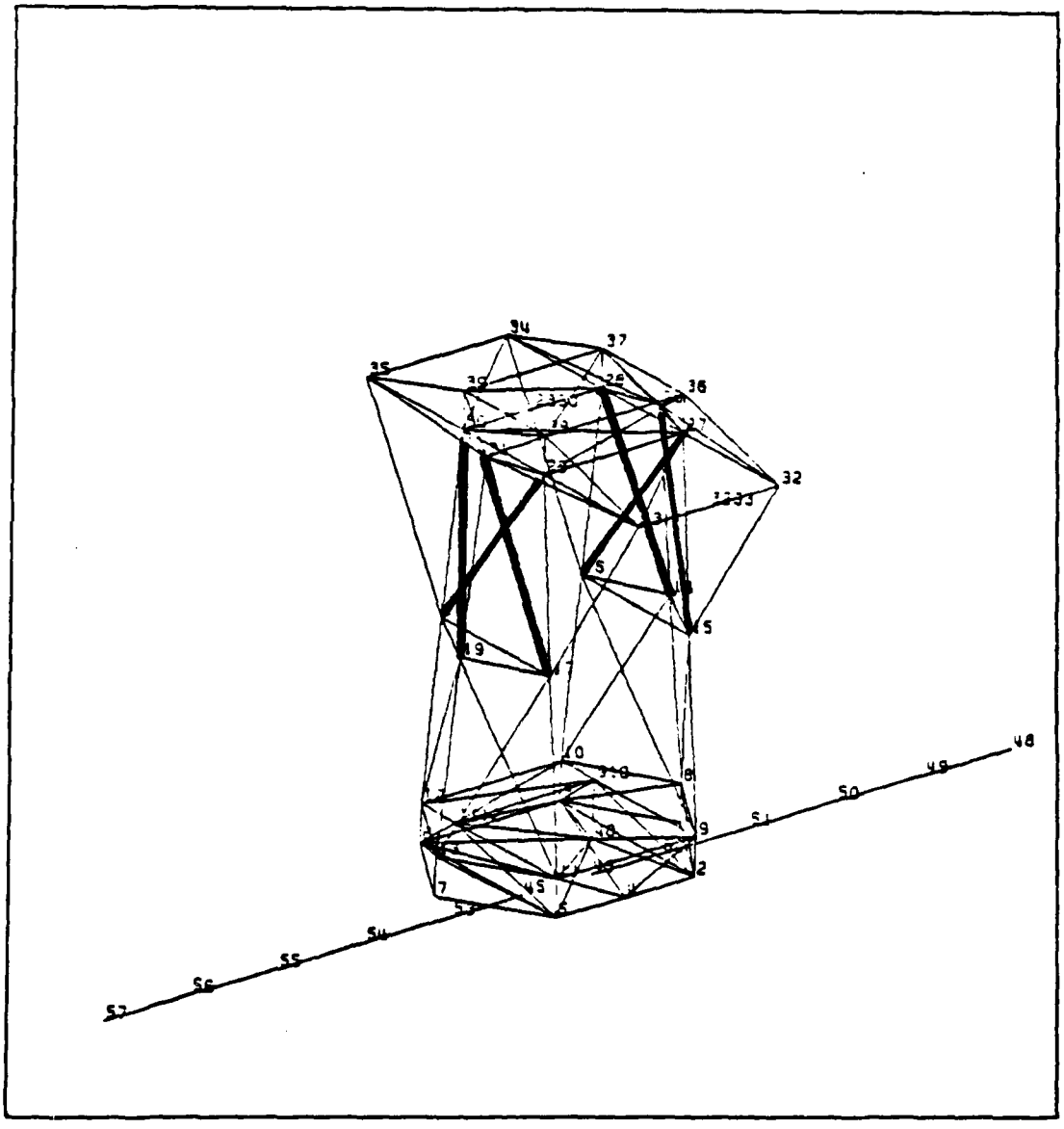

Figure 12. Perturbation Set 9

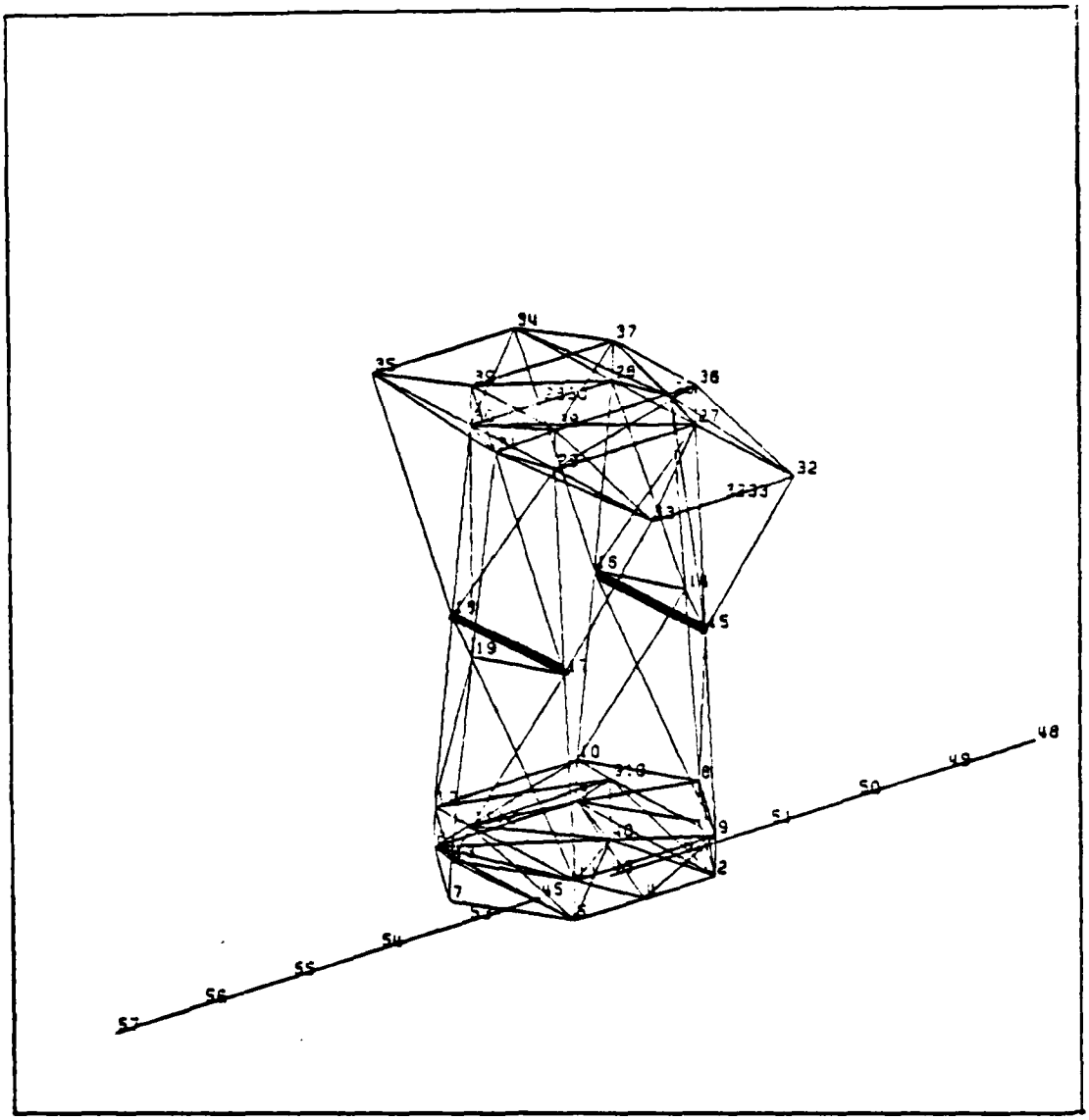

Figure 13. CBARs 44 and 45
(Midsection Mass Increases)

TABLE IV

NASTRAN DATA FOR ADDED MASS IN CBARs 44 and 45

Description of Perturbation	New Mass (kg)	New t(m)	r/t	New A (m^2)	New I (m^4)	New J (m^4)
Add 5 kg to mass of bar	6.433	.001668	26.7386	.467514E-03	.464890E-06	.929781E-06
Add 25 kg to mass of bar	26.433	.006855	6.5061	.192100E-02	.191062E-05	.382125E-05
Add 50 kg to mass of bar	51.433	.013315	3.3495	.373140E-02	.371117E-05	.742234E-05
Make the bars solid	85.988	-	-	.624913E-02	.621526E-05	.124305E-04

$$t = \frac{A}{2\pi r} = \frac{.001912}{2\pi(.0446)} = .006855 \text{ m}$$

$$r/t = \frac{.0446}{.006855} = 6.5061$$

$$I = \frac{\pi r^4}{r/t} = \frac{\pi(.0446)^4}{6.5061} = .191062E\text{-}05 \text{ m}^4$$

and

$$J = 2I = .382125E\text{-}05 \text{ m}^4$$

The analysis of changes in the damping factor will use data from the three perturbation groups just discussed. The appropriate changes are made to the NASTRAN input deck and the output is processed through DOFB34. The equation used to calculate the damping factor, as well as those used to find the B and C matrices, are the subject of the next chapter of this thesis.

III. Theory

B and C Matrices

NASTRAN is run to determine the modal frequencies and mode shape values at node points on the structure. The results of NASTRAN are the ϕ matrix, which is a row matrix containing the eigenvectors (mode shapes) of the structure, and a listing of the modal frequencies.

The equations of motion for a vibrating structure such as CSDL 2 are

$$M\ddot{\underline{q}} + E\dot{\underline{q}} + K\underline{q} = D\underline{u} \tag{7}$$

Where $\underline{q}$ is an n-vector of generalized coordinates that completely describe the motion of the system, M an n x n symmetric mass matrix, K an n x n symmetric stiffness matrix, E an n x n symmetric damping matrix, $\underline{u}$ an m-vector of inputs (disturbances), and D an n x m matrix of actuator coefficients. The vector $D\underline{u}$ therefore represents the input force vector. (Ref 6:1) Equation (7) can be rewritten in model coordinates, $\underline{\eta}$, where $\underline{q} = \phi\underline{\eta}$. The mode shape (represented by ϕ) is unique, but the amplitude is not. By rewriting equation (7) in modal coordinates, the elements of the natural modes are made unique (i.e., they are normalized). In this case, this was accomplished by setting $\phi^T M\phi$ equal to I. (Ref 5:141) Equation (7) is now written

$$\ddot{\underline{\eta}} + \left[\begin{smallmatrix} & 2\zeta\omega & \\ & & \end{smallmatrix}\right] \dot{\underline{\eta}} + \left[\begin{smallmatrix} & \omega^2 & \\ & & \end{smallmatrix}\right] \underline{\eta} = \phi^T D \underline{u} \tag{8}$$

Where ω is the natural (undamped) modal frequency and ζ is the damping factor. The matrix $\left[\begin{smallmatrix} & 2\zeta\omega & \\ & & \end{smallmatrix}\right]$ is therefore an n x n diagonal damping matrix and $\left[\begin{smallmatrix} & \omega^2 & \\ & & \end{smallmatrix}\right]$ is an n x n diagonal matrix of the eigenvalue of equation (7). Because $\phi^T M \phi = I$, the modal matrix ϕ is such that $\phi^T K \phi = \left[\begin{smallmatrix} & \omega^2 & \\ & & \end{smallmatrix}\right]$ and $\phi^T E \phi = \left[\begin{smallmatrix} & 2\zeta\omega & \\ & & \end{smallmatrix}\right]$. (Ref 5:141) Equation (8) can be written in the state vector form

$$\dot{\underline{x}} = A\underline{x} + B\underline{u} \tag{9}$$

Where

$$x = \left\{ \underline{\eta}^T, \ \dot{\underline{\eta}}^T \right\}$$

$$A = \left[\begin{array}{c|c} 0 & I \\ \hline -\left[\begin{smallmatrix} & \omega^2 & \\ & & \end{smallmatrix}\right] & \left[\begin{smallmatrix} & -2\zeta\omega & \\ & & \end{smallmatrix}\right] \end{array}\right]$$

and

$$B = \left[\begin{array}{c} 0 \\ \hline \phi^T D \end{array}\right]$$

The general output equation is of the form

$$\underline{Y} = C_p \underline{q} + C_v \dot{\underline{q}} \tag{10}$$

assuming that both position and velocity sensors are being used. In terms of $\underline{x}$,

$$\underline{Y} = c\underline{x} \tag{11}$$

Where

$$C = \{C_p\phi,\ C_v\phi\}$$

C_p is a matrix corresponding to the direction cosines of the position sensors and C_v corresponds to the direction cosines of the velocity (rate) sensors. The designated control set for this research uses only collocated rate sensors and force actuators (no position sensors). Thus, $C_p = 0$ and $B^T = C$ where the rows of the B matrix physically correspond to the amplitude of each mode at the various actuator locations and the columns of C represent the amplitude of each mode at the various sensor locations. Negating the zero half of the B matrix (from equation (9)) gives

$$B = \phi^T D \tag{12}$$

Therefore, an element of B can be written

$$B_{i,j} = \phi_{k,i} \cos\alpha_j + \phi_{k+1,i} \cos\beta_j + \phi_{k+2,i} \cos\gamma_j \tag{13}$$

where the cosine terms are the direction cosines of the D matrix. Equation (13) is used in the ZETA program to calculate the B and C^T matrices.

Damping Factor

Program DOFB34 calculates two eigenvector (complex conjugate) pairs per mode, each having a real value and an imaginary value. The magnitude of the real value is the

product of the damping factor and the natural frequency; the magnitude of the imaginary value is the damped frequency ω_d. In Figure 14, one of the eigenvalues is plotted in the s-plane. From this depiction

$$\tan \eta = \frac{\omega'}{\sigma'}$$

or

$$\eta = \tan^{-1} \frac{\omega'}{\sigma'} = \cos^{-1}\zeta$$

and

$$\zeta = \cos \tan^{-1} \frac{\omega'}{\sigma'} \qquad (14)$$

Equation (14) is used to calculate the damping factor for each mode that is analyzed in this research. One of the inputs to DOFB34 is the damping factor of the uncontrolled structure that occurs as a result of the structure's resistance to bending and twisting. For this research, a value of 0.01 was assigned. The purpose of a control system is to actively dampen vibrations in the structure. Thus, an increase in the damping factor (i.e., a value greater than 0.01) means that the control system is actively damping that particular mode to some extent. If the value stays at or very near .01, the control set is having little or no effect on that particular mode.

Using equations developed in this chapter, data points for determining the effects of perturbations on the damping factor can be generated. The next chapter presents this

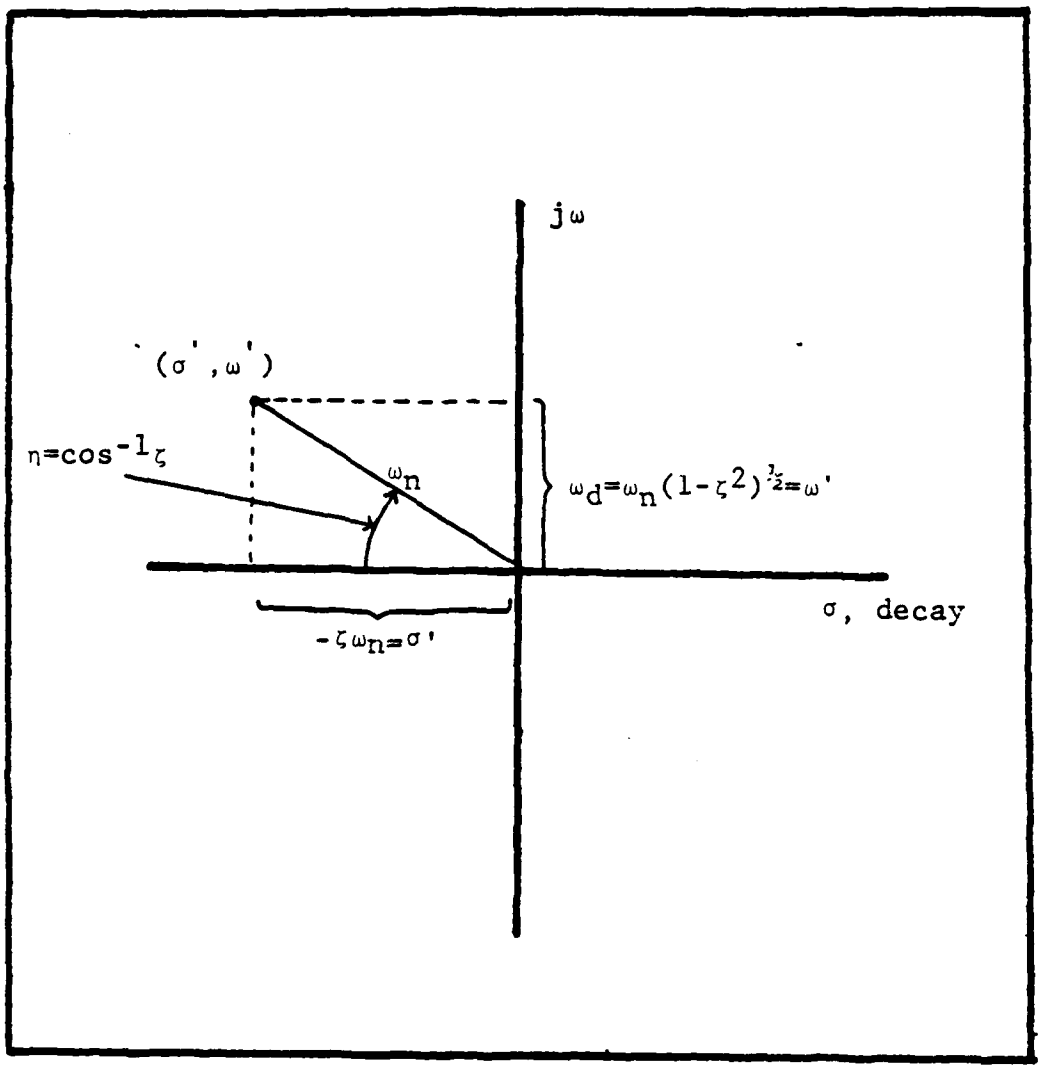

Figure 14. Location of the eigenvalue pairs in the complex plane (Ref 11:116)

data and discusses the impact that the control system orientation and the modeling of the structure have on the findings.

IV. Results

In this chapter, the mode shapes for the twelve modes are discussed and the effect of the perturbations on the damping factor for each mode are presented.

Mode Shapes

Appendix I (Figures 15 to 24) contains views of the twelve mode shapes from the unperturbed model under consideration in this research. These plots were made using GCSNAST, a program that uses the NASTRAN bulk data deck and a deflection file that is derived from the NASTRAN-produced modal frequencies and mode shapes. (See Appendix K for GCSNAST procedures.) In these plots, the dashed lines represent the deformed structure and the solid lines represent the original structure. The deformations have been magnified by a factor of ten for clarity. A brief description of the twelve modes follows.

Modes 4, 5, and 6 (Figure 15) are rigid body rotation modes encompasing rigid body rotation around each of the three axes.

Mode 7 (Figure 16) is a mode where the solar panels are deforming in the xy and xz planes and the structure rotates in the xz plane about a point near the middle of the equipment section. There is no noticeable deformation in the structure.

Mode 12 (Figure 17) involves rotation and bending in the xy and xz planes and a considerable deformation of the solar panels. The point of rotation is in the upper part of the optical support structure.

Mode 13 (Figure 18) has rotation in the yz plane and deformation of the solar panels in the xy and xz planes. The rotation is about a point in the upper mirror support truss.

Mode 17 (Figure 19) involves a slight rotation in the yz plane and deformation of the solar panels in the xy and xz planes. The structure rotates about a point near the outside edge of the primary mirror.

In Mode 21 (Figure 20) there is twisting and solar panel deformation in the xy plane and deformation of all three components of the optical support structure in all three planes.

Mode 22 (Figure 21) involves twisting and solar panel deformation in the xz plane.

Mode 24 (Figure 22) has the most radical deformation of the twelve modes. There is twisting in the xy and yz planes and deformation of the optical support structure and solar panels in all three planes.

Except for the solar panels, the deflections in mode 28 (Figure 23) are quite small. There is some deformation in the upper and lower mirror support trusses in the xy and yz planes.

Mode 29 (Figure 24) also has very small deformations

in the optical support structure. The metering truss is deformed slightly in the yz plane and the solar panels are deformed in the xy and xz planes.

In the CSDL 2 model, the equipment section is connected to the optical support structure by three springs at nodes 3, 4, and 6. These springs totally isolate the equipment section from the optical support structure and, therefore, the energy from the vibrating solar panels (cantilevered from the equipment section) is not passed upward to the optical support structure.

Damping Factor

Appendix J lists the damping factors calculated during this research. The damping factors associated with modes 12, 13, 17, and 24 of the perturbed models are portrayed in Figures 25 to 36. In these figures, the vertical scale is the damping factor in percent; the horizontal scale is the percent change in mass (for the mirror mass perturbations), the percent increase in cross-sectional area (for the stiffness perturbations), or the amount of mass that was added to the middle of the optical support structure. The horizontal scale is not linear and the lines connecting the various data points are there only to link the data points for a particular mode. Data points on the vertical axis are those for the unperturbed structure. The other eight of the original twelve modes are not plotted because their damping factors did not change or did not

contribute to the analysis.

Modes 4, 5, and 6 are rigid body modes and have a damping factor of zero. The eigenvalue pairs for these three modes lie on the imaginary axis (See Figure 14) and the response has sustained oscillations (Ref 11:242). The designated control set for this analysis uses only rate (velocity) sensors. Since the natural frequency for a rigid body mode is zero (the structure only translates or rotates, it does not deform) the ω terms in the A matrix (equation (9)) are zero and A is therefore zero. The sensors are sensing the motion but there is no control system input due to A being zero. The rigid body modes will not be controllable unless position sensors are added to the control set.

The eigenvalue pairs for mode 7 lie on the real axis but are not identical, hence the damping factor is greater than one, the mode is overdamped, and the oscillation is damped out in less than one cycle. The control system (Figure 3) is oriented such that there are three sensors/actuator pairs that sense motion in the x-direction and twelve in the z-direction, all of which are affected by this mode shape. This causes the overdamping in this mode. The overdamping remains throughout the research, so mode 7 will not be analyzed further.

Throughout the perturbations, the damping factors for modes 22, 28, and 29 have remained at .01, which is the value assumed to exist in the basic uncontrolled structure. Modes

28 and 29 show very little deformation in the optical support structure. Because of the small deformations, the sensors do not deflect very much. This limits their input to the control system processors and, hence, limits the control systems effectiveness in damping these modes. Mode 22 is primarily deformation in the z-direction, where there are twelve sensor/actuator pairs oriented to sense motion. But, because of the small deformations and the location of the sensors, the control system can not effectively damp the vibration. These three modes (22, 28, and 29) lie in uncontrollable modal space and are not controllable given the orientation of this particular control system. That is, the location and/or orientation of the sensors has to be changed such that they can more completely sense the motion of the vibration. Except for this observation, these modes present no other useful data for this research and will not be analyzed further.

The damping factor for mode 21 varies by only .00007 in this research (.01015 to .01022) and will be placed in the same category as modes 22, 28, and 29. Thus, the analysis will concentrate on modes 12, 13, 17, and 24 and focus on the changes in the damping factor with respect to the physical changes (perturbations) in the CSDL 2 model. Changes in the damping factor of less than .001 (10% of the passive damping factor, .01) will be assumed to be insignificant.

In some cases, there is a definite trend in the damping factor data as the magnitude of the perturbation is increased or decreased (Figure 25, Mode 13; Figure 31, Mode 13; Figure 32; Figure 33, Mode 13; Figure 34.) Conversely, there are many cases where the change in the damping factor does not follow a definite pattern (Figure 25, Mode 12; Figure 26, Mode 17; Figure 27 to 30; Figure 31, Modes 12 and 17; Figures 35 and 36). After looking at how the damping of each mode is affected by the three basic types of perturbations, there will be a discussion on the modeling of the structure, the orientation of the control system, and their impact on the results.

Mode 12: Due to the sensor/actuator configuration, there is only one sensor (at node 11) that senses the motion of the lower part of the structure in the x-direction. There is some twisting in the xy plane. This twisting is most notable in the upper mirror support truss, and, from Figure 17, it is noted that the tertiary mirror is deflected more than the primary mirror. There are sensors at node 34 (near the tertiary mirror) that sense x and y motion, and node 34 is at the point of maximum deflection. Both deflections that occur in mode 12 are, therefore, sensed by the control set and it is anticipated that there will be some degree of active damping in this mode.

The actual effects of mirror mass changes on this mode are portrayed in Figures 25 and 27. The only combination

whose damping factor was unchanged or better in every case is the addition of mass to the secondary mirror. It should be noted, however, that the +5% value is greater than the +10% value. Addition of mass to all three mirrors and to both the secondary and tertiary mirrors produced lower damping factors in every case except for the +10% value for the two mirrors. The other perturbations produced no trends in that the damping factors were not consistently higher or lower than the unperturbed value as the masses were increased. The changes to the secondary and tertiary mirrors by themselves produced results that were almost identical, but they do not show any consistent trend.

The results for the stiffness changes are shown in Figures 29 to 34. Perturbation sets 2, 5, 6, and 9 exhibit consistent trends (The damping factor stays the same or gets better/worse for both data points.). Set 2 stiffens the upper six vertical members in the metering truss (Figure 5). Sets 5 and 6 (Figures 8 and 9) stiffen all four, then two, of the upper diagonal members that link the outer edges of the primary and tertiary mirrors to the top of the structure. It is noted that set 6, which stiffens just the two members supporting the tertiary mirror, produces the same results as set 5. This is consistent with the observation that the tertiary mirror is most affected by the twisting motion. The data from these two sets implies that it is the stiffening of the tertiary mirror supports that causes the changes in the

damping factor. Set 9 (Figure 12) stiffens the six diagonal supports in the upper portion of the metering truss. This could increase the amount of the twisting motion that is passed downward. There are no sensor/actuator pairs to damp this motion in the middle of the structure, so the damping factor would decrease. Sets 1, 3, 4, 7, and 8 do not give consistent results.

The results from the midsection mass changes are shown in Figure 35. The process of adding mass has stiffened the two elements shown in Figure 13, so it is possible that this could increase the resistance to twisting in the z-direction. In this mode, the damping increases after approximately 50 kg have been added to each element, indicating that at this point, the motion/inertia in the middle of the structure is helping to damp the rotation.

Mode 13: The major component in this mode is rotation in the yz plane. This motion is large enough to result in significant displacement in the y and z directions. The primary mirror is deflected more than the tertiary mirror. The structure is also elongated in the z-direction. There are twice as many sensor/actuator pairs working in the y-direction as there are in the x-direction and twelve pairs oriented in the z-direction. Thus, it is expected that the damping factors for this mode will be larger than for mode 12.

The results of the mass changes for mode 13 are portrayed in Figures 25 and 27. The data for all three mirrors

depicts a consistent trend until the +10% value. When comparing the data from the two perturbations portrayed in Figure 25, it is noted that balanced increases in the upper mirror support truss (i.e., adding equal percentages of mass to both the primary and tertiary mirrors) results in better damping than unbalanced increases. The data for increases in the tertiary mirror by itself (Figure 27) concurs with this finding. It is also noted that the damping factors for mode 13 are considerably higher than for mode 12, as expected.

Increasing stiffness resulted in lower damping for every stiffness perturbation except for the +10% change in set 8, where there was a barely significant increase of .00149. All of the sets except 1 and 8 showed consistent results. Increasing the stiffness increases the frequency of the vibration, and this research has shown that lower frequencies, with their larger deformations, are generally more easily controlled. The results from the mode 13 stiffness perturbations confirm this in almost all cases.

The results from the midsection mass increases (Figure 35) are consistent except for the +50 kg data point. Increasing mass in the middle of the structure generally lowers the damping.

Mode 17: In this mode, there is a small rotation in the yz plane about a point near the primary mirror. The deflections in the mirror support trusses are quite small and there are only two sensor/actuator pairs in the lower part of the structure that can sense this motion. The

displacements in the z-direction are very small, so the twelve pairs that sense motion in the z-direction will not be displaced very much and are not expected to have much effect on the damping of this mode. Damping is expected to be lower than for modes 12 and 13.

Data for the mirror mass changes is shown in Figures 26 and 28. In all cases, the damping factor increased or remained the same. There is not a consistent trend as the mirror masses were varied from -10% to +10% of their original values. Every perturbation group (i.e., all mirrors, tertiary only, etc.) has at least two data points that are inconsistent with the others.

The stiffness changes (Figure 29 to 34) produced more consistent results and point out two perturbations that had a very detrimental effect on the damping of this mode. The damping factors were unchanged or higher except for those two cases. Sets 2, 5, 6, and 9 showed increasing damping as stiffnesses were increased. Sets 1, 3, and 4 had more damping at the 10% increase in area than at the 50% point. The two detrimental cases, the 10% increases for sets 7 and 8, showed almost no active damping at all. Both of these sets increased the area of the lower six vertical members of the metering truss; set 8 also increased the area of the corresponding vertical members in the upper part of the metering truss. It would appear then that the structure is very sensitive to stiffness changes in the lower vertical members. When the areas of the members in these

two perturbation sets were increased by 50%, active damping returned and the damping factor was greater than for the unperturbed structure.

One data point in the midsection mass increases (Figure 36) showed a drastic decrease in damping. Except for this point (25 kg increase), the damping was the same or better than that of the unperturbed case.

Mode 24: This mode is characterized by large deformations in all three planes. Thus, all 21 sensor/actuator pairs get involved and there is some degree of active damping even though the frequency (1.773 hz) is higher than the other modes where active damping was subsequently employed. The damping factors for all three perturbation groups are lumped very closely around a value of .012, with no data points varying by more than the .001 value that has been defined as the significant amount for this research. It can be stated, then, that mode 24 is actively damped and that the perturbations had no significant effect on the damping factor. It is possible that more sensor/actuator pairs oriented in the x and y directions would increase the damping for this mode.

This chapter has discussed the mode shapes and the changes in the damping factor as the structure was perturbed. The next chapter will discuss the possible causes for the lack of consistent results, summarize the findings, and present recommendations for further research to remove or lessen the uncertainty in these results.

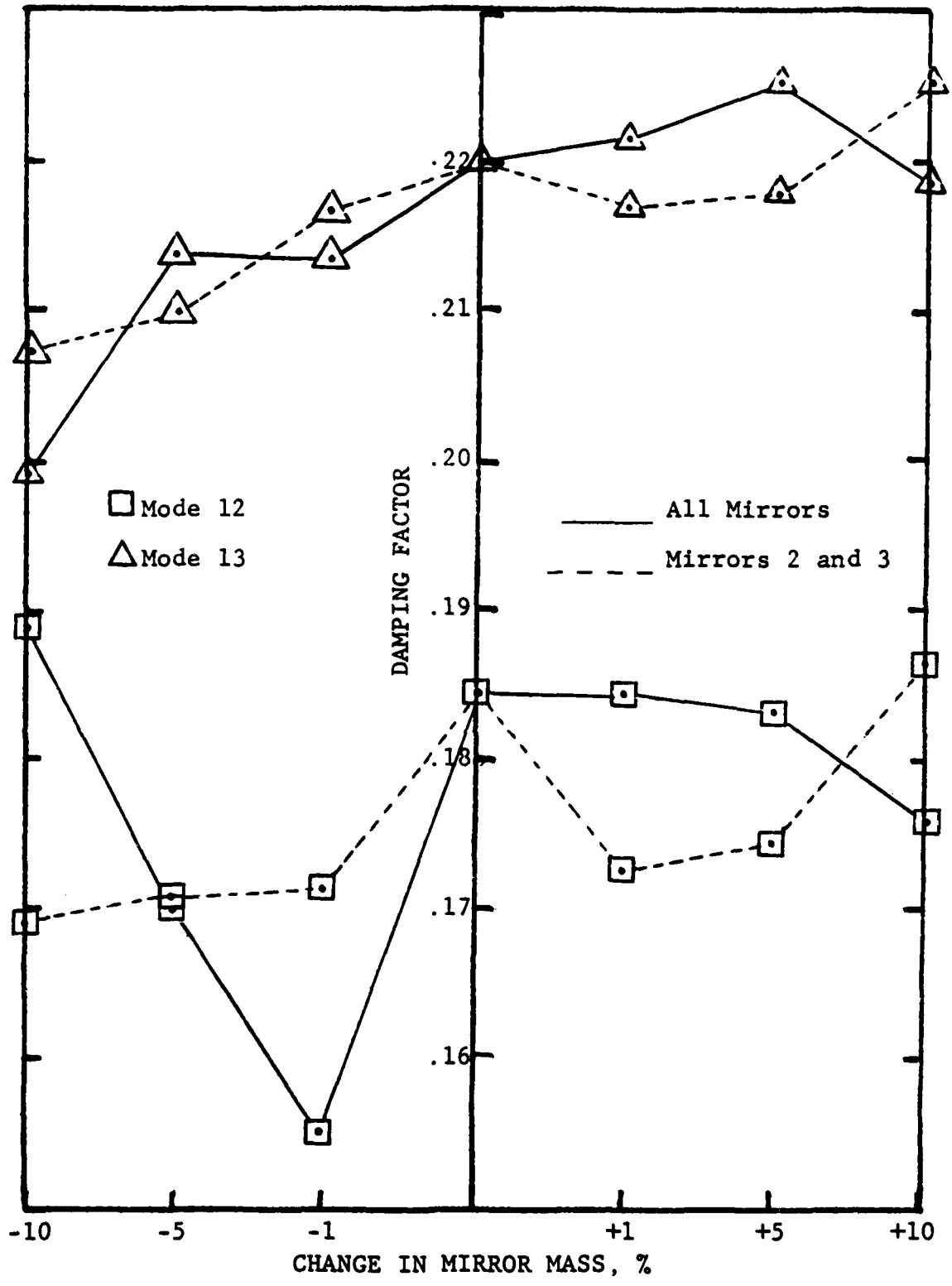

Figure 25. Mirror Mass Changes

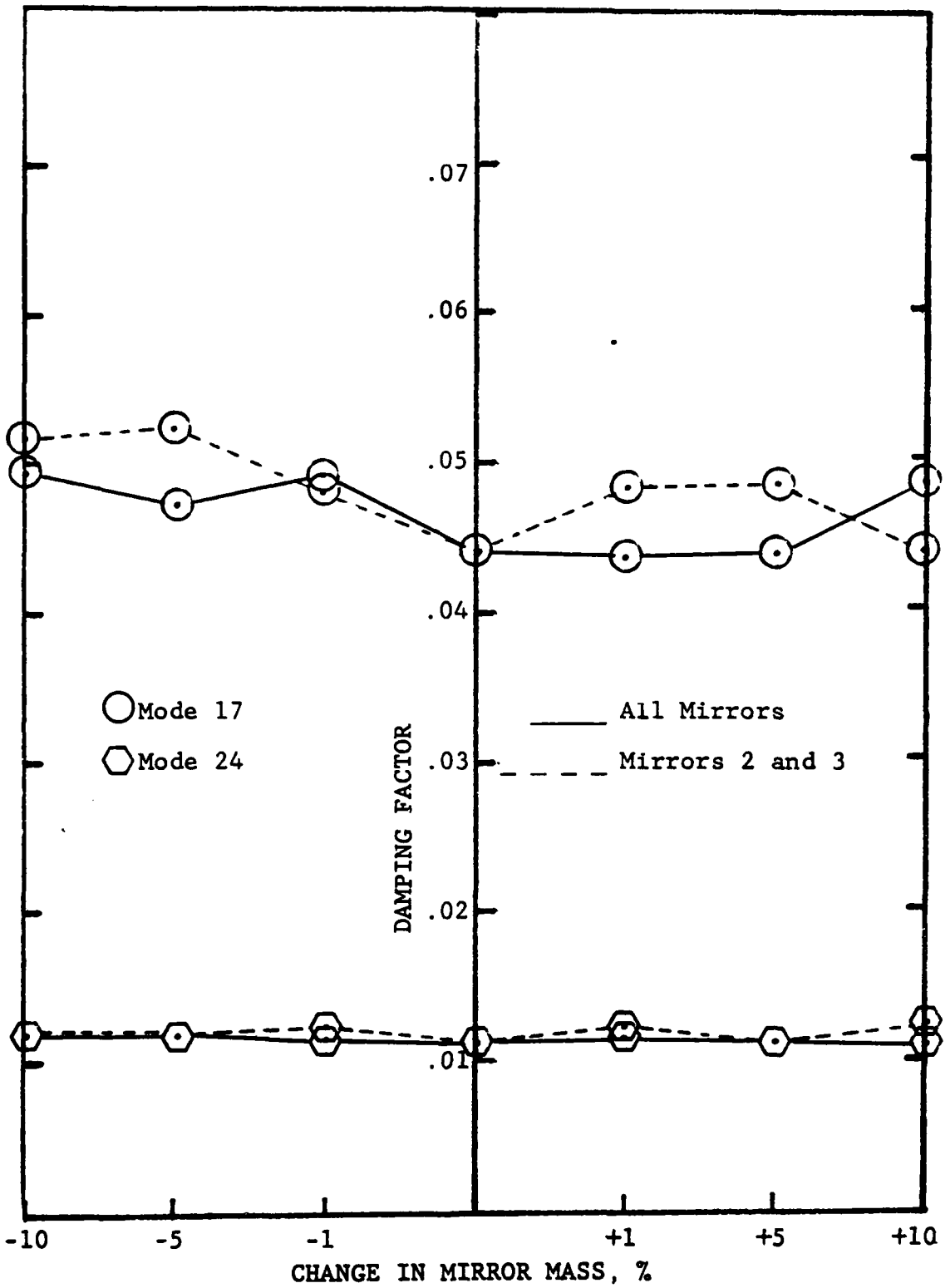

Figure 26. Mirror Mass Changes

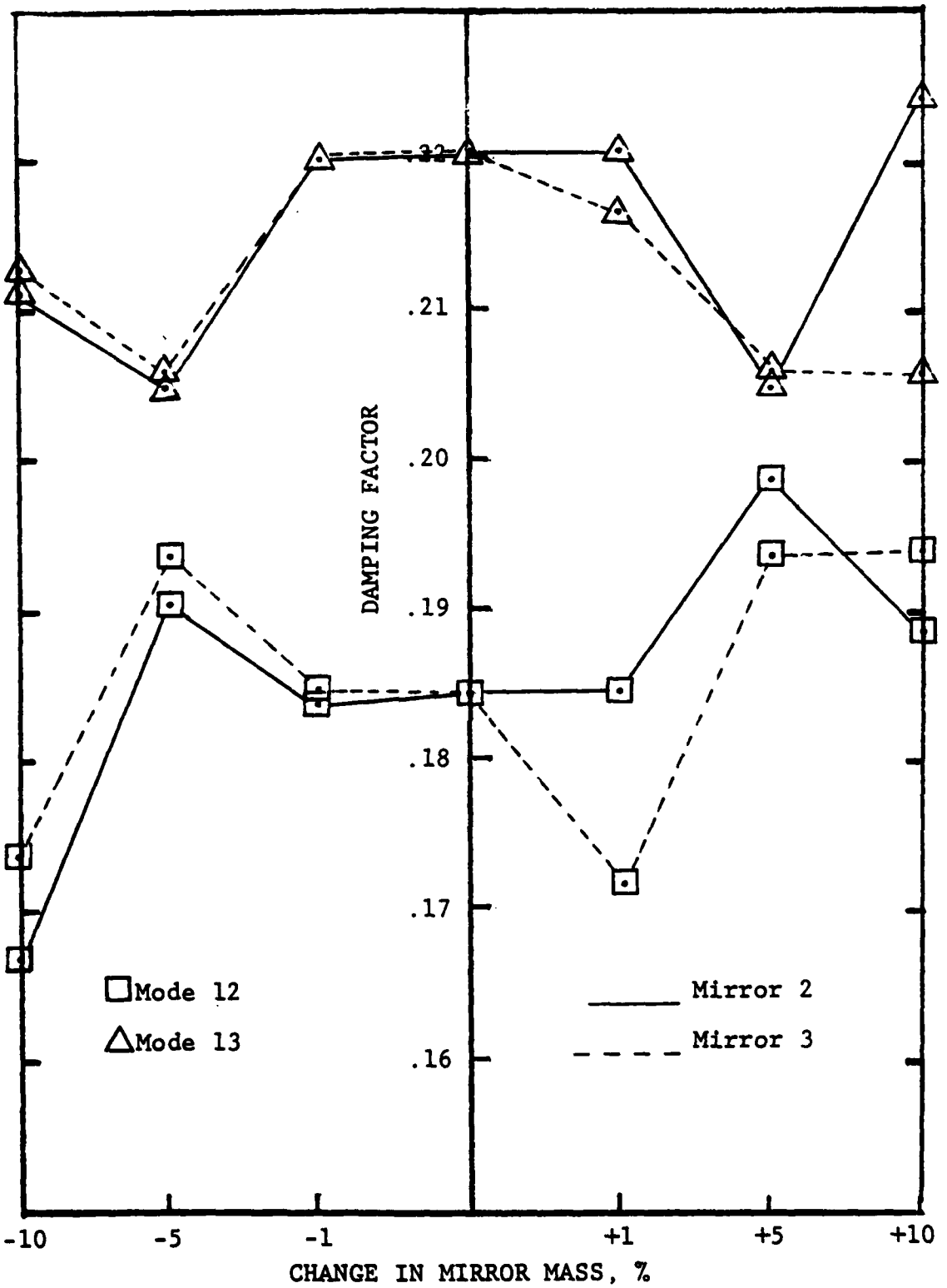

Figure 27. Mirror Mass Changes

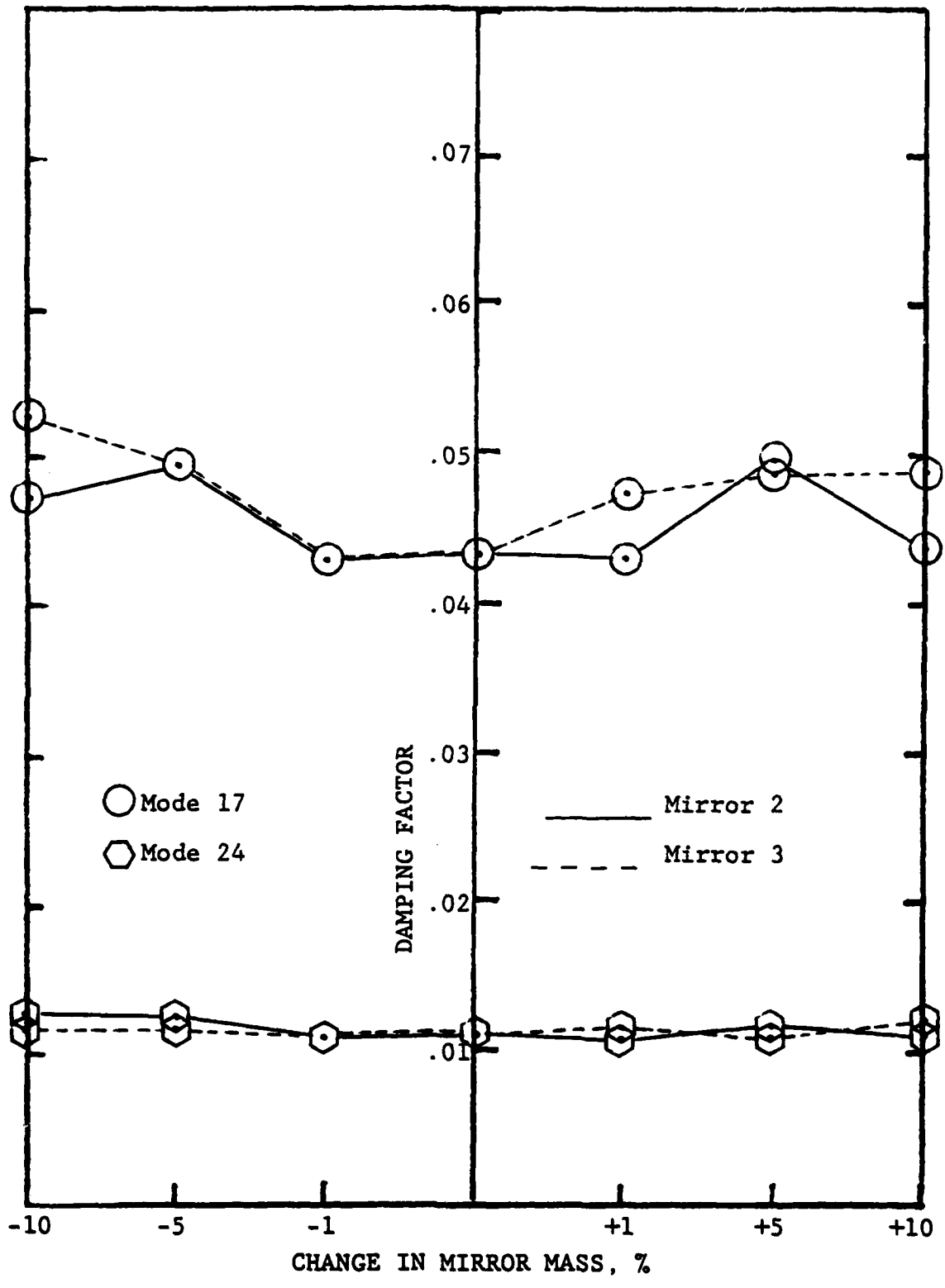

Figure 28. Mirror Mass Changes

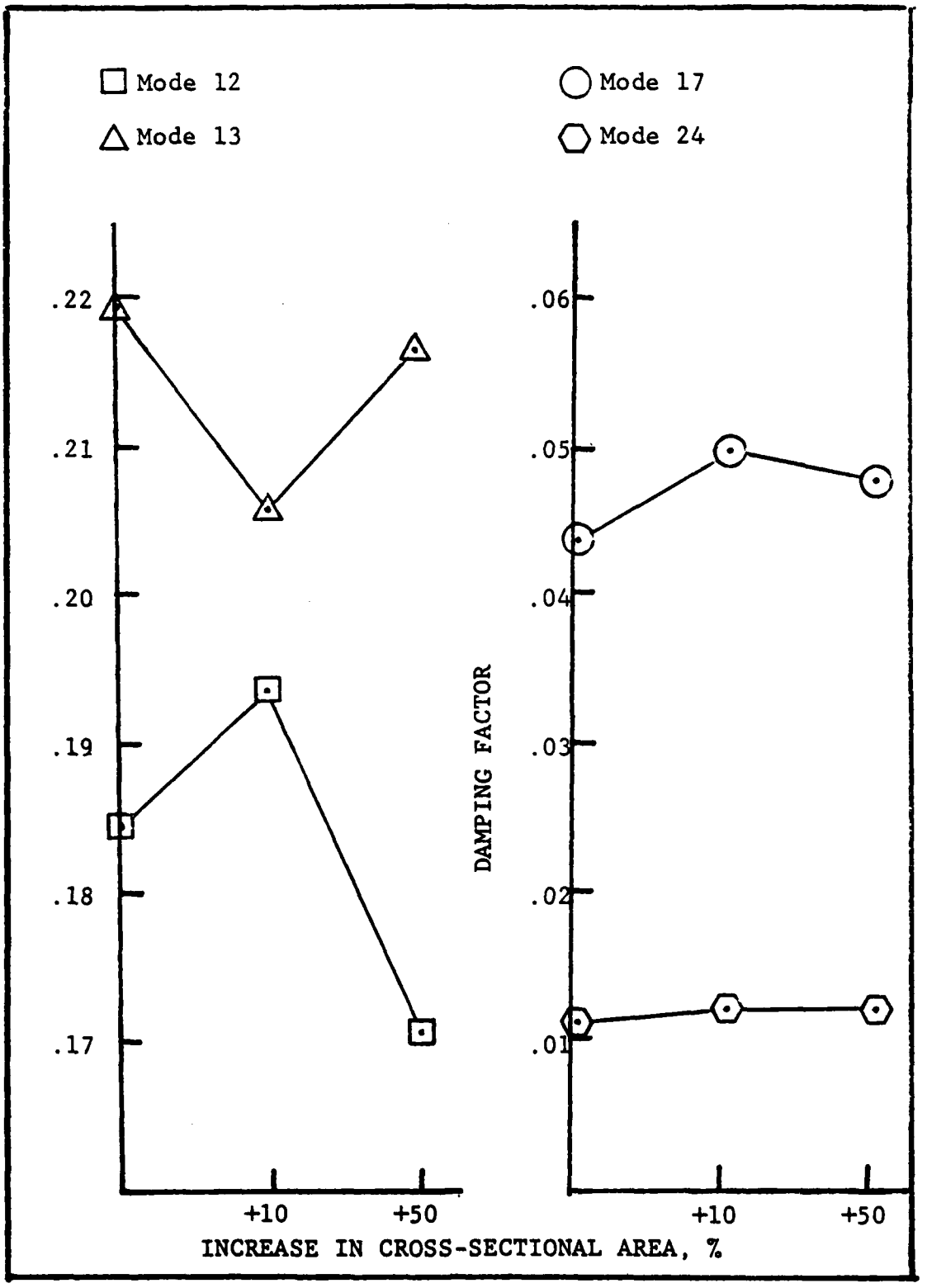

Figure 29. Stiffness Changes, Set 1

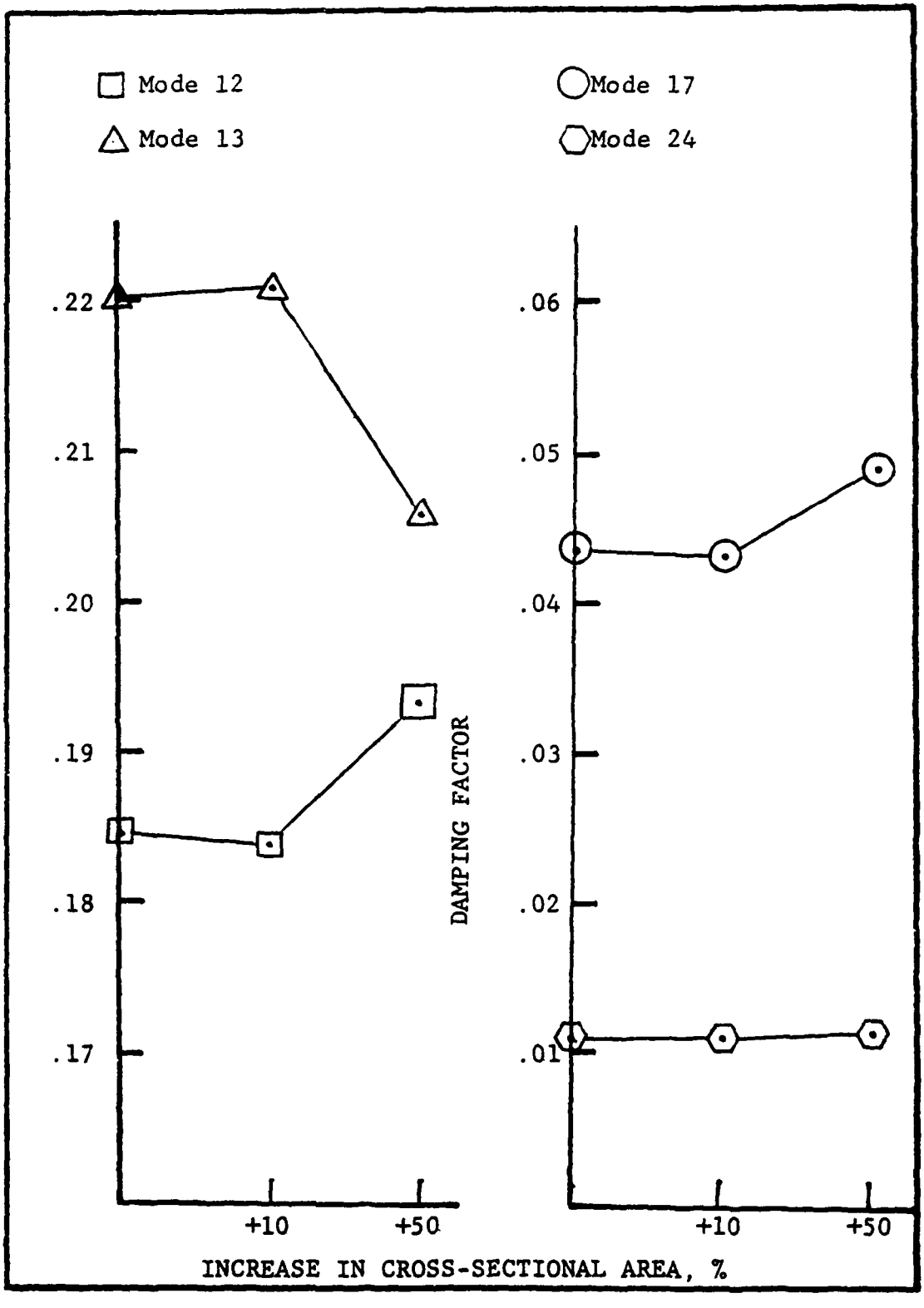

Figure 30. Stiffness Changes, Set 2

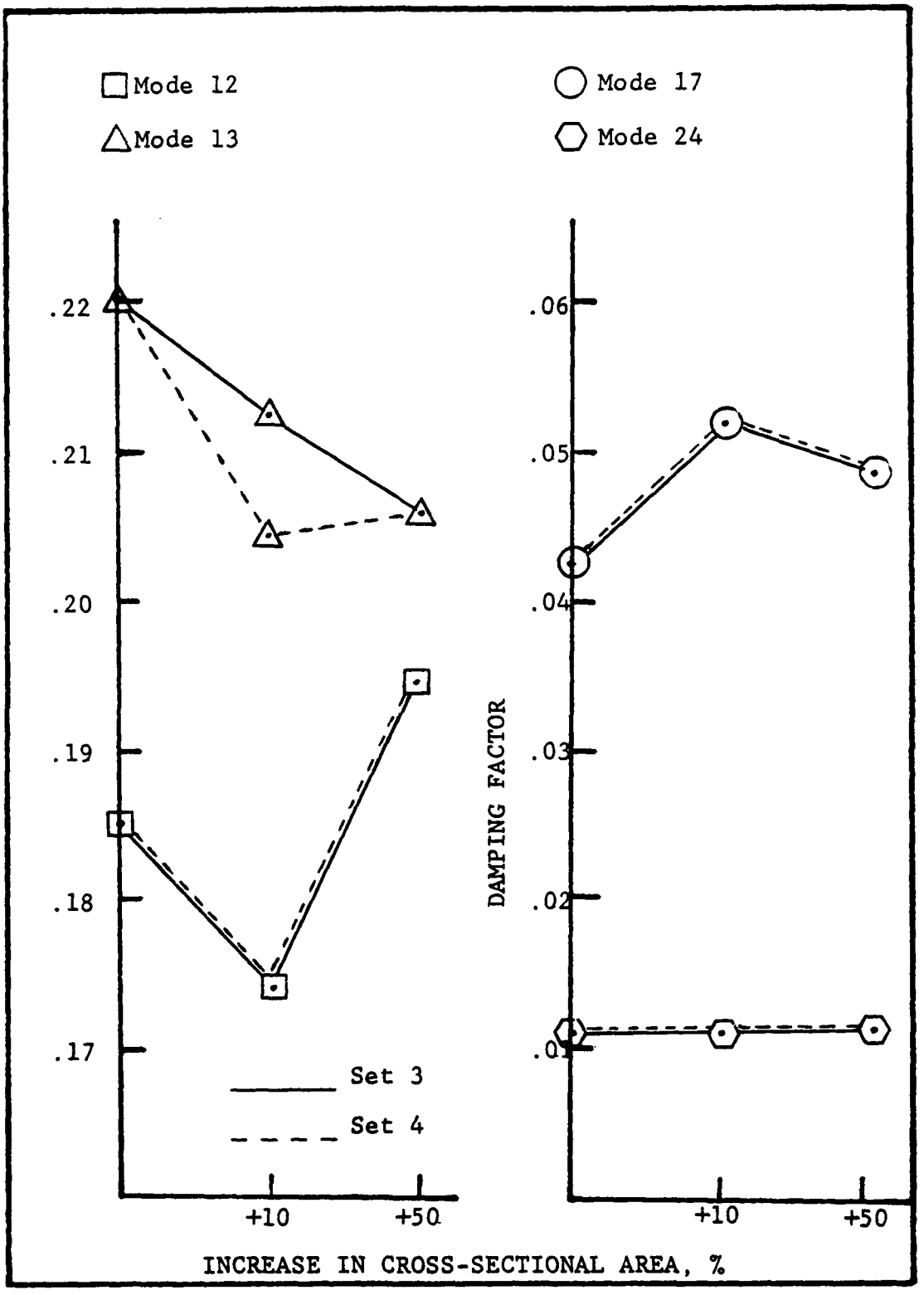

Figure 31. Stiffness Changes, Sets 3 and 4

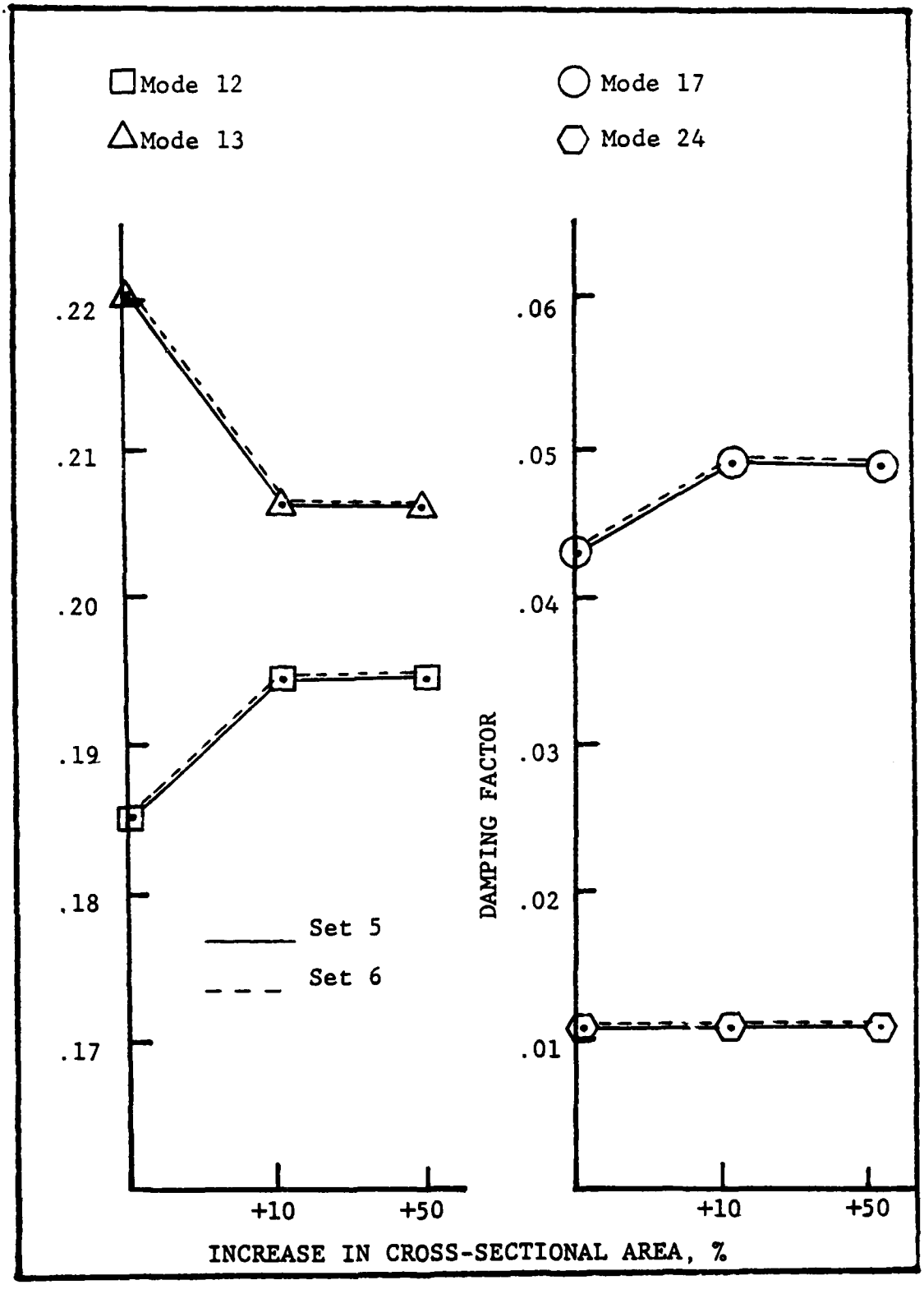

Figure 32. Stiffness Changes, Sets 5 and 6

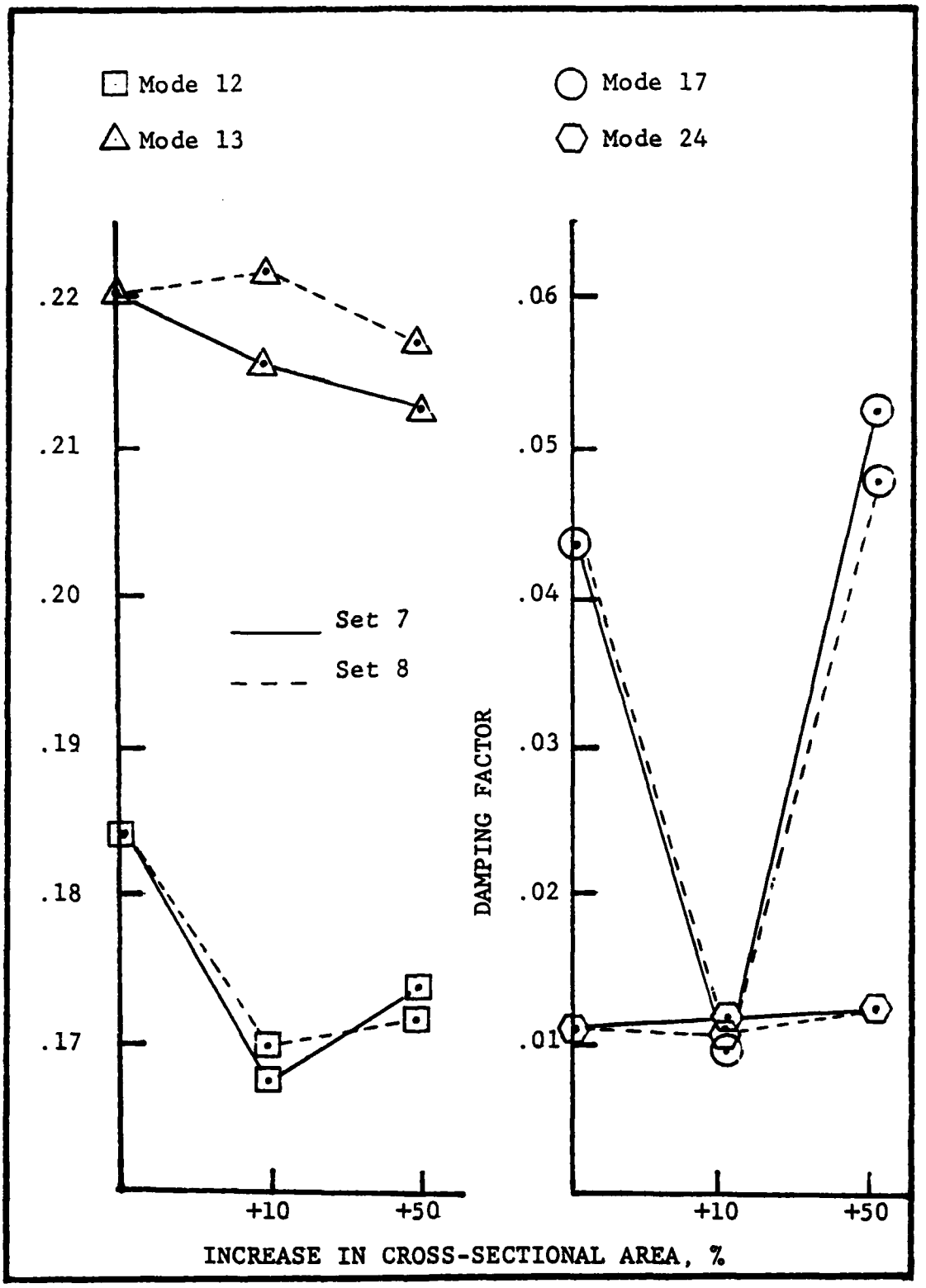

Figure 33. Stiffness Changes, Sets 7 and 8

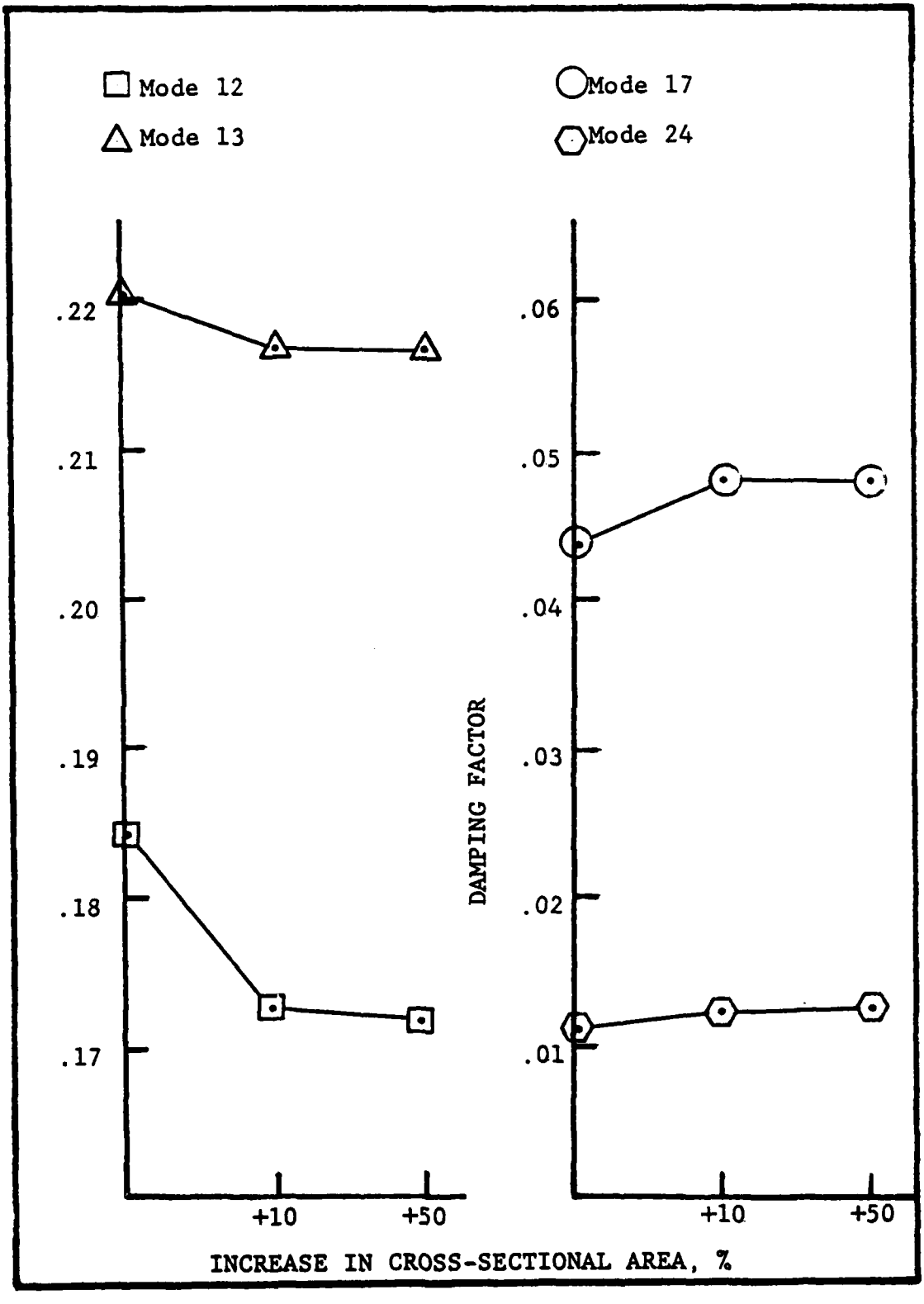

Figure 34. Stiffness Changes, Set 9

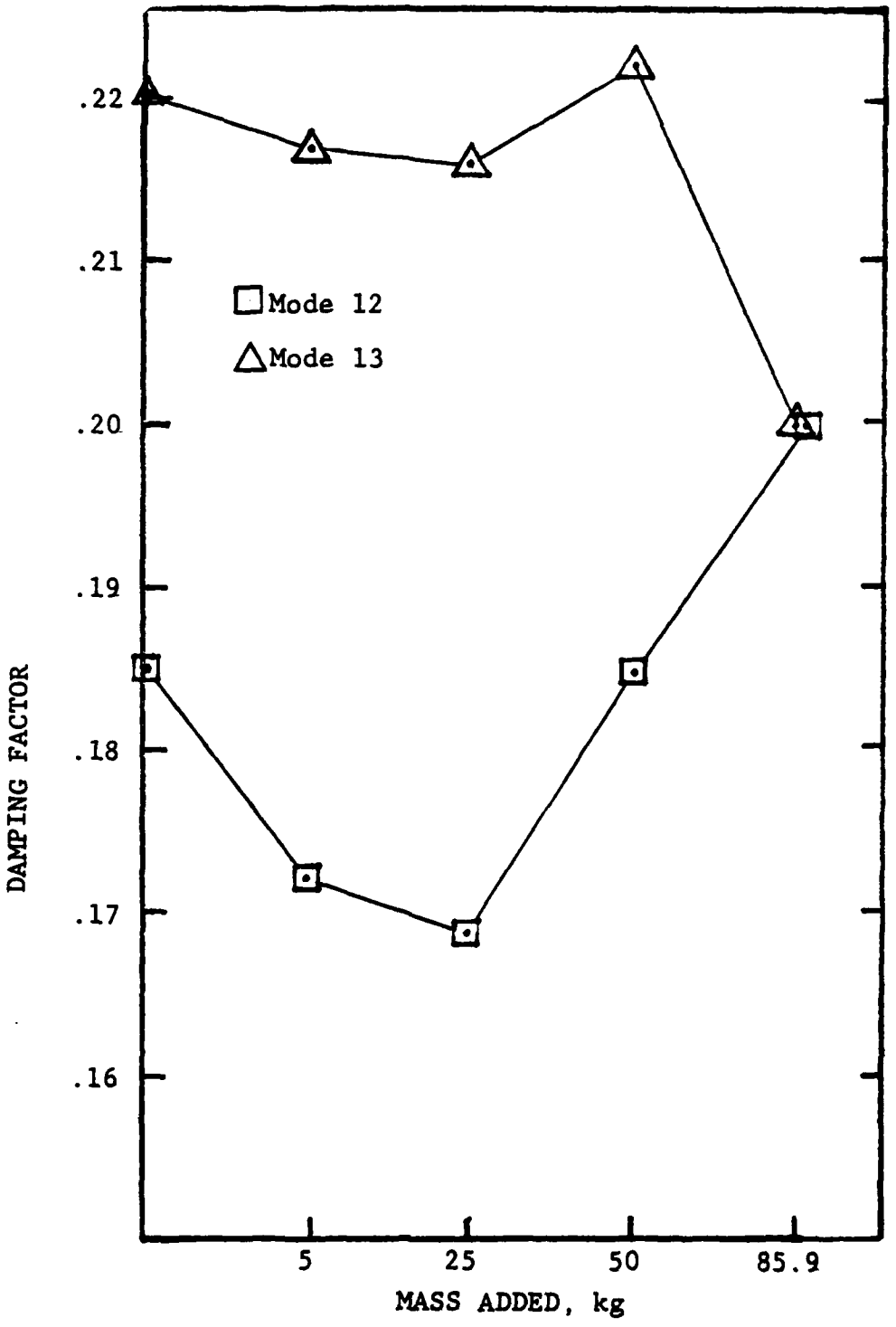

Figure 35. Mid-section Mass Increases

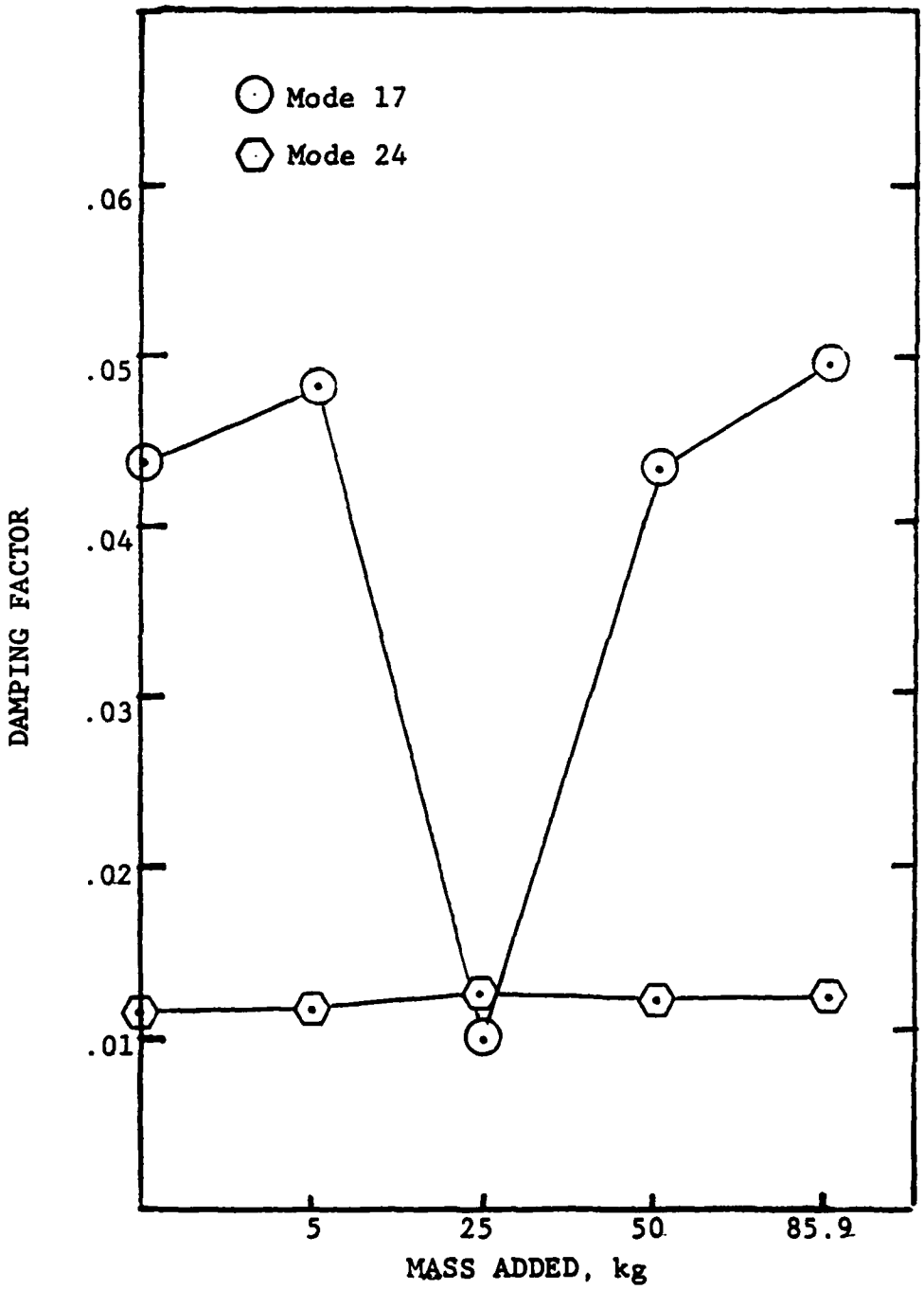

Figure 36. Mid-section Mass Increases

V. Conclusions and Recommendations

Discussion on Inconsistencies in the Data

Due to the inconsistency of portions of the data, the modeling of the CSDL 2 structure and the particular VCOSS derivation were studied. In Revision 1 of the CSDL 2 model, the cross-members that go from node points 28 to 30 and from 32 to 33 are strengthened to support the masses of the primary and tertiary mirrors, respectively. (This research used the revision 1 model). The cross-section of the stiffened mirror support beams is depicted in Figure 37. They are tubular trusses and were designed to prevent line-of-sight errors due to bending at frequencies less than 40 hz. (Ref 3:9) The cross members and exterior members of these trusses do not run the full length of the truss and are assumed to have no effect on its bending stiffness. The mass per unit length is set at 1.5 times that of the four tubes by themselves to account for the cross members. In the NASTRAN input deck, this tubular truss is modeled as a circular beam with the same cross-sectional area as the four tubes combined. The moments of inertia for the equivalent circular beam are the same as the summed moments of inertia for the individual tubes around the center of the truss. The inertia of the cross members and exterior members has not been included. The assumption has been made through this modeling technique

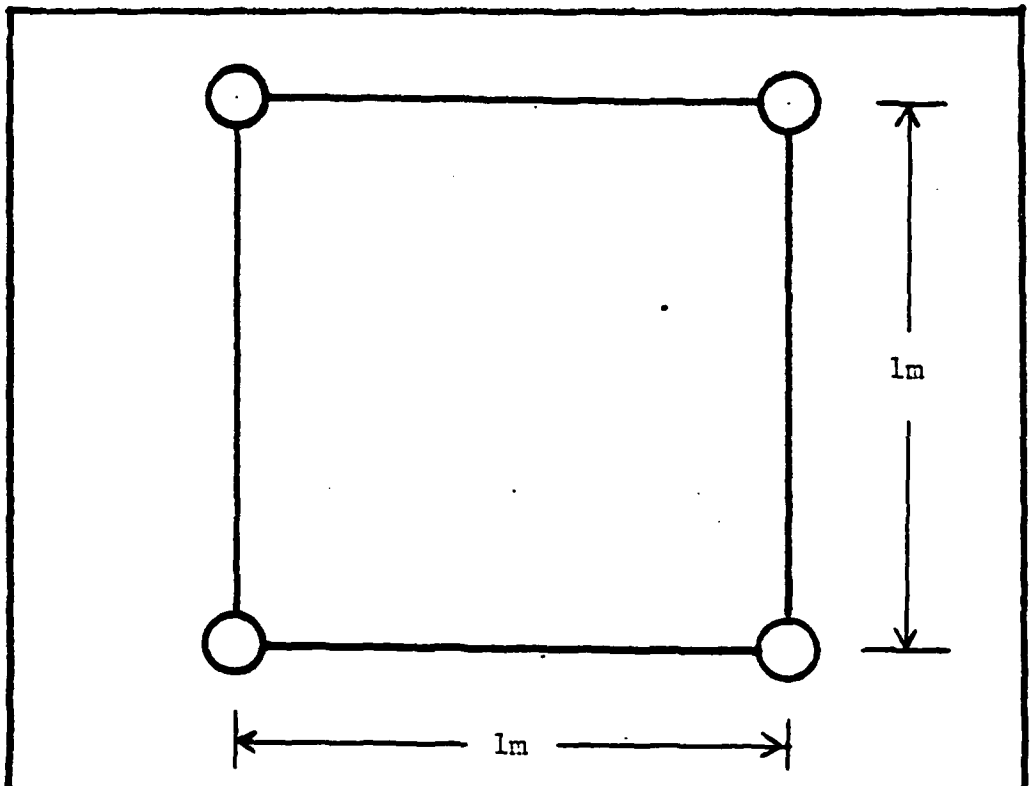

Tube Properties:
Radius = 0.11m
t = 0.0022m
Area = 0.00152m^2

Section Properties:
Area = $4A_{tube}$ = 0.00608m^2
I = 0.00152m^4
J = 0.00304m^4
Mass/L = 15.69 kg/m

Figure 37. Stiffened Mirror Support Beam (Ref 3:11)

that the equivalent circular beam will bend and twist in the same manner as the tubular truss. This is a very questionable structural modeling technique and could be a factor in the inconsistency of the damping factor data from this research.

The approach used in the design of the VCOSS version of the CSDL 2 model was to reduce the size of the structural elements to the minimum values that would still prevent structural failure. The structure is therefore very flexible and has very low natural frequencies. (Ref 3:17) Resizing these elements downward from the basic model (revision 1) lowered the total mass by 373 kg to 8963 kg, a reduction of slightly over 4%. If an LSS such as this telescope was to be launched into space on the shuttle, the LSS mass of 8963 kg would be small compared to the shuttle capacity of around 27000 kg. A savings of 373 kg could be insignificant due to the fact that the tubular elements would occupy a large volume in the payload bay without approaching the constraint on total payload weight. The VCOSS structure, then, is perhaps unrealistic and does not model the characteristics of the type of LSS that will be erected in the future. This research has indicated that the structure, as it exists in the VCOSS configuration, does not exhibit much consistency in its response to small changes in mass and stiffness. This could indicate serious problems in its basic design, and, since the goals of the VCOSS program include realistic design and control hardware

specification, the effectiveness of the VCOSS program could be degraded.

The control system of 21 sensor/actuator pairs emphasizes the focusing of the telescope (rather than the pointing of it) in that twelve pairs are oriented to sense motion in the z-direction. (Displacements in the z-direction would cause the mirrors to deflect and result in an unfocused image.) There are three sensor/actuator pairs for the x-direction and six pairs for y. The analysis of modes 21, 24, 28, and 29 has shown that it is difficult to actively damp these modes because of their higher frequencies and smaller displacements. Mode 24, however, is actively damped; it involves motion of many more sensor/actuator pairs than do the other three uncontrollable modes due to the severity of its deformation. It is possible, then, that if more sensor/actuator pairs were oriented in the x and y directions, modes 21, 28, and 29 could be actively damped. It is important to damp these modes, because, of the twelve modes studied in this research, modes 21, 24, and 29 have the largest impact on the line-of-sight problem that is critical in a telescope. During a Lockheed Missiles and Space Company, Inc., control design effort using CSDL 2, a maximum line-of-sight error of 50 nanoradians (nrad) was specified. It was found that modes 21, 24, and 29 contributed 633, 815, and 630 nrad, respectively, to the line-of-sight error during this analysis. (Ref 1:4-23) These values are significantly higher than the allowable limit

and emphasize the need to damp these modes.

The methodology used in this research assumed that the perturbations to the CSDL 2 model do not significantly change the mode shapes or frequencies from their values in the unperturbed model. This is important because NASTRAN orders its output as a function of the eigenvalue of the mode, starting with the lowest value. (The eigenvalue is the square of the natural frequency.) The rest of the data reduction assumes that the frequencies do not change enough to cause the mode shapes to swap positions in the output. For example, the natural frequency for mode 7 is .145 hz; for mode 8 it is .263 hz. If the perturbations to the model caused the frequency associated with mode shape 8 to be less than the frequency of mode 7, the output from NASTRAN would have the two modes reversed and the analysis of the results would be comparing the damping factor for two different mode shapes. This comparison would be invalid. To verify that the results of this research do not reflect the above problem, three additional sets of GCSNAST mode shape plots (similar to those in Figures 15 to 24) were made. These three sets are plots of the mode shapes from three of the perturbations whose damping factors varied significantly from the rest of the data points in the particular perturbation group. These points seemed to be the most likely to be affected by a swap in the order of mode shapes. They are (1) the addition of 10% mass to the secondary mirror, (2) the set that made

CBARs 44 and 45 (near the middle of the structure) solid, and (3) the 50% increase in area for stiffness perturbation set 1 (CBARs 99-102 in the upper part of the metering truss). Inspection of the GCSNAST plots showed that, even when the mode shapes are magnified by a factor of 10, there are no noticeable differences in mode shapes between these three perturbations and the unperturbed structure. (There must be some, otherwise the damping factor would not change.) The important point to be made is that the overall shapes did not change, indicating, for example, that the mode shape associated with the twelvth eigenvalue in the NASTRAN output remained essentially the same throughout the research and that the analysis is not comparing the damping for two different mode shapes. The grouping of the data (i.e., the damping factors for mode 12 are all near .185, mode 13 is around .22, etc.) supports this conclusion. The assumption remains, however, that the mode shapes for modes that have frequencies very close together are different.

Conclusions

This research has shown that the damping in a LSS can be affected by very small changes in mass and stiffness. A structure in space could be "fine tuned" to increase the damping for a particular mode. It was noted, however, that not all modes are affected in the same way. One mode may show increased damping while another modes damping may decrease. Any attempt to increase damping, therefore, must

consider all of the modes that are to be controlled.

The amount of active damping in the CSDL 2 model is dependent upon the mode shape, the natural frequency, and the orientation of the control system. The lower frequency modes have larger deflections associated with them and are more easily controlled than the higher frequency modes. Mode 24, one of the higher frequency modes, indicated that if enough sensor/actuator pairs are affected by the deflection associated with the mode shape, active damping can be successfully employed. Similarly, in the lower frequency modes, the number of sensor/actuator pairs involved affects the damping factor. Modes 12 and 13 have basically the same kind of mode shape (rotation about a point in the upper mirror support truss) but they rotate in different planes. Mode 12 has one sensor/actuator pair in the lower mirror support truss to control the vibration and had a damping factor around .185. Mode 13 affected two pairs in the lower mirror support truss and had a damping factor of .22. The addition of more control pairs in the lower mirror support truss oriented to sense motion in the x and y directions would very likely increase the damping of those two modes.

It seems logical that, as the magnitude of a perturbation is increased, the damping factor would show a consistent trend, either up or down. It also seems likely that, if the trend in the change of the damping factor is not consistent, there should be some point where the damping

factor reaches a maximum/minimum value and then goes down/up as the magnitude of the perturbation changes. These trends are absent in much of the data developed in this research. Possible explanations for this include inaccuracies in the computer modeling of the structure and the extreme flexibility of the structure. More research on the structural characteristics of the CSDL 2 model is required if this model is to be used to develop methods of specifying the actual control system hardware for a large space structure.

Recommendations

Several areas need to be researched in detail to confirm the results of this thesis. The first approach that should be taken is to determine if the discrepancy in the modeling of the two stiffened mirror support beams has an effect on the results. The tubular truss should be modeled as a truss and not as an equivalent circular beam. This can be done by designating appropriate GRID points and "building" a beam in the NASTRAN input deck. Damping factors in this remodeled structure should then be compared to those discussed in this thesis.

Secondly, the doubts about the suitability of the VCOSS version of this model should be resolved. The CSDL 2, Revision 1 model should be analyzed and then perturbed in a manner similar to that done in this thesis. This will indicate if the extreme flexibility in the VCOSS version

of this model (Revision 3) is responsible for the erratic damping behavior discovered in this research.

Third, the effect of changing the orientation of the control set and the number of sensor/actuator pairs should be studied, with emphasis on determining a control system configuration that can damp the modes that are not damped by the current control system.

Finally, the predictability of the effects of small perturbations must be improved. In order to accomplish this, the data base must be expanded. There are an infinite number of possible perturbations; this research has looked at 46 of them. Several of these perturbations indicate that small deviations in mass or stiffness, if they exist in the wrong place, can negate the active damping in a vibrational mode (Figures 33 and 36). Other cases have shown that the damping in some modes is increased by small deviations. The predictability of these occurrences must be improved if large space structures are to be built at an affordable cost.

Large space structures, whether in the form of a telescope, a solar power station, or manned space stations, are becoming increasingly important in the plans for development of space. In order to be able to afford these structures, the specifications for their components, be they control systems or epoxy-graphite tubes, must be developed to reflect the minimum precision required to accomplish the mission. This thesis has explored the sensitivity of

a LSS to small deviations in mirror mass, beam stiffness, and mass distribution. Space structures, once erected, may exhibit poor controllability due to small manufacturing deviations in their components or inaccuracies in the design or specification of the control system. This thesis has shown that the concept of "fine-tuning" a structure in orbit is valid, at least in the engineering sense. The ability to control a large space structure is dependent on knowledge of the interactions between active damping, passive damping, bending, twisting, rotating, and the inertial characteristics of the large masses. Once these are understood, the large space structure will be ready to support the development of space.

Bibliography

1. Aubrun, J. A., et al. ACOSS Five (Active Control of Space Structures) Phase IA. Final Technical Report. Rome Air Development Center TR-82-21. Griffiss Air Force Base, New York, March 1982.

2. Henderson, T. Active Control of Space Structures (ACOSS) Model 2. Final Technical Report. Cambridge, MA, The Charles Stark Draper Laboratory, Inc., September, 1981.

3. Henderson T. Modifications to ACOSS Model #2 Design. Cambridge, MA, The Charles Stark Draper Laboratory, Inc., March 1983.

4. Schaeffer, H. G. MSC/NASTRAN Static and Normal Modes Analysis. Milford, NH: Wallace Press, Inc., 1979.

5. Meirovitch, L. Elements of Vibration Analysis. New York: McGraw-Hill, Inc., 1975.

6. Calico, R. A., Jr. and Wm. T. Miller. "Decentralized Control for a Flexible Spacecraft," AIAA/AAS Astrodynamics Conference. New York: AIAA, August 1982.

7. Vierck, R. K. Vibration Analysis. New York: Harper and Row, 1979.

8. Aldridge, E. A. Decentralized Control of a Large Space Structure As Applied to the CSDL 2 Model. MS Thesis. Wright-Patterson AFB, Ohio: Air Force Institute of Technology, December 1982.

9. Henderson, T. Telephone Interview. The Charles Stark Draper Laboratory, Inc., 1 September 1983.

10. Henderson, T. VCOSS Design Model. The Charles Stark Draper Laboratory, Inc., Cambridge, MA, November 1981.

11. D'Azzo, J. J. and C.H. Houpis. Linear Control System Analysis and Design. Second Edition, New York: McGraw-Hill, Inc., 1981.

Appendix A. NASTRAN Bulk Data Listing

```
ID DRAPER,MODEL2
SOL 3
CHKPNT YES
CEND
TITLE = ACOSS MODEL #2  - REVISION 3
SUBTITLE = ACOSS DESIGN MODEL
LABEL = 156 MODES AND FREQUENCIES
MPC = 100
METHOD = 600
DISP = ALL
$ESE = ALL
BEGIN BULK
PARAM,USETPRT,1
PARAM   GRDPNT  0
EIGR    600     GIV                                     200                     +10
+10     MASS
$
$       KINEMATIC MOUNT:  TERTIARY MIRROR
$
RBE1,1003,27,123,29,23,3233,3,,+RB31
+RB31,UM,1003,123456
$
$       KINEMATIC MOUNT:  PRIMARY MIRROR
$
RBE1,1001,34,123,35,23,2830,3,,+RB11
+RB11,UM,1001,123456
$
$       KINEMATIC MOUNT:  FOCAL PLANE
$
RBE1,1004,11,123,9,23,40,3,,+RB41
+RB41,UM,1004,123456
$
$       KINEMATIC MOUNT:  SECONDARY MIRROR
$
RBE1,1002,910,123,1112,23,40,3,,+RB21
+RB21,UM,1002,123456
$
$        RIGID EQUIPMENT SECTION
$
RBE2    141     44      123456  42      43      45      46      47
$
$   NODE POINT LOCATIONS
$     NODE#             X (M)   Y (M)   Z (M)
$
GRID    1               -7.0    0.0     0.0
GRID    2               -4.0    5.0     0.0
GRID    3               -4.0    -5.0    0.0
GRID    4               0.0     5.0     0.0
GRID    5               4.0     5.0     0.0
GRID    6               4.0     -5.0    0.0
GRID    7               7.0     0.0     0.0
GRID    8               -7.0    0.0     2.0
GRID    9               -4.0    5.0     2.0
GRID    1004            0.0     4.0     2.0
GRID    10              -4.0    -5.0    2.0
GRID    11              4.0     5.0     2.0
GRID    12              4.0     -5.0    2.0
```

```
GRID     910             -4.0     -2.5     2.0
GRID     1112            4.0      -2.5     2.0
GRID     13              7.0      0.0      2.0
GRID     14              -6.0     0.0      12.
GRID     15              -4.0     4.0      12.
GRID     16              -4.0     -4.0     12.
GRID     17              4.0      4.0      12.
GRID     18              4.0      -4.0     12.
GRID     19              6.0      0.0      12.0
GRID     26              -5.0     0.0      22.0
GRID     27              -4.0     3.0      22.0
GRID     28              -4.0     -3.0     22.0
GRID     2830            0.0      -3.0     22.0
GRID     1001            0.0      -6.5     22.0
GRID     29              4.0      3.0      22.0
GRID     30              4.0      -3.0     22.0
GRID     31              5.0      0.0      22.0
GRID     32              -4.0     10.0     22.0
GRID     3233            0.0      10.0     22.0
GRID     1003            0.0      6.5      22.0
GRID     33              4.0      10.0     22.0
GRID     34              -4.0     -10.0    22.0
GRID     35              4.0      -10.0    22.0
GRID     36              -4.0     3.0      24.0
GRID     37              -4.0     -3.0     24.0
GRID     38              4.0      3.0      24.0
GRID     39              4.0      -3.0     24.0
GRID     40              0.0      2.5      2.0
GRID     1002            0.0      0.0      2.0
GRID     42              0.0      5.0      -0.3
GRID     43              -2.0     0.0      -1.3
GRID     44              0.0      -1.667   -1.3
GRID     45              2.0      0.0      -1.3
GRID     46              -4.0     -5.0     -0.3
GRID     47              4.0      -5.0     -0.3
GRID     48              -26.0    0.0      -1.3
GRID     49              -21.00   0.0      -1.3
GRID     50              -16.0    0.0      -1.3
GRID     51              -11.0    0.0      -1.3
GRID     52              -6.0     0.0      -1.3
GRID     53              6.0      0.0      -1.3
GRID     54              11.0     0.0      -1.3
GRID     55              16.0     0.0      -1.3
GRID     56              21.00    0.0      -1.3
GRID     57              26.0     0.0      -1.3
GRID     100             0.0      0.0      0.0              456
$
$    ELEMENT CONNECTION DATA
$
$     ELEM#   PROP#   NODE     NODE      LOCAL AXIS ORIENTATION VECTOR
$                       A        B
$
BARCR                                     1.0      0.0      0.0      1
CBAR     1       1       1        2
CBAR     2       2       1        3
CBAR     3       3       2        3
CBAR     4       4       2        4       0.0      1.0      0.0      1
```

```
CBAR    5       5       3       4
CBAR    6       6       4       5       0.0     1.0     0.0     1
CBAR    7       7       4       6
CBAR    8       8       3       6       0.0     1.0     0.0     1
CBAR    9       9       5       6
CBAR    10      10      5       7
CBAR    11      11      6       7
CBAR    12      12      1       8
CBAR    13      13      2       9
CBAR    14      14      3       10
CBAR    15      15      5       11
CBAR    16      16      6       12
CBAR    17      17      7       13
CBAR    18      18      3       8
CBAR    19      19      2       8
CBAR    21      21      4       9
CBAR    22      22      4       11
CBAR    24      24      5       13
CBAR    25      25      6       13
CBAR    26      26      1112    3
CBAR    27      27      6       10
CBAR    30      30      8       9
CBAR    31      31      8       10
CBAR    32      32      9       910
CBAR    232     232     910     10
CBAR    33      33      9       40
CBAR    34      34      910     40
CBAR    35      35      11      40
CBAR    36      36      1112    40
CBAR    37      37      9       11      0.0     1.0     0.0     1
CBAR    38      38      10      12      0.0     1.0     0.0     1
CBAR    39      39      11      1112
CBAR    239     239     1112    12
CBAR    201     201     910     1112    0.0     1.0     0.0     1
CBAR    202     202     2       910
CBAR    203     203     3       910
CBAR    204     204     5       1112
CBAR    205     205     6       1112
CBAR    207     207     12      910
CBAR    40      40      11      13
CBAR    41      41      12      13
CBAR    42      42      14      15
CBAR    43      43      14      16
CBAR    44      44      16      15
CBAR    45      45      17      18
CBAR    46      46      17      19
CBAR    47      47      18      19
CBAR    54      54      26      27
CBAR    55      55      26      28
CBAR    56      56      27      28
CBAR    57      57      29      30
CBAR    58      58      29      31
CBAR    59      59      30      31
CBAR    60      60      27      29      0.0     1.0     0.0     1
CBAR    61      61      27      30
CBAR    62      62      28      2830    0.0     1.0     0.0     1
CBAR    184     184     2330    30      0.0     1.0     0.0     1
```

CBAR	63	63	27	36				
CBAR	64	64	28	37				
CBAR	65	65	30	39				
CBAR	66	66	29	38				
CBAR	67	67	29	36				
CBAR	68	68	27	37				
CBAR	69	69	28	39				
CBAR	70	70	30	38				
CBAR	71	71	36	37				
CBAR	72	72	37	39	0.0	1.0	0.0	1
CBAR	73	73	39	38				
CBAR	74	74	36	38	0.0	1.0	0.0	1
CBAR	75	75	37	38				
CBAR	127	127	26	37				
CBAR	128	128	26	36				
CBAR	129	129	31	39				
CBAR	130	130	31	38				
CBAR	76	76	8	14				
CBAR	77	77	10	14				
CBAR	78	78	10	16				
CBAR	79	79	16	9				
CBAR	80	80	9	15				
CBAR	181	181	8	15				
CBAR	182	182	6	40				
CBAR	183	183	2	40				
CBAR	186	186	3	40				
CBAR	187	187	5	40				
CBAR	81	81	11	17				
CBAR	82	82	11	18				
CBAR	83	83	12	18				
CBAR	84	84	12	19				
CBAR	85	85	13	19				
CBAR	86	86	13	17				
CBAR	87	87	14	26				
CBAR	88	88	14	28				
CBAR	89	89	16	28				
CBAR	90	90	16	27				
CBAR	91	91	15	27				
CBAR	92	92	15	26				
CBAR	93	93	17	29				
CBAR	94	94	18	29				
CBAR	95	95	18	30				
CBAR	96	96	19	30				
CBAR	97	97	19	31				
CBAR	98	98	17	31				
CBAR	99	99	15	32				
CBAR	100	100	16	34				
CBAR	101	101	17	33				
CBAR	102	102	18	35				
CBAR	111	111	26	32				
CBAR	112	112	27	32				
CBAR	113	113	27	33				
CBAR	114	114	29	33				
CBAR	115	115	31	33				
CBAR	116	116	32	3233	0.0	1.0	0.0	1
CBAR	185	185	3233	33	0.0	1.0	0.0	1
CBAR	117	117	26	34				

```
CBAR    118     118     28      34
CBAR    119     119     30      34
CBAR    120     120     30      35
CBAR    121     121     31      35
CBAR    122     122     34      35      0.0     1.0     0.0     1
CBAR    123     123     32      36
CBAR    124     124     33      38
CBAR    125     125     34      37
CBAR    126     126     35      39
CBAR    131     131     48      49      0.0     1.0     0.0     1
CBAR    132     132     49      50      0.0     1.0     0.0     1
CBAR    133     133     50      51      0.0     1.0     0.0     1
CBAR    134     134     51      52      0.0     1.0     0.0     1
CBAR    135     135     52      43      0.0     1.0     0.0     1
CBAR    136     136     45      53      0.0     1.0     0.0     1
CBAR    137     137     53      54      0.0     1.0     0.0     1
CBAR    138     138     54      55      0.0     1.0     0.0     1
CBAR    139     139     55      56      0.0     1.0     0.0     1
CBAR    140     140     56      57      0.0     1.0     0.0     1
$
$     ISOLATOR SPRINGS
$
$       ELEM#       K     NODE    DOF     NODE    DOF
$                 (N/M)   A       A       B       B
$
CELAS2  142     5.79E3  4       1       42      1
CELAS2  143     5.79E3  4       2       42      2
CELAS2  144     5.79E3  4       3       42      3
CELAS2  145     5.79E3  3       1       46      1
CELAS2  146     5.79E3  3       2       46      2
CELAS2  147     5.79E3  3       3       46      3
CELAS2  148     5.79E3  6       1       47      1
CELAS2  149     5.79E3  6       2       47      2
CELAS2  150     5.79E3  6       3       47      3
$
$     MATERIAL PROPERTY DATA
$
$       MAT#    E               NU      RHO
$
MAT1    100     1.24E+11        0.3     1720.
MAT1    200     1.24E+11        0.3     1720.
MAT1    300     1.24E+11        0.3     2579.70
$
$     LUMPED MASS DATA
$
$CONM2  ELEM#   NODE#           MASS                                    +XXXX
$+XXXX    IXX           IYY                     IZZ
$
$       MIRRORS
$
CONM2   1001    1001            1000.                                   +1001
+1001   4083.33         5333.33                 9416.67
CONM2   1002    1002            800.                                    +4040
+4040   1666.67         4266.67                 5933.33
CONM2   1003    1003            1200.                                   +1003
+1003   4900.           6400.                   11300.
CONM2   1004    1004            600.                                    +1004
```

```
+1004   200.            800.                    1000.
$
$       EQUIPMENT SECTION
$
CONM2   544     44              3500.                                   +544
+544    20611.          10500.                  28777.
$
$    SOLAR PANELS   .
$
CONM2   548     48              81.91                                   +548
+548    270.0
CONM2   550     50              163.82                                  +550
+550    540.0
CONM2   552     52              73.82                                   +552
+552    270.0
CONM2   553     53              73.82                                   +553
+553    270.0
CONM2   557     57              81.91                                   +557
+555    540.0
CONM2   555     55              163.82                                  +555
+557    270.0
$
$       ADDITIONAL NON-STRUCTURAL MASS AT MIRROR SUPPORTS
$
CONM2   501     27              69.5
CONM2   502     28              6.74
CONM2   503     29              69.5
CONM2   504     30              6.74
CONM2   505     32              6.74
CONM2   506     33              6.74
CONM2   507     34              69.5
CONM2   508     35              69.5
CONM2   509     9               67.4
CONM2   510     10              67.4
CONM2   511     11              67.4
CONM2   512     12              67.4
$
$       BEAM SECTION PROPERTIES
$
$PBAR             PROP#  MAT#            AREA            I11      *XXXXXXX
$*XXXXXXX         I22             J
$
PBAR*                   1   100         0.678583E-04    0.439721E-07*       1
*       1   0.439721E-07    0.879442E-07
PBAR*                   2   100         0.678583E-04    0.439721E-07*       2
*       2   0.439721E-07    0.879442E-07
PBAR*                   3   100         0.255098E-03    0.621422E-06*       3
*       3   0.621422E-06    0.124284E-05
PBAR*                   4   100         0.678583E-04    0.439721E-07*       4
*       4   0.439721E-07    0.879443E-07
PBAR*                   5   100         0.343532E-03    0.112695E-05*       5
*       5   0.112695E-05    0.225391E-05
PBAR*                   6   100         0.678583E-04    0.439721E-07*       6
*       6   0.439721E-07    0.879443E-07
PBAR*                   7   100         0.343532E-03    0.112695E-05*       7
*       7   0.112695E-05    0.225391E-05
PBAR*                   8   100         0.104152E-03    0.103587E-06*       8
```

```
*      8    0.103587E-06   0.207174E-06
PBAR*                 9  100          0.255098E-03   0.621422E-06*      9
*      9    0.621422E-06   0.124284E-05
PBAR*                10  100          0.678583E-04   0.439721E-07*     10
*     10    0.439721E-07   0.879442E-07
PBAR*                11  100          0.678583E-04   0.439721E-07*     11
*     11    0.439721E-07   0.879442E-07
PBAR*                12  100          0.678583E-04   0.439721E-07*     12
*     12    0.439721E-07   0.879443E-07
PBAR*                13  100          0.678583E-04   0.439721E-07*     13
*     13    0.439721E-07   0.879443E-07
PBAR*                14  100          0.678583E-04   0.439721E-07*     14
*     14    0.439721E-07   0.879443E-07
PBAR*                15  100          0.678583E-04   0.439721E-07*     15
*     15    0.439721E-07   0.879443E-07
PBAR*                16  100          0.678583E-04   0.439721E-07*     16
*     16    0.439721E-07   0.879443E-07
PBAR*                17  100          0.678583E-04   0.439721E-07*     17
*     17    0.439721E-07   0.879442E-07
PBAR*                18  100          0.678583E-04   0.439721E-07*     18
*     18    0.439721E-07   0.879442E-07
PBAR*                19  100          0.678583E-04   0.439721E-07*     19
*     19    0.439721E-07   0.879442E-07
PBAR*                21  100          0.678583E-04   0.439721E-07*     21
*     21    0.439721E-07   0.879443E-07
PBAR*                22  100          0.678583E-04   0.439721E-07*     22
*     22    0.439721E-07   0.879443E-07
PBAR*                24  100          0.678583E-04   0.439721E-07*     24
*     24    0.439721E-07   0.879442E-07
PBAR*                25  100          0.678583E-04   0.439721E-07*     25
*     25    0.439721E-07   0.879442E-07
PBAR*                26  100          0.140494E-03   0.188490E-06*     26
*     26    0.188490E-06   0.376979E-06
PBAR*                27  100          0.140494E-03   0.188490E-06*     27
*     27    0.188490E-06   0.376979E-06
PBAR*                30  100          0.678583E-04   0.439721E-07*     30
*     30    0.439721E-07   0.879442E-07
PBAR*                31  100          0.678583E-04   0.439721E-07*     31
*     31    0.439721E-07   0.879442E-07
PBAR*                32  100          0.804583E-04   0.618177E-07*     32
*     32    0.618177E-07   0.123635E-06
PBAR*                33  100          0.678583E-04   0.439721E-07*     33
*     33    0.439721E-07   0.879443E-07
PBAR*                34  100          0.678583E-04   0.439721E-07*     34
*     34    0.439721E-07   0.879443E-07
PBAR*                35  100          0.678583E-04   0.439721E-07*     35
*     35    0.439721E-07   0.879443E-07
PBAR*                36  100          0.678583E-04   0.439721E-07*     36
*     36    0.439721E-07   0.879443E-07
PBAR*                37  100          0.104152E-03   0.103587E-06*     37
*     37    0.103587E-06   0.207174E-06
PBAR*                38  100          0.104152E-03   0.103587E-06*     38
*     38    0.103587E-06   0.207174E-06
PBAR*                39  100          0.804583E-04   0.618177E-07*     39
*     39    0.618177E-07   0.123635E-06
PBAR*                40  100          0.678583E-04   0.439721E-07*     40
*     40    0.439721E-07   0.879442E-07
```

```
FBAR*                41   100              0.678583E-04   0.439721E-07*    41
*     41   0.439721E-07    0.879442E-07
FBAR*                42   100              0.678583E-04   0.439721E-07*    42
*     42   0.439721E-07    0.879443E-07
FBAR*                43   100              0.678583E-04   0.439721E-07*    43
*     43   0.439721E-07    0.879443E-07
FBAR*                44   100              0.104152E-03   0.103587E-06*    44
*     44   0.103587E-06    0.207174E-06
FBAR*                45   100              0.104152E-03   0.103587E-06*    45
*     45   0.103587E-06    0.207174E-06
FBAR*                46   100              0.678583E-04   0.439721E-07*    46
*     46   0.439721E-07    0.879443E-07
FBAR*                47   100              0.678583E-04   0.439721E-07*    47
*     47   0.439721E-07    0.879443E-07
FBAR*                54   100              0.678583E-04   0.439721E-07*    54
*     54   0.439721E-07    0.879442E-07
FBAR*                55   100              0.678583E-04   0.439721E-07*    55
*     55   0.439721E-07    0.879442E-07
FBAR*                56   100              0.678583E-04   0.439721E-07*    56
*     56   0.439721E-07    0.879442E-07
FBAR*                57   100              0.678583E-04   0.439721E-07*    57
*     57   0.439721E-07    0.879442E-07
FBAR*                58   100              0.678583E-04   0.439721E-07*    58
*     58   0.439721E-07    0.879442E-07
FBAR*                59   100              0.678583E-04   0.439721E-07*    59
*     59   0.439721E-07    0.879442E-07
FBAR*                60   100              0.104152E-03   0.103587E-06*    60
*     60   0.103587E-06    0.207174E-06
FBAR*                61   100              0.255098E-03   0.621422E-06*    61
*     61   0.621422E-06    0.124284E-05
FBAR*                62   300              0.0060821      0.0015205  *     62
*     62   0.0015205       0.0030410
FBAR*                63   100              0.678583E-04   0.439721E-07*    63
*     63   0.439721E-07    0.879443E-07
FBAR*                64   100              0.678583E-04   0.439721E-07*    64
*     64   0.439721E-07    0.879443E-07
FBAR*                65   100              0.678583E-04   0.439721E-07*    65
*     65   0.439721E-07    0.879443E-07
FBAR*                66   100              0.678583E-04   0.439721E-07*    66
*     66   0.439721E-07    0.879443E-07
FBAR*                67   100              0.117640E-03   0.132154E-06*    67
*     67   0.132154E-06    0.264308E-06
FBAR*                68   100              0.678583E-04   0.439721E-07*    68
*     68   0.439721E-07    0.879442E-07
FBAR*                69   100              0.117640E-03   0.132154E-06*    69
*     69   0.132154E-06    0.264308E-06
FBAR*                70   100              0.678583E-04   0.439721E-07*    70
*     70   0.439721E-07    0.879442E-07
FBAR*                71   100              0.678583E-04   0.439721E-07*    71
*     71   0.439721E-07    0.879442E-07
FBAR*                72   100              0.104152E-03   0.103587E-06*    72
*     72   0.103587E-06    0.207174E-06
FBAR*                73   100              0.678583E-04   0.439721E-07*    73
*     73   0.439721E-07    0.879442E-07
FBAR*                74   100              0.104152E-03   0.103587E-06*    74
*     74   0.103587E-06    0.207174E-06
FBAR*                75   100              0.255098E-03   0.621422E-06*    75
```

*	75	0.621422E-06	0.124284E-05			
PBAR*		76	100	0.259503E-03	0.643065E-06*	76
*	76	0.643065E-06	0.128613E-05			
PBAR*		77	100	0.424114E-03	0.171765E-05*	77
*	77	0.171765E-05	0.343531E-05			
PBAR*		78	100	0.259503E-03	0.643065E-06*	78
*	78	0.643065E-06	0.128613E-05			
PBAR*		79	100	0.833904E-03	0.664055E-05*	79
*	79	0.664055E-05	0.132811E-04			
PBAR*		80	100	0.259503E-03	0.643065E-06*	80
*	80	0.643065E-06	0.128613E-05			
PBAR*		81	100	0.259503E-03	0.643065E-06*	81
*	81	0.643065E-06	0.128613E-05			
PBAR*		82	100	0.833904E-03	0.664055E-05*	82
*	82	0.664055E-05	0.132811E-04			
PBAR*		83	100	0.259503E-03	0.643065E-06*	83
*	83	0.643065E-06	0.128613E-05			
PBAR*		84	100	0.424114E-03	0.171765E-05*	84
*	84	0.171765E-05	0.343531E-05			
PBAR*		85	100	0.259503E-03	0.643065E-06*	85
*	85	0.643065E-06	0.128613E-05			
PBAR*		86	100	0.398135E-03	0.151367E-05*	86
*	86	0.151367E-05	0.302735E-05			
PBAR*		87	100	0.259503E-03	0.643065E-06*	87
*	87	0.643065E-06	0.128613E-05			
PBAR*		88	100	0.325124E-03	0.100942E-05*	88
*	88	0.100942E-05	0.201883E-05			
PBAR*		89	100	0.259503E-03	0.643065E-06*	89
*	89	0.643065E-06	0.128613E-05			
PBAR*		90	100	0.566323E-03	0.306267E-05*	90
*	90	0.306267E-05	0.612533E-05			
PBAR*		91	100	0.259503E-03	0.643065E-06*	91
*	91	0.643065E-06	0.128613E-05			
PBAR*		92	100	0.348640E-03	0.116072E-05*	92
*	92	0.116072E-05	0.232143E-05			
PBAR*		93	100	0.259503E-03	0.643065E-06*	93
*	93	0.643065E-06	0.128613E-05			
PBAR*		94	100	0.566323E-03	0.306267E-05*	94
*	94	0.306267E-05	0.612533E-05			
PBAR*		95	100	0.259503E-03	0.643065E-06*	95
*	95	0.643065E-06	0.128613E-05			
PBAR*		96	100	0.325124E-03	0.100942E-05*	96
*	96	0.100942E-05	0.201883E-05			
PBAR*		97	100	0.259503E-03	0.643065E-06*	97
*	97	0.643065E-06	0.128613E-05			
PBAR*		98	100	0.348640E-03	0.116072E-05*	98
*	98	0.116072E-05	0.232143E-05			
PBAR*		99	100	0.470559E-03	0.211446E-05*	99
*	99	0.211446E-05	0.422892E-05			
PBAR*		100	100	0.470559E-03	0.211446E-05*	100
*	100	0.211446E-05	0.422892E-05			
PBAR*		101	100	0.470559E-03	0.211446E-05*	101
*	101	0.211446E-05	0.422892E-05			
PBAR*		102	100	0.470559E-03	0.211446E-05*	102
*	102	0.211446E-05	0.422892E-05			
PBAR*		111	100	0.259503E-03	0.643065E-06*	111
*	111	0.643065E-06	0.128613E-05			

```
FBAR*              112   100              0.678583E-04    0.439721E-07*   112
*    112   0.439721E-07    0.879443E-07
FBAR*              113   100              0.325124E-03    0.100942E-05*   113
*    113   0.100942E-05    0.201883E-05
FBAR*              114   100              0.678583E-04    0.439721E-07*   114
*    114   0.439721E-07    0.879443E-07
FBAR*              115   100              0.259503E-03    0.643065E-06*   115
*    115   0.643065E-06    0.128613E-05
FBAR*              116   300              0.0060821       0.0015205  *    116
*    116   0.0015205       0.0030410
FBAR*              117   100              0.259503E-03    0.643065E-06*   117
*    117   0.643065E-06    0.128613E-05
FBAR*              118   100              0.678583E-04    0.439721E-07*   118
*    118   0.439721E-07    0.879443E-07
FBAR*              119   100              0.325124E-03    0.100942E-05*   119
*    119   0.100942E-05    0.201883E-05
FBAR*              120   100              0.678583E-04    0.439721E-07*   120
*    120   0.439721E-07    0.879443E-07
FBAR*              121   100              0.259503E-03    0.643065E-06*   121
*    121   0.643065E-06    0.128613E-05
FBAR*              122   100              0.104152E-03    0.103587E-06*   122
*    122   0.103587E-06    0.207174E-06
FBAR*              123   100              0.716806E-04    0.490653E-07*   123
*    123   0.490653E-07    0.981305E-07
FBAR*              124   100              0.716806E-04    0.490653E-07*   124
*    124   0.490653E-07    0.981305E-07
FBAR*              125   100              0.716806E-04    0.490653E-07*   125
*    125   0.490653E-07    0.981305E-07
FBAR*              126   100              0.716806E-04    0.490653E-07*   126
*    126   0.490653E-07    0.981305E-07
FBAR*              127   100              0.678583E-04    0.439721E-07*   127
*    127   0.439721E-07    0.879443E-07
FBAR*              128   100              0.678583E-04    0.439721E-07*   128
*    128   0.439721E-07    0.879443E-07
FBAR*              129   100              0.678583E-04    0.439721E-07*   129
*    129   0.439721E-07    0.879443E-07
FBAR*              130   100              0.678583E-04    0.439721E-07*   130
*    130   0.439721E-07    0.879443E-07
FBAR*              131   100              6.107256E-04    3.561752E-06*   131
*    131   3.561752E-06    7.123504E-06
FBAR*              132   100              6.107256E-04    3.561752E-06*   132
*    132   3.561752E-06    7.123504E-06
FBAR*              133   100              6.107256E-04    3.561752E-06*   133
*    133   3.561752E-06    7.123504E-06
FBAR*              134   100              6.107256E-04    3.561752E-06*   134
*    134   3.561752E-06    7.123504E-06
FBAR*              135   100              6.107256E-04    3.561752E-06*   135
*    135   3.561752E-06    7.123504E-06
FBAR*              136   100              6.107256E-04    3.561752E-06*   136
*    136   3.561752E-06    7.123504E-06
FBAR*              137   100              6.107256E-04    3.561752E-06*   137
*    137   3.561752E-06    7.123504E-06
FBAR*              138   100              6.107256E-04    3.561752E-06*   138
*    138   3.561752E-06    7.123504E-06
FBAR*              139   100              6.107256E-04    3.561752E-06*   139
*    139   3.561752E-06    7.123504E-06
FBAR*              140   100              6.107256E-04    3.561752E-06*   140
```

```
*     140     3.561752E-06     7.123504E-06
PBAR*                  181    100                0.398135E-03    0.151367E-05*     181
*     181     0.151367E-05     0.302735E-05
PBAR*                  182    100                0.343532E-03    0.112695E-05*     182
*     182     0.112695E-05     0.225391E-05
PBAR*                  183    100                0.343532E-03    0.112695E-05*     183
*     183     0.112695E-05     0.225391E-05
PBAR*                  184    300                0.0060821       0.0015205  *      184
*     184     0.0015205        0.0030410
PBAR*                  185    300                0.0060821       0.0015205  *      185
*     185     0.0015205        0.0030410
PBAR*                  186    100                0.343532E-03    0.112695E-05*     186
*     186     0.112695E-05     0.225391E-05
PBAR*                  187    100                0.343532E-03    0.112695E-05*     187
*     187     0.112695E-05     0.225391E-05
PBAR*                  201    100                0.104620E-03    0.104520E-06*     201
*     201     0.104520E-06     0.209040E-06
PBAR*                  202    100                0.923628E-04    0.814640E-07*     202
*     202     0.814640E-07     0.162928E-06
PBAR*                  203    100                0.678583E-04    0.439721E-07*     203
*     203     0.439721E-07     0.879442E-07
PBAR*                  204    100                0.923628E-04    0.814640E-07*     204
*     204     0.814640E-07     0.162928E-06
PBAR*                  205    100                0.678583E-04    0.439721E-07*     205
*     205     0.439721E-07     0.879442E-07
PBAR*                  207    100                0.140494E-03    0.188490E-06*     207
*     207     0.188490E-06     0.376979E-06
PBAR*                  232    100                0.678583E-04    0.439721E-07*     232
*     232     0.439721E-07     0.879442E-07
PBAR*                239100                       0.678583E-04    0.439721E-07*     239
*     239     0.439721E-07     0.879442E-07
$
$       MULTI-POINT CONSTRAINT EQUATION FOR X-AXIS LOS ERROR (NODE 100 DOF 1)
$
MPC*    100                              100              1            -1.0*1000000
*1000000                  34               2  -0.01855287570                 *1000001
*1000001                                   34               3  -0.14285714286*1000002
*1000002                  35               2  -0.0185528757                  *1000003
*1000003                                   35               3  -0.14285714286*1000004
*1000004                2830               3   0.28571428572                 *1000005
*1000005                                   30               3   0.0           *1000006
*1000006                  27               2   0.08065681999                 *1000007
*1000007                                   27               3  -0.35489000795*1000008
*1000008                  29               2   0.08065681999                 *1000009
*1000009                                   29               3  -0.35489000795*1000010
*1000010                3233               3   0.70978001590                 *1000011
*1000011                                   33               3   0.0           *1000012
*1000012                1004               4  -3.48423005566                 *1000013
*1000013                                   11               2  -0.06210394429*1000014
*1000014                   9               2  -0.06210394429
$
$       MULTI-POINT CONSTRAINT EQUATION FOR Y-AXIS LOS ERROR (NODE 100 DOF 2)
$
MPC*    100                              100              2            -1.0*2000000
*2000000                  34               1  -0.03710575139                 *2000001
*2000001                                   34               2  -0.04638218924*2000002
*2000002                  34               3  -0.2500000000                  *2000003
```

AD-A136 984 THE EFFECT OF MASS AND STIFFNESS CHANGES ON THE DAMPING FACTOR IN A LARGE..(U) AIR FORCE INST OF TECH WRIGHT-PATTERSON AFB OH SCHOOL OF ENGI.. D E OLSEN

UNCLASSIFIED DEC 83 AFIT/GSO/AA/83D-2 F/G 22/2 NL

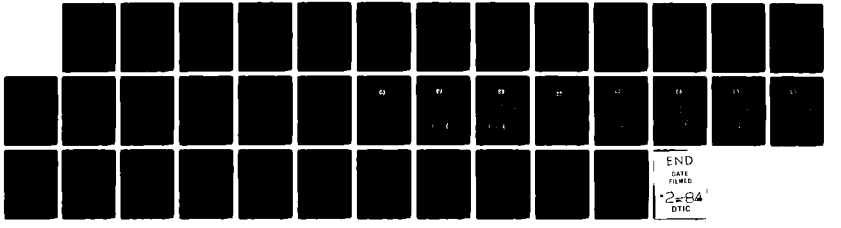

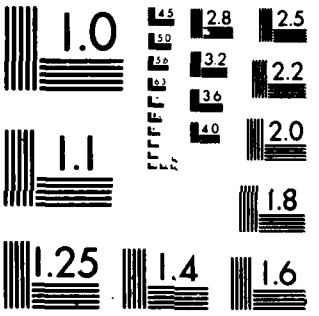

```
*2000003                              35              2   0.04638218924*2000004
*2000004              35               3   0.2500000000                *2000005
*2000005                              27              1   0.16131363998*2000006
*2000006              27               2  -0.06049261499                *2000007
*2000007                              27              3  -0.62105751391*2000008
*2000008              29               2   0.06049261499                *2000009
*2000009                              29              3   0.62105751391*2000010
*2000010            1002               5   3.48423005566                *2000011
*2000011                              11              1  -0.12420788859*2000012
*2000012              11               2  -0.07762993037                *2000013
*2000013                               9              2   0.07762993037*2000014
*2000014
$
$       MULTI-POINT CONSTRAINT EQUATION FOR DEFOCUS (NODE 100 DOF 3)
$
MPC*    100                         100              3             -1.0*3000000
*3000000              34               3  -0.01912393776                *3000001
*3000001                              35              3  -0.01912393776*3000002
*3000002            2830               3   0.12749291836                *3000003
*3000003                              30              3   0.0          *3000004
*3000004              27               3   0.77803217347                *3000005
*3000005                              29              3   0.77803217347*3000006
*3000006            3233               3  -0.46681930408                *3000007
*3000007                            1002              3  -0.17849008571*3000008
*3000008               9               3   0.50000000000                *3000009
*3000009                              11              3   0.50000000000*3000010
*3000010              40               3  -2.00000000000
$
$       RIGID BODY SUPPORT
$
SUPORT,44,123456
ENDDATA

******** END OF MEMBER REV03      659 RECORDS ********
```

Appendix B. Computer Methodology

The damping ratio, used as the performance index in this research, is the end result of a lengthy computational process. The programs used include NASTRAN, FORMAT, SELECT, ZETA, and DOFB34. NASTRAN is widely used and well documented (Ref 4) and will not be discussed here. FORMAT, SELECT, ZETA, and DOFB34 were developed at the Air Force Institute of Technology to aid in the analysis of the CSDL 2 model. Various forms of these programs exist; the users must ascertain that they use the appropriate ones. DOFB34 is documented and validated in reference 6. These programs, as listed in the following appendices, were used on the CDC 170/750 computer system at Wright-Patterson AFB, OH. The first task in the generation of data was to run NASTRAN for the finite element analysis of the CSDL 2 model.

NASTRAN was run using the NASTJCL control cards listed in Appendix C. The data deck, called BULK1 in NASTJCL, contains the finite element model of the LSS. It is listed in Appendix A. The output from the NASTRAN program is filed as ACOSSPUN and contains a six line NASTRAN header, followed by the eigenvalue, mode number, and ϕ matrix for each mode. The entry in line three of the header, titled LABEL, is used to keep track of the particular bulk data deck used as input to NASTRAN. This variable, labeled DATASET in succeeding

programs, is passed through the rest of the computer analysis and printed on the final product.

Program FORMAT (Appendix D) is used to reformat ACOSSPUN into the format required for the SELECT program. FORMAT reads ACOSSPUN (relabeled TAPE5) and prints out (on TAPE8) the number of critical modes (12 in this case) and the specific mode numbers to be analyzed (4,5,6,7,12,...29), followed by DATASET, the mode number, eigenvalue, and ϕ matrix for each mode. This program should be compiled using the FORTRAN IV compiler.

SELECT (Appendix E) reads TAPE8 and then outputs DATASET, the ϕ matrix for each of the 12 modes, and the 12 eigenvalues onto TAPE6. Next, the number of modes being analyzed, the number of actuators, the number of sensors, and the location and orientation of the sensors/actuators are added to the front of TAPE6. An example of this set of data is listed in Appendix G.

Program ZETA (Appendix F) prepares the data for input to DOFB34. ZETA reads the revised TAPE6 and computes the B and C matrices. It also takes the square root of the eigenvalue to get the natural frequency in radians per second. As discussed earlier, the B and C matrices are the transpose of each other if the sensors and actuators are collocated. DOFB34, the next program used in the analysis, requires C in its transposed form and then transposes it back to its original form. The B matrix is therefore printed by ZETA

to represent the transposed C matrix. Various other parameters for DOFB34 are also printed by ZETA on an output file. These parameters are explained in reference 6. Thus, the output from ZETA contains DATASET, 2 lines of parameters for DOFB34, the B matrices for the 12 modes, the C matrix for the 12 modes (represented by B in this case), the 12 natural frequencies, and finally, 9 lines of parameters for DOFB34.

DOFB34 reads the output file from ZETA, relabeled TAPE8, and calculates the complex conjugate pairs that are used to calculate the damping factor for the various modes. These pairs are titled "Eigenvalues A1+(BSTAR1)(KSTAR1)(C1), A2+(BSTAR2)(KSTAR2)(C2), and A3+(BSTAR3)(KSTAR3)(C3)." Each of the 12 modes is represented by two eigenvalue pairs having the same real value and only different signs on the imaginary value. Thus, the original NASTRAN data has been reduced to the 24 eigenvalue pairs output by DOFB34.

The damping factor calculation (equation 14) uses the absolute value of the real and imaginary values.

Appendix C. NASTRAN Job Control Listing (NASTJCL)

The commands listed below are used to run the NASTRAN program. The job control card should include a time limit of at least 800 seconds, an input/output limit of 1000 seconds, and 170000 units of core memory. The NASTRAN input deck is labeled BULK1 in this listing, and the NASTRAN output (punch file) goes to the file called PUN. ACOSSPUN is the permanent file name assigned to PUN during filing.

```
(Job Control Card)
ATTACH,NASTRAN, NASTRAN,ID=NASTRAN,SN=AFFDL,MR=1.
ATTACH,NAS1,NAS1,ID=TRAN,SN=ASDAD.
ATTACH,NAS2,NAS2,ID=TRAN,SN=ASDAD.
LIBRARY,NAS1,NAS2.
ATTACH,DATA,BULK1.
REQUEST,PUN,*PF.
RFL,17000.
NASTRAN,DATA,PUN. ATTACH
REWIND,PUN.
CATALOG,PUN,ACOSSPUN,CY=1,RP=999.
*EOF
```

Appendix D. Program FORMAT

The first two WRITE statements write the number of modes to be selected and the particular modes that make up the selection onto the output, TAPE8. This data is required by SELECT. The program then searches for the name "TITLE" in the NASTRAN output file (called ACOSSPUN and relabeled TAPE5) by assigning the variable ANAME to the first ten letters of every line and continuing when ANAME=TITLE. It then reads SUBTI, which is the subtitle, and DATASET, the variable assigned to the LABEL block in the NASTRAN input deck. After reading the next three lines (not used for anything here), it reads EIGEN (the eigenvalue of the mode) and MODEN (the mode number) and writes DATASET, MODEN, and EIGEN on TAPE8. The ϕ matrix for each of the modes (T1,T2,T3,R1,R2,R3) is then read and written onto TAPE8. This process continues until the data for all of the modes has been reformatted and written onto TAPE8.

```
      PROGRAM FORMAT(INPUT,OUTPUT,TAPE5,TAPE8)
      DIMENSION CARD(8)
      WRITE(8,11) 12
      WRITE(8,12) 4,5,6,7,12,13,17,21,22,24,28,29
   11 FORMAT(I2)
   12 FORMAT(12(I2,1X))
    1 READ(5,100) ANAME
      IF(EOF(5))1000,15
  100 FORMAT(A10)
   15 IF (ANAME.EQ.10H$TITLE  =) GO TO 150
      GO TO 1
  150 READ(5,100) SUBTI
      READ(5,235) DATASET
```

```
      DO 200 I=1,3
      READ(5,205)(CARD(J),J=1,8)
  205 FORMAT(8A10)
  200 CONTINUE
   10 FORMAT(I3,E13.6)
  235 FORMAT(10X,2A10)
      READ(5,210) EIGEN,MODEN
  210 FORMAT(14X,E14.6,11X,I3)
      WRITE(8,235) DATASET
      WRITE(8,10) MODEN,EIGEN
      DO 220 I=1,59
      READ(5,215) T1,T2,T3
  215 FORMAT(23X,3(E13.6,5X))
      READ(5,215) R1,R2,R3
      WRITE(8,225) T1,T2,T3
  225 FORMAT(3E15.6)
      WRITE(8,225) R1,R2,R3
  220 CONTINUE
      GO TO 1
 1000 STOP
      END
```

Appendix E. Program SELECT

This program reads the TAPE8 prepared by FORMAT. The variables are defined as follows:

N is the number of modes to be selected.

ID(I) is a matrix of the mode numbers to be selected.

DATASET(K) is a matrix of the bulk data identifier.

MODE(K) is the matrix of mode numbers.

EIGEN(K) is the matrix of eigenvalues.

MAT(I,J,K) is a 59 by 6 x 30 matrix of the ϕ matrices.

DATASET is printed onto TAPE6, followed by the ϕ matrix for the selected modes. Finally, the eigenvalues of the selected modes are listed. The MODES READ and MODES FILED statements are displayed on the output device (the screen) to assure the user that the proper actions have been accomplished.

```
      PROGRAM SELECT(INPUT,OUTPUT,TAPE8,TAPE6)
      DIMENSION MAT(59,6,30),MODE(30),ID(30),DATASET(30)
      DIMENSION EIGEN(30)
      CHARACTER*40,DATASET
      READ(8,*)N
      READ(8,*)(ID(I),I=1,N)
      DO 1 K=1,30
      READ(8,'(A40)') DATASET(K)
      READ(8,100)MODE(K),EIGEN(K)
      READ(8,200)((MAT(I,J,K),J=1,6),I=1,59)
    1 CONTINUE
      WRITE(6,'(A40)') DATASET(1)
      DO 2 K=1,N
      M=ID(K)
      WRITE(6,300)((MAT(I,J,M),J=1,6),I=1,59)
    2 CONTINUE
      DO 3 K=1,N
      M=ID(K)
      WRITE(6,400) EIGEN(M)
    3 CONTINUE
```

```
      PRINT*,'MODES READ ARE : ',(MODE(I),I=1,30)
      PRINT*,'MODES FILED ARE : ',(ID(I),I=1,N)
  100 FORMAT(I3,E13.6)
  200 FORMAT(3E15.6)
  300 FORMAT(3E15.6)
  400 FORMAT(E13.6)
      END
```

Appendix F. Program ZETA

This program reads the TAPE6 output from SELECT with the control system orientation added onto the front of TAPE6. The variables are defined as follows:

N is the number of modes to be analyzed.

NA is the number of actuators.

NS is the number of sensors.

ALPHA(I), BETA(I), and GAMMA(I) are the orientation of the actuators.

NODE(I) is the location (node point) of the actuators.

ALPHS(I), BETS(I), GAMMS(I) and NODS(I) represent the orientation and location of the sensors.

ID(I) is a 59 unit array of the node point numbers of CSDL 2. (This is added onto TAPE6 with the control system data.)

PHI(354,12) are the ϕ matrices of the 12 selected modes. (Note that 59 nodes times 6 values per node equals 354 values.)

B(12,21) and C(21,12) are the B and C matrices calculated in this program.

FREQ(I) is the natural frequency in radians per second, it is the square root of EIGEN(I).

EIGEN(I) and DATASET remain the same from SELECT.

After reading in the revised TAPE6, the six angles (ALPHA, BETA, etc.) are converted from degrees to radians by CON.

Next, the program matches up the node numbers and the actuator/sensor locations, finds the proper part of the ϕ matrix using K = 6*K-5, and calculates the B and C matrices using equation (13) for B and the transpose of that for C. After writing DATASET, 2 lines of input for DOFB34 are written, followed by the B matrix twice (DOFB34 wants C^T and C^T = B). This output is not automatically written onto a TAPE; the disposition of the output must be specified when the program is run. After taking the square root of EIGEN, FREQ is written. Finally, the other parameters for DOFB34 are written and the program ends.

```
      PROGRAM ZETA(INPUT,OUTPUT,TAPE5,TAPE6)
      DIMENSION PHI(354,12),ALPHA(21),BETA(21),GAMMA(21)
      DIMENSION ALPHS(21),BETS(21),GAMMS(21),NODE(21),NODS(21)
      DIMENSION ID(59),B(12,21),C(21,12),EIGEN(12),FREQ(12)
      CHARACTER*40,DATASET
      READ(6,*)N,NA,NS
      READ(6,*)(ALPHA(I),I=1,NA)
      READ(6,*)(BETA(I),I=1,NA)
      READ(6,*)(GAMMA(I),I=1,NA)
      READ(6,*)(NODE(I),I=1,NA)
      READ(6,*)(ALPHS(I),I=1,NS)
      READ(6,*)(BETS(I),I=1,NS)
      READ(6,*)(GAMMS(I),I=1,NS)
      READ(6,*)(NODS(I),I=1,NS)
      READ(6,*)(ID(I),I=1,59)
      READ(6,*'(A40)') DATASET
      READ(6,400)((PHI(I,J),I=1,354),J=1,N)
      READ(6,230)(EIGEN(K),K=1,N)
      PI=3.14159265E0
      CON=PI/180.0
      DO 30 J=1,NA
      ALPHA(J)=ALPHA(J)*CON
      BETA(J)=BETA(J)*CON
      GAMMA(J)=GAMMA(J)*CON
      DO 10 K=1,59
   10 IF(ID(K).EQ.NODE(J))GO TO 20
   20 CONTINUE
      K=6*K-5
      DO 30 I=1,N
```

```
      B(I,J)=PHI(K,I)*COS(ALPHA(J))+PHI(K+1,I)*COS(BETA(J))
     1  +PHI(K+2,1)*COS(GAMMA(J))
   30 CONTINUE
      DO 60 I=1,NS
      ALPHS(I)=ALPHS(I)*CON
      BETS(I)=BETS(I)*CON
      GAMMS(I)=GAMMS(I)*CON
      DO 40 K=1,59
   40 IF (ID(K).EQ.NODS(I))GO TO 50
   50 CONTINUE
      K=6*K-5
      DO 60 J=1,N
      C(I,J)=PHI(K,J)*COS(ALPHS(I))+PHI(K+1,J)*COS(BETS(I))
     1  +PHI(K+2,J)*COS(GAMMS(I))
   60 CONTINUE
      WRITE(*,'(A40)') DATASET
      PRINT'("3")'
      PRINT'("3 4 5 0 21 21 0.01")'
      DO 500 I=1,N
  500 PRINT 220,(B(I,J),J=1,NA)
      DO 600 I=1,N
  600 PRINT 220,(B(I,J),J=1,NS)
      DO 700 I=1,N
      FREQ(I)=SQRT(EIGEN(I))
      PRINT 230,FREQ(I)
  700 CONTINUE
      PRINT'("1 2 3")'
      PRINT'("4 5 6 7")'
      PRINT'("8 9 10 11 12")'
      PRINT'("0")'
      PRINT'("0")'
      PRINT'("2 2 2 5000 5000 5000 5000 5000 5000 5000 5000 5000")'
      PRINT'("2")'
      PRINT'("2")'
      PRINT'("3")'
  220 FORMAT(1X,/,6(/,6X,4F10.6))
  230 FORMAT(E13.6)
  400 FORMAT(3E15.8)
      END
```

Appendix G. Sensor/Actuator Orientation

ORIENTATION OF SENSORS

M	NODE	ALPHA	BETA	GAMMA
1	9	90.00	0.00	90.00
2	9	90.00	90.00	0.00
3	10	90.00	90.00	0.00
4	11	0.00	90.00	90.00
5	11	90.00	0.00	90.00
6	11	90.00	90.00	0.00
7	12	90.00	90.00	0.00
8	27	0.00	90.00	90.00
9	27	90.00	0.00	90.00
10	27	90.00	90.00	0.00
11	28	90.00	90.00	0.00
12	29	90.00	0.00	90.00
13	29	90.00	90.00	0.00
14	30	90.00	90.00	0.00
15	32	90.00	90.00	0.00
16	33	90.00	90.00	0.00
17	34	0.00	90.00	90.00
18	34	90.00	0.00	90.00
19	34	90.00	90.00	0.00
20	35	90.00	0.00	90.00
21	35	90.00	90.00	0.00

Sensor/Actuator location as input to Program ZETA.

```
12 21 21
90. 90. 90. 0. 90. 90. 90. 0. 90. 90. 90. 90. 90. 90. 90.
90. 0. 90. 90. 90. 90.
0. 90. 90. 90. 0. 90. 90. 90. 0. 90. 90. 0. 90. 90. 90.
90. 90. 0. 90. 0. 90.
90. 0. 0. 90. 90. 0. 0. 90. 90. 0. 0. 90. 0. 0. 0.
0. 90. 90. 0. 90. 0.
9 9 10 11 11 11 12 27 27 27 28 29 29 30 32 33 34 34 34 35 35
90. 90. 90. 0. 90. 90. 90. 0. 90. 90. 90. 90. 90. 90. 90.
90. 0. 90. 90. 90. 90.
0. 90. 90. 90. 0. 90. 90. 90. 0. 90. 90. 0. 90. 90. 90.
90. 90. 0. 90. 0. 90.
90. 0. 0. 90. 90. 0. 0. 90. 90. 0. 0. 90. 0. 0. 0.
0. 90. 90. 0. 90. 0.
9 9 10 11 11 11 12 27 27 27 28 29 29 30 32 33 34 34 34 35 35
1 2 3 4 5 6 7 8 9 10 11 12 13 14 15 16 17 18 19 26 27 28 29
30 31 32 33 34 35 36 37 38 39 40 42 43 44 45 46 47 48 49 50
51 52 53 54 55 56 57 100 910 1001 1002 1003 1004 1112 2830
3233
```

Appendix H. B Matrix for the Unperturbed Model

This appendix shows the B matrix computed by program ZETA for the unperturbed model. B is a 12 by 21 matrix; the printout lists the row number, followed by the 21 elements in that row.

B MATRIX

1

.004775	.004476	-.004430	.000000
.004775	.004476	-.004430	-.000000
-.313837	.003015	-.002568	-.013837
.003015	-.002568	.009529	.009529
-.000000	-.013837	-.009092	-.013837
-.009092			

2

.000001	.003619	.003618	-.004642
.000001	-.003619	-.003619	.013452
-.000002	.003619	.003618	-.000002
-.003619	-.003619	.003620	-.003617
.013452	-.000002	.003617	-.000002
-.003620			

3

-.006023	.000267	.000266	-.009232
.006023	-.000266	-.000266	-.013837
-.006023	.000266	.000266	.006023
-.000266	-.000266	.000267	-.000266
.015637	-.006023	.000266	.006023
-.000267			

4

.000126	-.001570	-.001532	.002816
-.000126	.001569	.001532	-.006275
.000097	-.001564	-.001541	-.000096
.001563	.00154	-.001565	.001563
-.006567	.000090	-.001520	-.000066
.001519			

5

-.000453	-.000859	-.000903	.010105
.000431	.000869	.000927	-.001877
-.000831	-.000680	-.000909	.000535
.000991	.000929	-.000922	.000824
-.000105	-.000570	-.000940	.000577
.000971			

6

-.016036	-.002014	.006244	.000073
-.016045	-.002002	.006279	-.000012
.000644	-.000401	.004528	.000666
-.000363	.004651	-.006268	-.006263
.000033	.000658	.010503	.000686
.010546			

7

-.000011	-.000616	-.000255	.000002
-.000812	-.000619	-.000257	-.000000
-.000065	-.000550	-.000331	-.000056
-.000552	-.000333	-.000810	-.000812
-.000000	-.000035	-.000073	-.000086
-.000075			

8

-.001653	-.001165	.000620	-.001659
.001953	.001152	-.000527	.001115
.001646	-.000647	.000291	-.001636
.000340	-.000271	-.002043	.002337
-.004343	.001618	.001326	-.001621
-.001337			

9

.003981	-.002849	-.003470	.001225
-.003980	.002659	.003479	.000638
-.000292	-.002955	-.003364	.000293
.002965	.003343	-.002561	.002570
.001357	-.000201	-.003782	.000206
.003795			

10

-.019403	-.005697	.005622	-.017699
.019407	.005625	-.005680	.001840
.002955	-.003584	.004155	-.002991
.003342	-.004167	-.011645	.011593
-.008292	.002726	.011238	-.002757
-.011342			

11

-.000000	-.000004	.000001	-.000003
-.000004	-.000005	.000001	-.000000
-.000008	.000001	-.000003	-.000006
-.000000	-.000003	.000004	.000002
.000000	-.000009	-.000008	-.000009
-.000007			

12

.000003	-.000010	-.000015	.000005
.000009	-.000000	-.000016	-.000000
.000004	-.000016	-.000016	.000004
-.000016	-.000016	-.000023	-.000016
-.000000	.000015	-.000011	.000004
-.000014			

Appendix I. Mode Shapes of the Unperturbed Model

Figure 15 through 24 show the mode shapes for the 12 modes under consideration in this research. These plots were made using the GCSNAST plotting program.

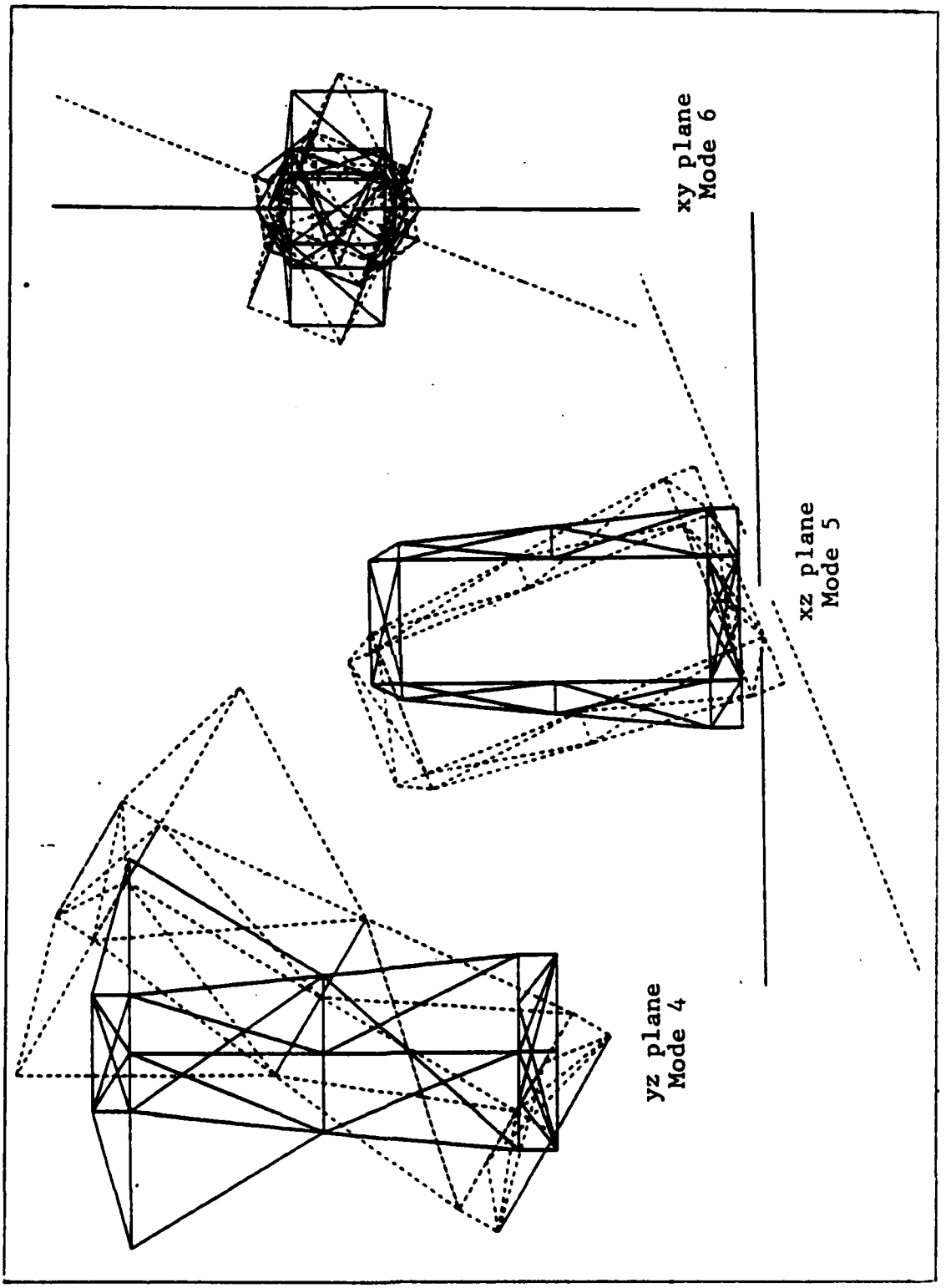

Figure 15. Mode Shapes 4, 5, and 6

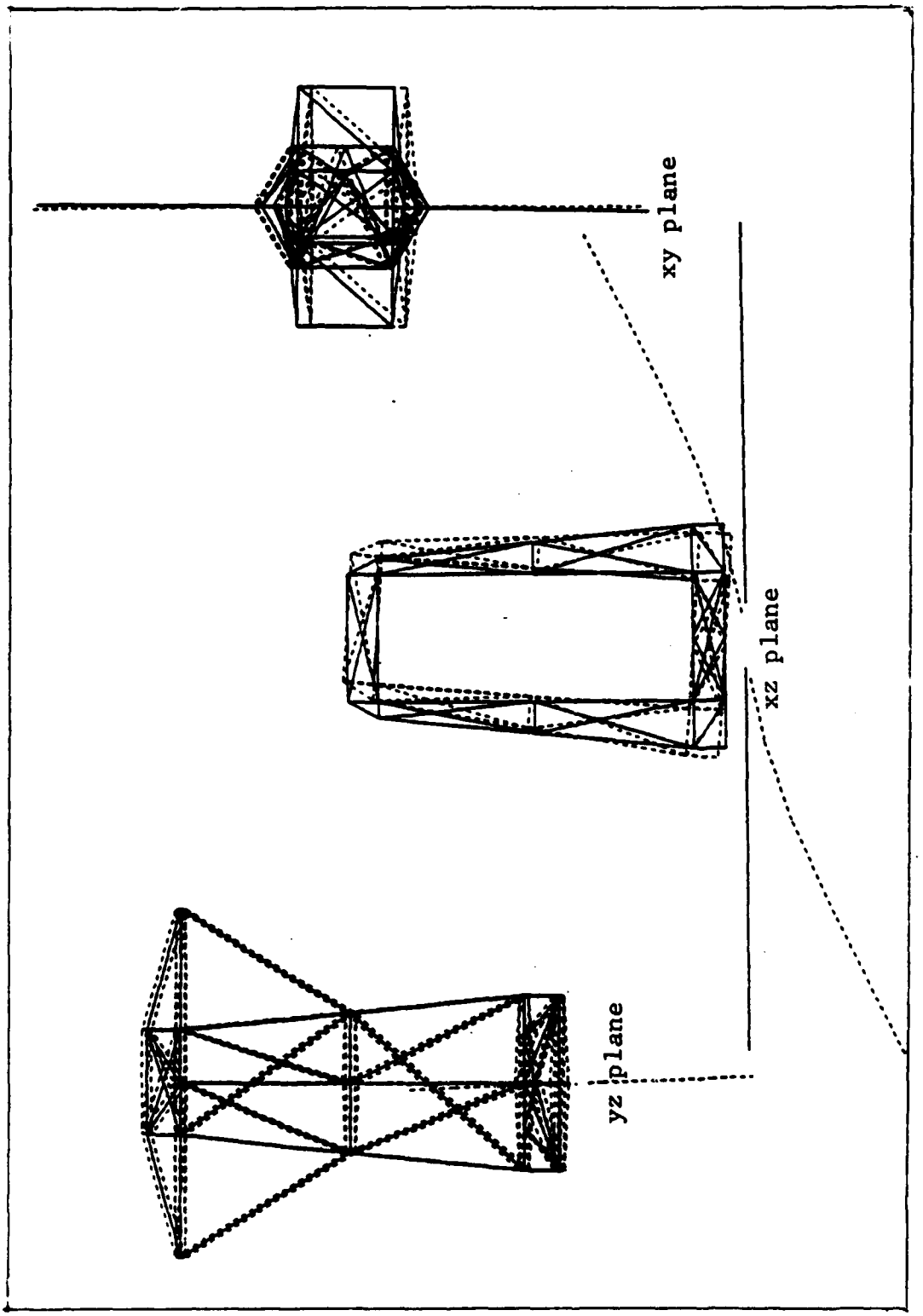

Figure 16. Mode Shape 7

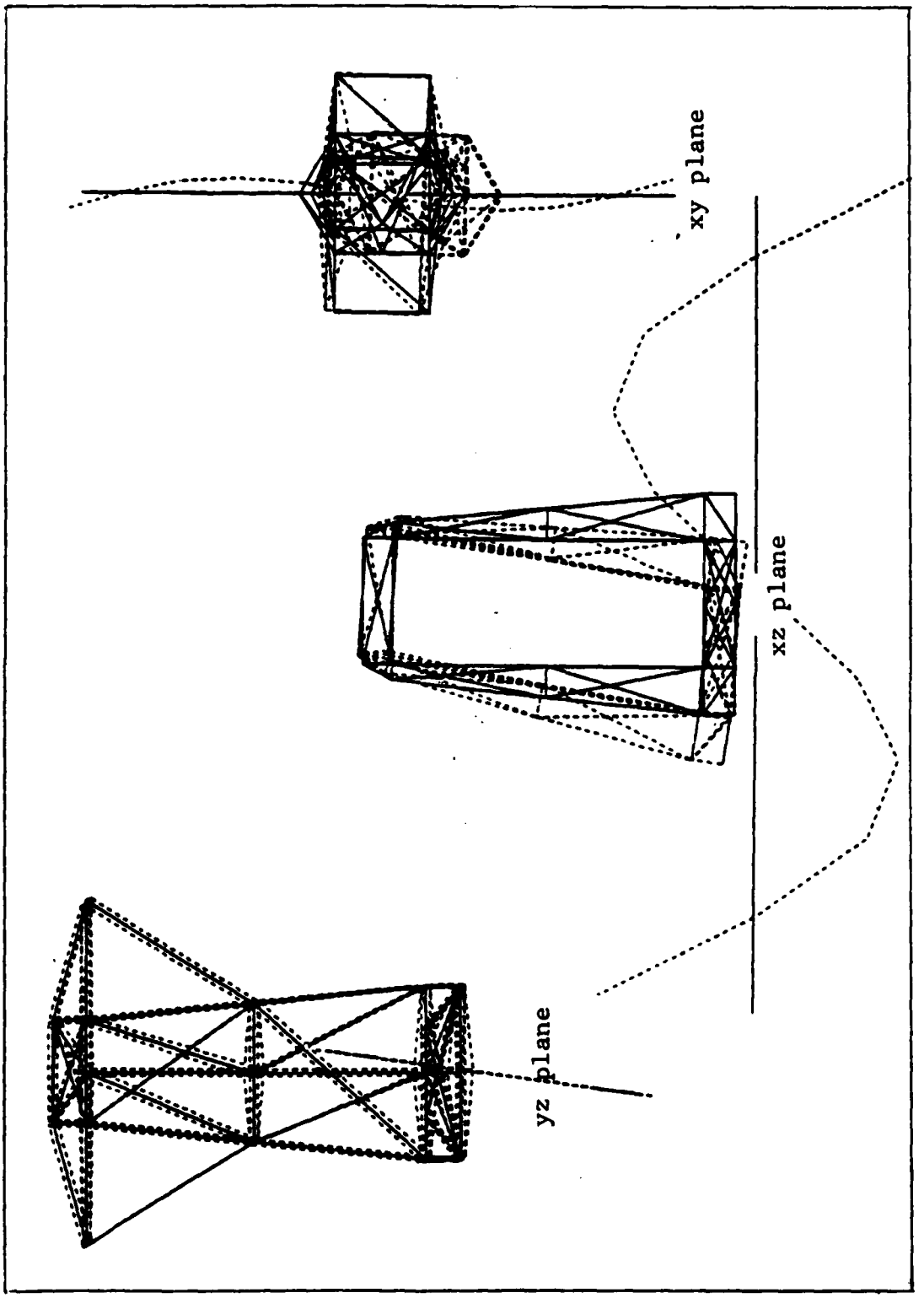

Figure 17. Mode Shape 12

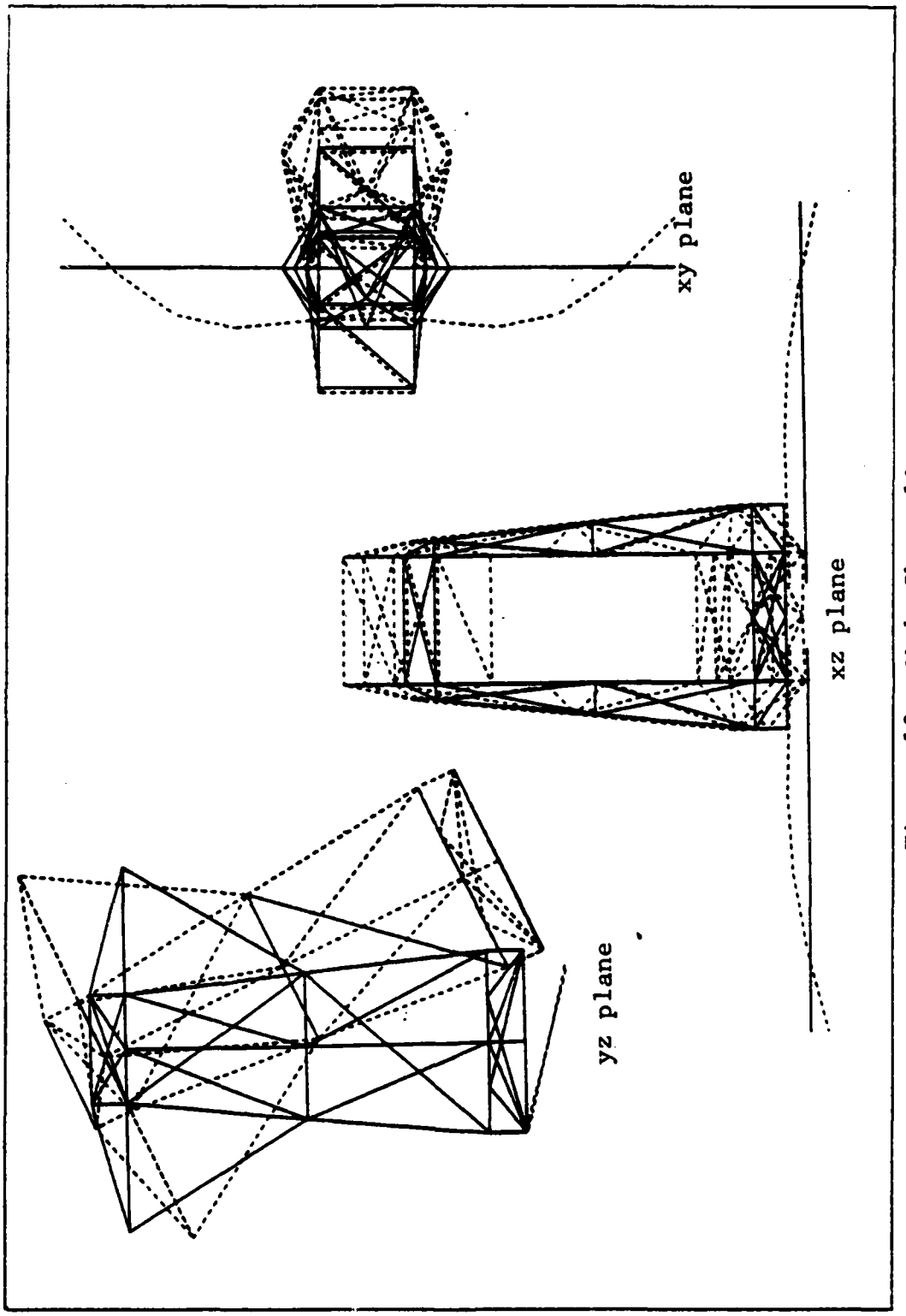

Figure 18. Mode Shape 13

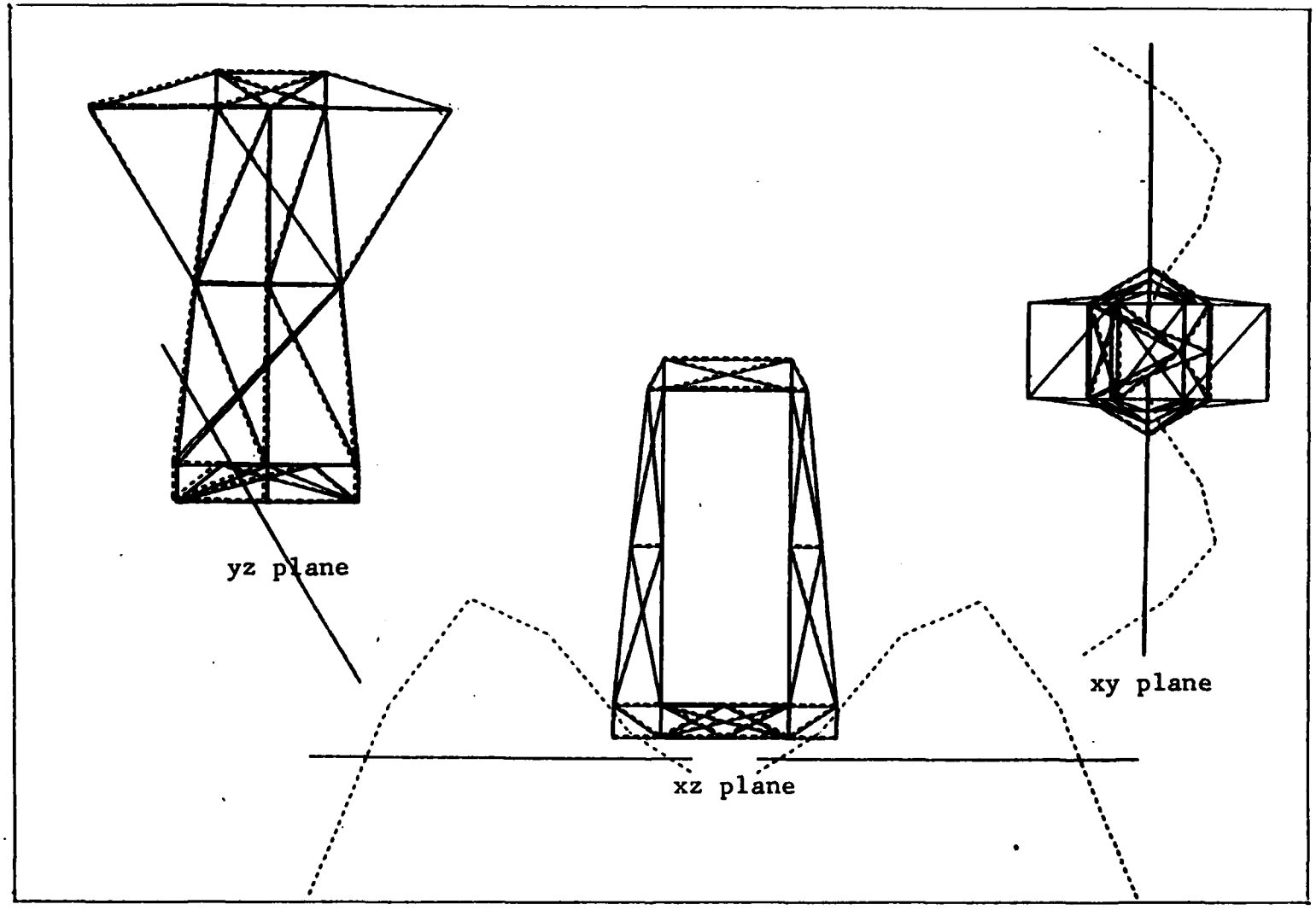

Figure 19. Mode Shape 17

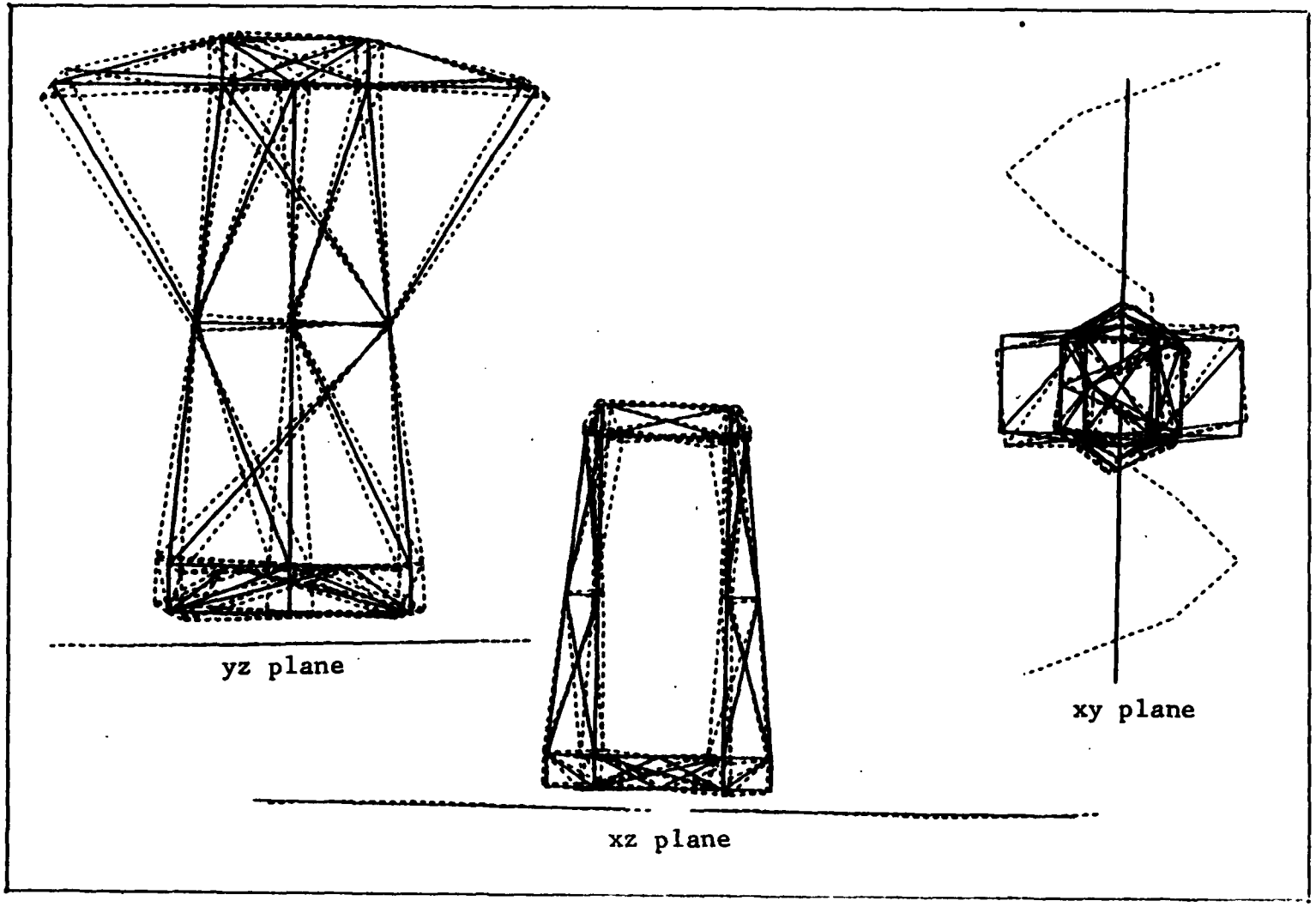

Figure 20. Mode Shape 21

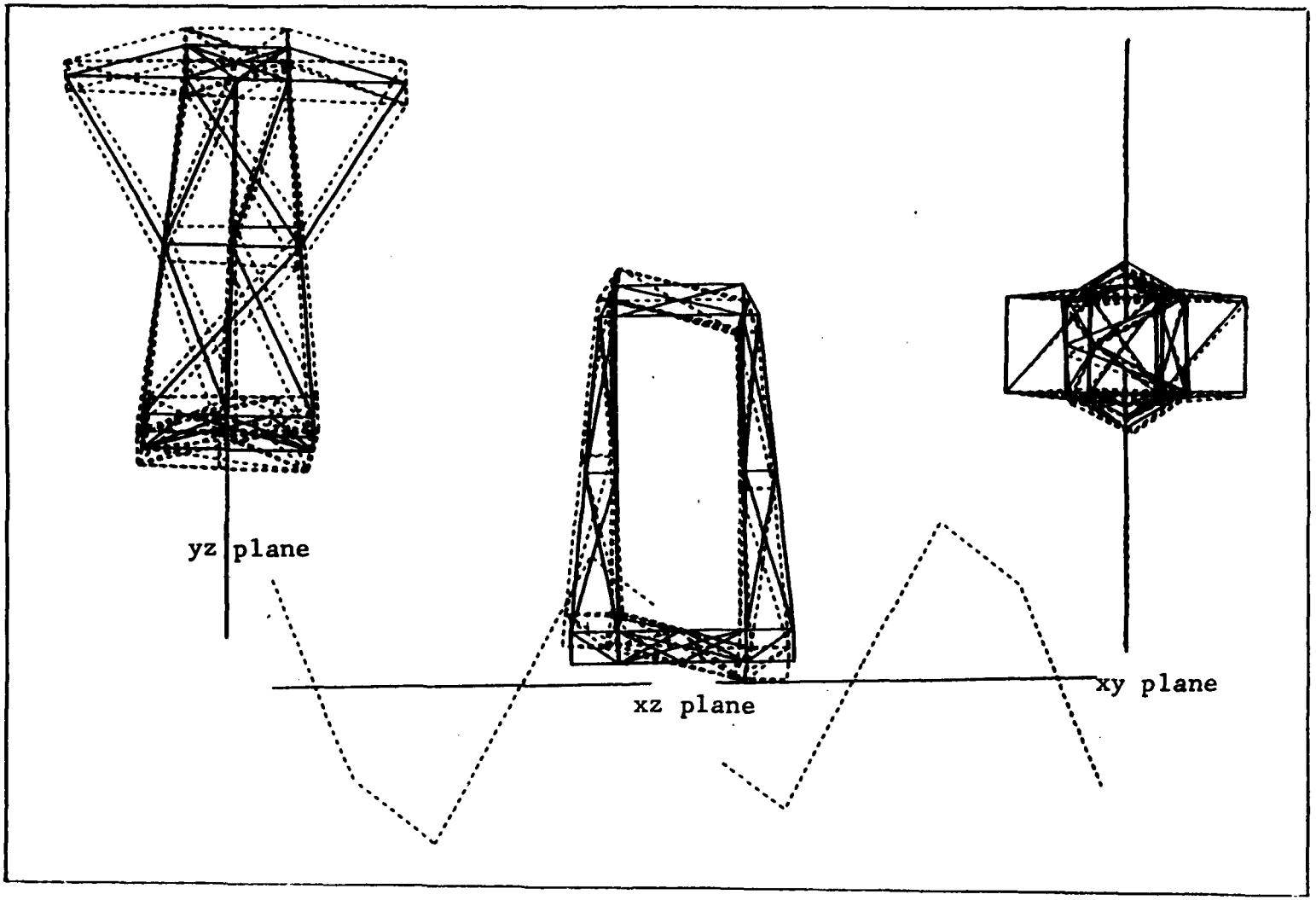

Figure 21. Mode Shape 22

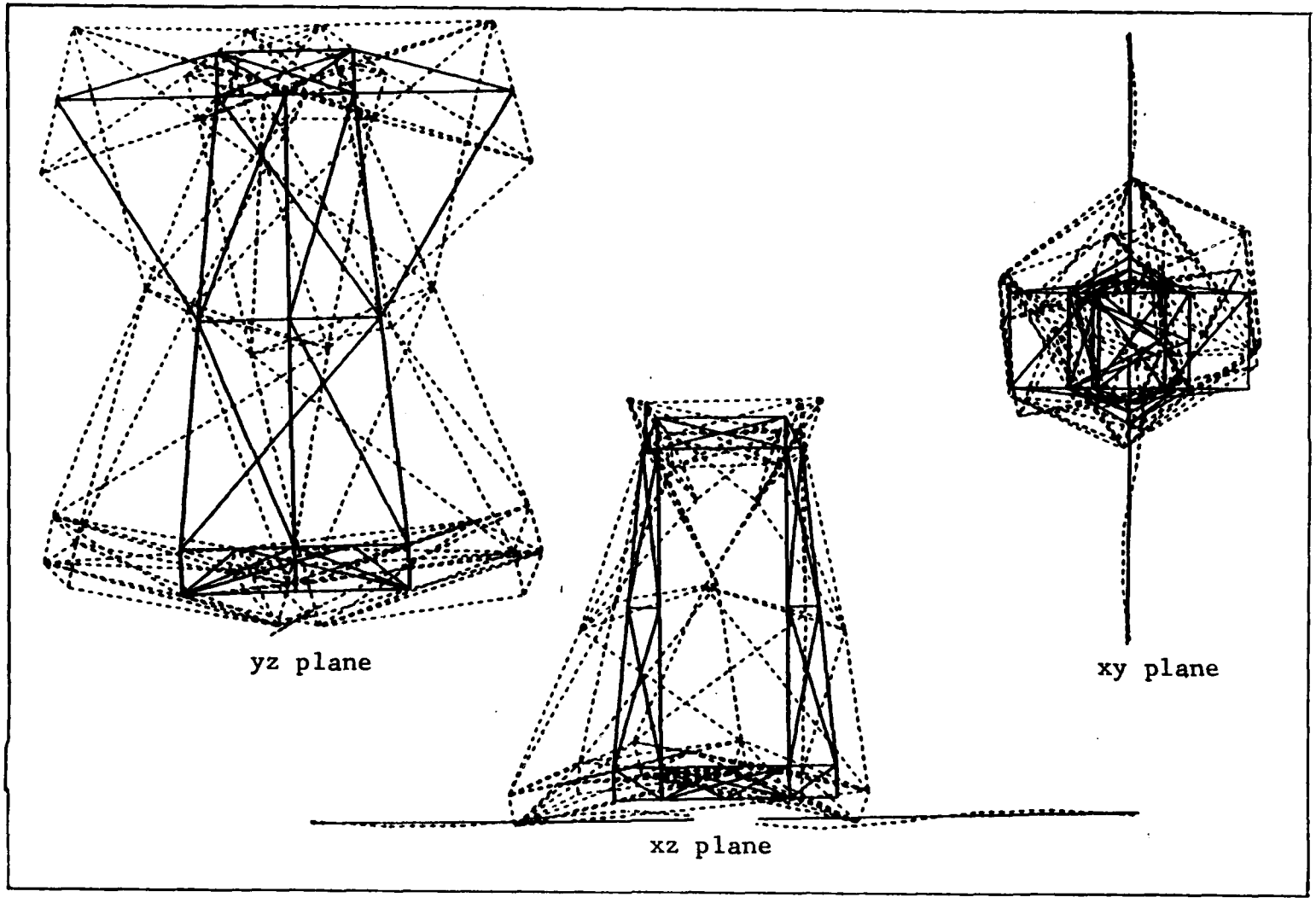

Figure 22. Mode Shape 24

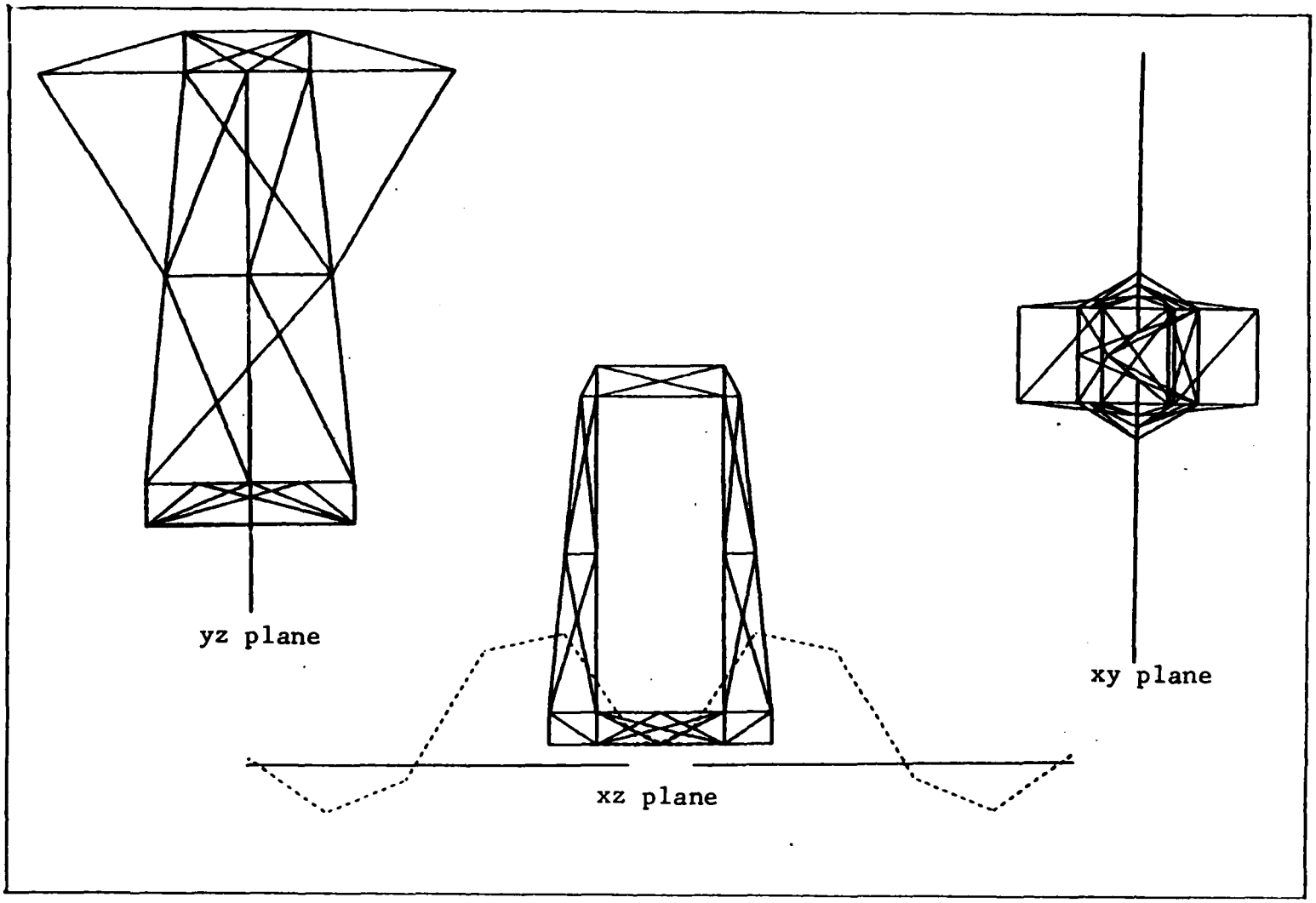

Figure 23. Mode Shape 28

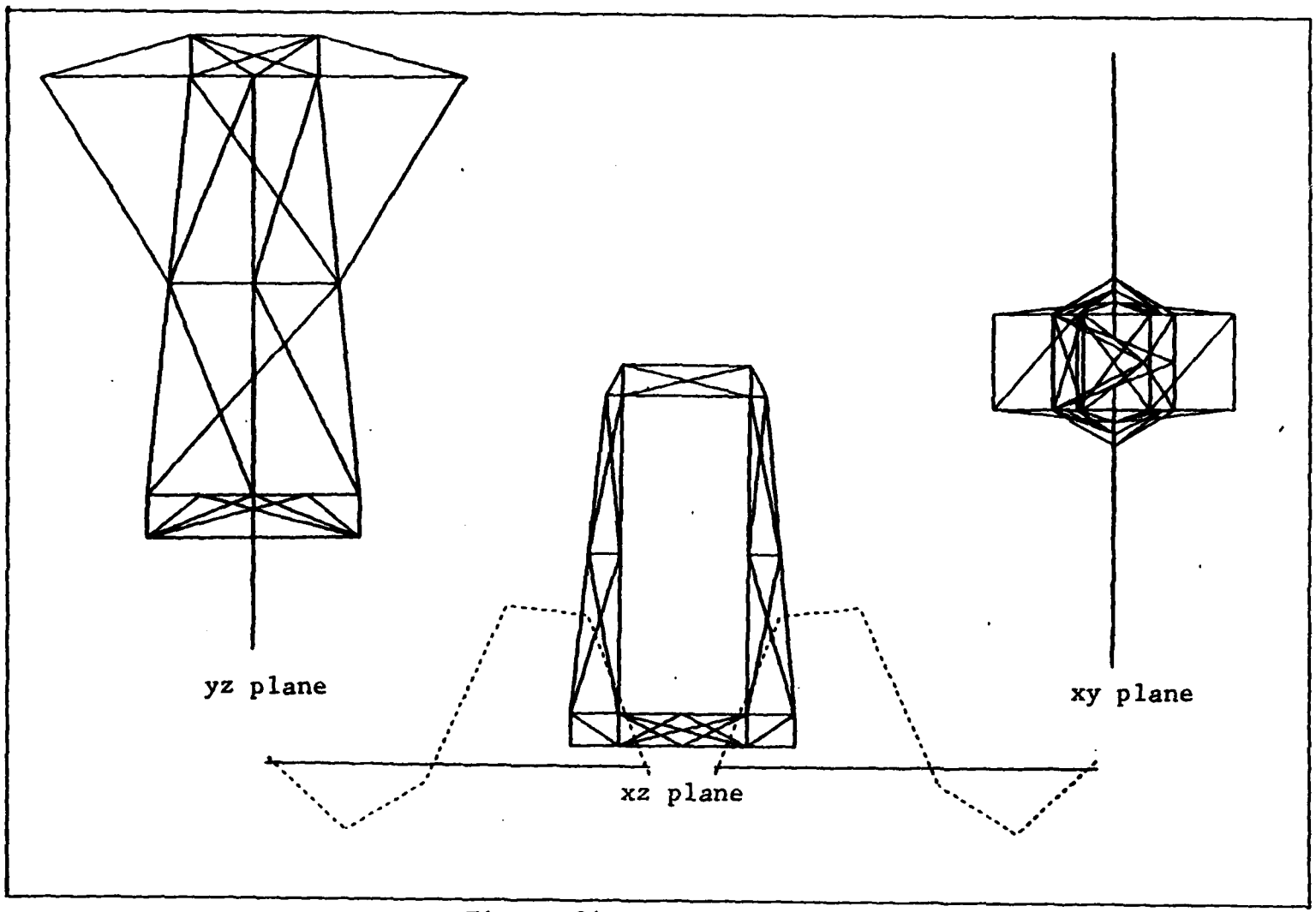

Figure 24. Mode Shape 29

Appendix J. Damping Factors

This appendix contains the actual damping factors for the 12 modes and the various perturbations. Modes 4, 5, and 6 always had a damping factor of zero. The damping factor for mode 7 was always greater than one. Modes 22, 28, and 29 had damping factors of .01000 throughout the research. The values for the remaining modes are listed below.

Table V. Damping Factors for the Unperturbed Model

Mode	Damping Factor
12	.04386
13	.22070
17	.18471
21	.01013
24	.01159

Table VI. Damping Factors for Mirror Mass Changes

Affected Mirrors	% Change	Damping Factor For Mode				
		12	13	17	21	24
All	-10	.18910	.19923	.04902	.01016	.01188
	- 5	.17009	.21432	.04771	.01020	.01231
	- 1	.15497	.21392	.04877	.01015	.01176
	+ 1	.18453	.22180	.04392	.01015	.01183
	+ 5	.18355	.22611	.04413	.01015	.01178
	+10	.17654	.21962	.04850	.01013	.01154
2 and 3	-10	.16899	.20711	.05167	.01015	.01184
	- 5	.17130	.21043	.05210	.01018	.01164
	- 1	.17160	.21691	.04796	.01018	.01210
	+ 1	.17259	.21759	.04808	.01022	.01254
	+ 5	.17462	.21851	.04831	.01016	.01183
	+10	.18685	.22607	.04434	.01020	.01237
2	-10	.16720	.21154	.04753	.01021	.01247
	- 5	.19068	.20516	.04935	.01020	.01228
	- 1	.18428	.22024	.04380	.01019	.01120
	+ 1	.18516	.22109	.04391	.01015	.01174
	+ 5	.19900	.20527	.05006	.01017	.01198
	+10	.18900	.22381	.04437	.01015	.01179
3	-10	.17394	.21279	.05239	.01014	.01174
	- 5	.19421	.20608	.04974	.01017	.01199
	- 1	.18485	.22053	.04386	.01014	.01170
	+ 1	.17207	.21724	.04804	.01017	.01195
	+ 5	.19446	.20604	.04969	.01016	.01183
	+10	.19451	.20605	.04965	.01022	.01252

Table VII. Damping Factors for Stiffness Increases (See Figures 4-12)

Perturbation Set	% Change in Area	Damping Factor for Mode				
		12	13	17	21	24
1	+10	.19415	.20606	.04967	.01018	.01217
	+50	.17090	.21740	.04871	.01015	.01215
2	+10	.18406	.22113	.04382	.01014	.01174
	+50	.19358	.20590	.04950	.01013	.01194
3	+10	.17376	.21252	.05249	.01015	.01174
	+50	.19461	.20598	.04970	.01015	.01182
4	+10	.17375	.20471	.05249	.01013	.01161
	+50	.19446	.20605	.04970	.01016	.01192
5	+10	.19435	.20606	.04972	.01016	.01182
	+50	.19436	.20606	.04972	.01016	.01187
6	+10	.19435	.20606	.04972	.01016	.01192
	+50	.19437	.20605	.04972	.01019	.01223
7	+10	.16815	.21613	.01004	.01018	.01215
	+50	.17422	.21292	.05254	.01018	.01213
8	+10	.16972	.22219	.01070	.01014	.01173
	+50	.17238	.21774	.04804	.01020	.01256
9	+10	.17293	.21729	.04802	.01020	.01231
	+50	.17200	.21733	.04801	.01019	.01234

Table VIII. Damping Factors for Midsection Mass Increases (See Figure 13)

Increase in mass per bar, kg	Damping Factor for Mode				
	12	13	17	21	24
5	.17216	.21734	.04801	.01016	.01195
25	.16889	.21527	.01003	.01018	.01222
50	.18547	.22218	.04378	.01018	.01215
85.9	.20089	.20314	.04951	.01019	.01226

Appendix K. GCSNAST Procedures

The GSCNAST plotting program was used to produce the deflected view of the CSDL 2 model in Appendix I. GCSNAST uses the NASTRAN bulk data deck for data on the shape and size of the structure and then refers to a deflection file that is processed from the NASTRAN output for data on the shape of the deflected structure. The first step in running GCSNAST is to create the deflection file. The following commands accomplish this:

```
ATTACH,NASTPP,NASTPP,ID=GCSNAST,SN=AFFDL.
ATTACH,NAS1,NAS1,ID=TRAN,SN=ASDAD.
ATTACH,NAS2,NAS2,ID=TRAN,SN=ASDAD.
LIBRARY,NAS1,NAS2.
ATTACH,PUN,ACOSSPUN,CY=1
REQUEST,DEFORM,*PF.
NASTPP,PUN.
```

The command NASTPP,PUN runs the program and puts the deflection file into the file labeled DEFORM. ACOSSPUN is the permanent file name used for the NASTRAN output (punch) file.

After creating the deflection file, GCSNAST can be run. The following two commands retrieve the GCSNAST program and set up its files:

```
ATTACH,GCSNAST,GCSNAST,ID=GCSNAST,SN=ASDAD.
GCSNAST.
```

Next, the program asks for the number of grid points and elements in the model, the type of data (NAST), and, finally, the name and location of the file that contains the NASTRAN input deck. At this point, the program is ready

to use and the user can refer to the GCSNAST manual for the specific commands used in GCSNAST. The figures in Appendix I were drawn using the DEFORM command and the deflection file.

VITA

David Eymer Olsen was born on 1 December 1952 in Takoma Park, Maryland. He graduated from high school in Colorado Springs, Colorado in 1970 and attended the United States Air Force Academy where he received the degree of Bachelor of Science in Civil Engineering in June 1974.. Upon graduation, he received a regular commission in the USAF. He attended pilot training in Lubbock, Texas and received his wings in September 1975. After completing mission qualification training in the RF-4C, he served tours at Kadena AB, Japan and Bergstrom AFB, Texas as an RF-4C pilot and flight instructor in the 15th and 12th Tactical Reconnaissance Squadrons. He entered the School of Engineering, Air Force Institute of Technology, in June 1982.

Permanent Address: 1485 Northfield Rd.
Colorado Springs, Colorado 80919

Unclassified

SECURITY CLASSIFICATION OF THIS PAGE

REPORT DOCUMENTATION PAGE

1a. REPORT SECURITY CLASSIFICATION Unclassified	1b. RESTRICTIVE MARKINGS
2a. SECURITY CLASSIFICATION AUTHORITY	3. DISTRIBUTION/AVAILABILITY OF REPORT Approved for public release; Distribution unlimited.
2b. DECLASSIFICATION/DOWNGRADING SCHEDULE	
4. PERFORMING ORGANIZATION REPORT NUMBER(S) AFIT/GSO/AA/83D-2	5. MONITORING ORGANIZATION REPORT NUMBER(S)
6a. NAME OF PERFORMING ORGANIZATION School of Engineering AF Institute of Technology 6b. OFFICE SYMBOL (If applicable) AFIT/EN	7a. NAME OF MONITORING ORGANIZATION
6c. ADDRESS (City, State and ZIP Code)	7b. ADDRESS (City, State and ZIP Code)
8a. NAME OF FUNDING/SPONSORING ORGANIZATION 8b. OFFICE SYMBOL (If applicable)	9. PROCUREMENT INSTRUMENT IDENTIFICATION NUMBER
8c. ADDRESS (City, State and ZIP Code)	10. SOURCE OF FUNDING NOS. PROGRAM ELEMENT NO. / PROJECT NO. / TASK NO. / WORK UNIT NO.
11. TITLE (Include Security Classification) See Box 19	
12. PERSONAL AUTHOR(S) David E. Olsen, B.S., Captain, USAF	
13a. TYPE OF REPORT MS Thesis 13b. TIME COVERED FROM _____ TO _____	14. DATE OF REPORT (Yr., Mo., Day) 1983 December 15. PAGE COUNT 127
16. SUPPLEMENTARY NOTATION Lynn Wolaver Dean for Professional Development Air Force Institute of Technology (AIC) Wright-Patterson AFB OH 45433 3 JAN 1984	

17. COSATI CODES		
FIELD	GROUP	SUB. GR.
1	2	
22	2	

18. SUBJECT TERMS (Continue on reverse if necessary and identify by block number)
ACOSS Large Space Structures
VCOSS

19. ABSTRACT (Continue on reverse if necessary and identify by block number)

Title: THE EFFECT OF MASS AND STIFFNESS CHANGES ON THE DAMPING FACTOR IN A LARGE SPACE STRUCTURE AS REPRESENTED BY THE CSDL 2 MODEL

Thesis Chairman: Martin M. Wallace, Major, USAF

20. DISTRIBUTION/AVAILABILITY OF ABSTRACT UNCLASSIFIED/UNLIMITED ☒ SAME AS RPT. ☐ DTIC USERS ☐	21. ABSTRACT SECURITY CLASSIFICATION Unclassified
22a. NAME OF RESPONSIBLE INDIVIDUAL Martin M. Wallace, Major, USAF	22b. TELEPHONE NUMBER (Include Area Code) 513-255-2998 22c. OFFICE SYMBOL AFIT/EN

DD FORM 1473, 83 APR EDITION OF 1 JAN 73 IS OBSOLETE.

Unclassified

SECURITY CLASSIFICATION OF THIS PAGE

This investigation was undertaken to determine the sensitivity of the damping factor in a large space structure (LSS) to small changes in non-structural mass and structural element stiffness. Revision 3 of the ACOSS 2 model, developed by the Charles Stark Draper Laboratory, Inc. (CSDL), was used as the model of the LSS. Various combinations of the mirror masses in this large space telescope were varied by up to 10%, selected structural elements were stiffened by increasing their cross-sectional areas by 10 and 50%, and, finally, two structural elements in the middle of the telescope were stiffened to represent the addition of a lumped mass located away from the control system sensors and actuators. A control system of 21 collocated sensors and actuators, positioned at the top and bottom of the telescope, was used in this analysis.

The analysis was accomplished using NASTRAN for the finite element analysis, and, after selecting certain vibration modes for further study, the complex conjugate pairs used to determine the damping factors were calculated. This last step was accomplished through spillover reduction and reduction of the closed loop matrix to a lower triangular form. This procedure was repeated for each of the 46 perturbations applied to the model in this research. The results indicate that the damping factors for the CSDL model are quite sensitive to small perturbations and that it is very difficult to predict the effect that a perturbation to the model will have on the damping factors. If the vibrations in an LSS are to be altered by changing mass or stiffness, a thorough analysis is required to ensure that increasing the damping for one mode does not result in an undesirable change in the damping for another mode.

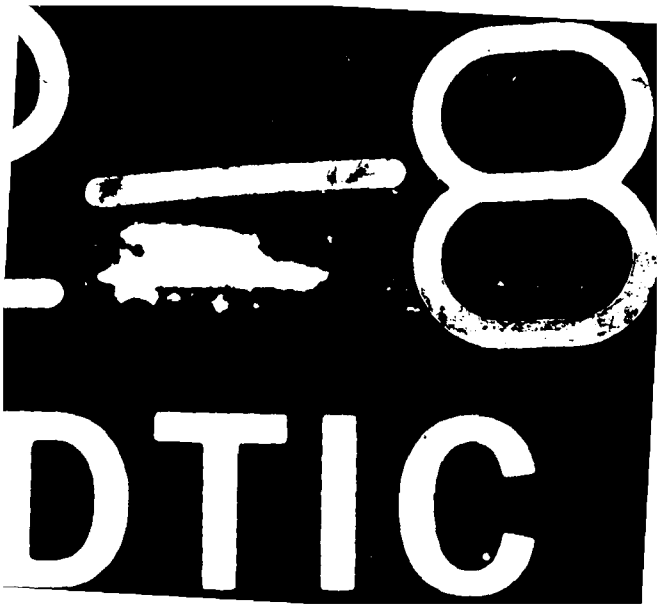
8
DTIC